AD-A085 349 ROYAL AIRCRAFT ESTABLISHMENT FARNBOROUGH (ENGLAND) F/G 1/4
THE DESIGN OF AIRCRAFT AUTOMATIC RIDE-SMOOTHING SYSTEMS USING D--ETC(U)
MAY 79 D E FRY, J S WINTER
UNCLASSIFIED RAE-TR-79045 DRIC-BR-70063 NL

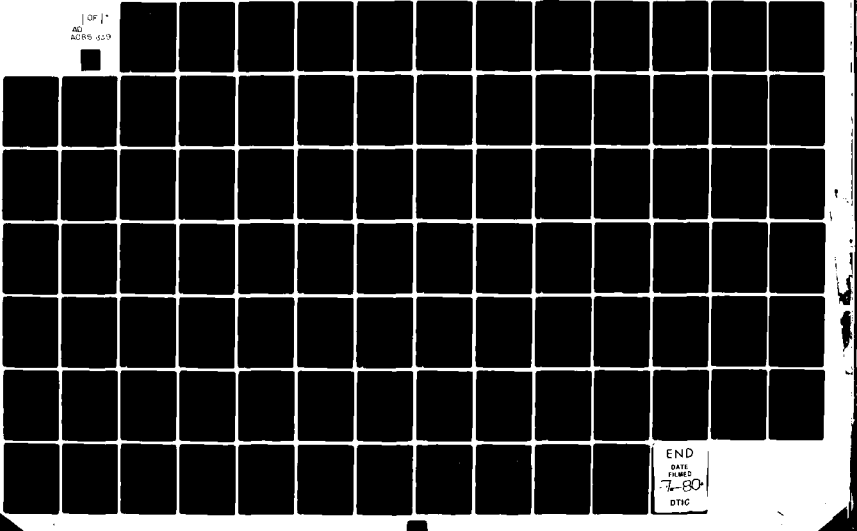

UNLIMITED

ROYAL AIRCRAFT ESTABLISHMENT

Technical Report 79045

May 1979

THE DESIGN OF AIRCRAFT AUTOMATIC RIDE-SMOOTHING SYSTEMS USING DIRECT-LIFT CONTROL

by

D.E. Fry

J.S. Winter

*

Procurement Executive, Ministry of Defence
Farnborough, Hants

UDC 533.694.1 : 533.6.013.61 : 629.13.074 : 623.746.3

(12) 93 (18) DRIC (19) BR-70063

ROYAL AIRCRAFT ESTABLISHMENT

(1) Technical Report 79045

(11) May 79

Received for printing 8 May 1979

(6) THE DESIGN OF AIRCRAFT AUTOMATIC RIDE-SMOOTHING SYSTEMS USING DIRECT-LIFT CONTROL

by

(10) D. E. Fry

J. S. Winter

(14) RAE-TR-79045

SUMMARY

This Report shows how a direct-lift motivator can be used to alleviate the response to vertical turbulence of a rigid, combat-type aircraft. Optimal-control and parameter-optimisation techniques are used to design both 'open' and 'closed' loop control systems. Alternative criteria other than simply reducing the normal acceleration response are discussed. The effects of system non-linearities such as position and rate limits are explored. Both discrete and continuous models of turbulence are used in the analysis. Some nonlinear control solutions are discussed.

Departmental Reference: FS 98

LIST OF CONTENTS

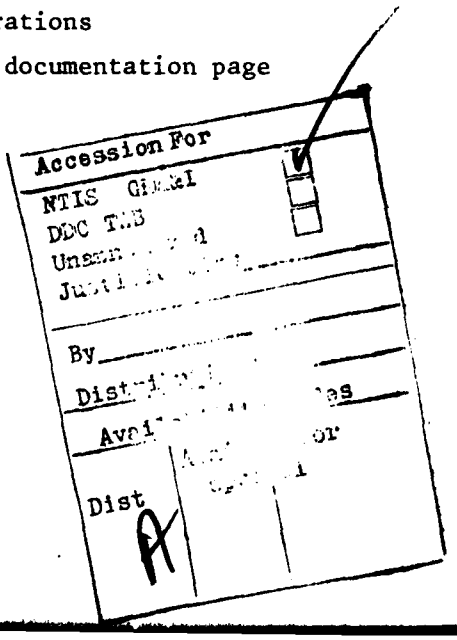

1 INTRODUCTION

This Report deals with the problem of designing a control system incorporating direct-lift-control (DLC) to improve the ride performance of a modern fighter aircraft. It is one of a series dealing with the implementation of possible performance benefits of active control, as applied to military combat aircraft. Active control is defined here as the use of feedback or feedforward control to change the dynamic characteristics of the aircraft. There are basically two types of benefit: firstly, that associated with pilot handling characteristics including tracking, weapon aiming, 'care-free' manoeuvring etc, and secondly, that associated with fully automatic control systems, independent of pilot input, including ride control, gust and load alleviation and flutter control. 'Active control' also implies the use of any available motivator, including not only the conventional elevator, aileron, flap and rudder, but also other possible motivators such as suitably placed canards or deflected thrust jets. From basic principles, the more motivators available to the control engineer the more the design flexibility and range of control he has over the aircraft dynamic response.

Research into ride quality of aircraft began more than 50 years ago and the benefits of high wing loading and a low lift-curve slope were established. The advent of high wing loading aircraft with their inherently improved ride qualities somewhat negated the need for ride smoothing control systems. However, the modern requirement for multipurpose aircraft having both good manoeuvring characteristics at high altitude (ideally requiring low wing loading and high lift curve slope) and good ride performance at low altitude has revived interest in ride control. There is now the possibility that the poor ride qualities near ground level of a low wing loading aircraft may be significantly improved through the use of active control.

A synopsis of the current knowledge of ride qualities can be found in Ref 1. At present, few generally accepted criteria for defining good or acceptable ride qualities are available, but clearly the motion of aircraft in response to atmospheric turbulence is the major factor.

A pre-requisite for the design of a ride-smoothing system is a quantitative specification of the atmospheric environment[2]. Atmospheric turbulence is usually modelled analytically as a statistical process and aircraft motion resulting from the turbulence excitation is generally deduced on the basis of random process theory. However, since the standard statistical models do not completely describe atmospheric turbulence other discrete forms of input must not be ignored[3-5].

Only the longitudinal axis has been considered in this Report and the control system has been implemented using two motivators: the conventional elevator, and split flaps to generate DLC. The design of the system was also constrained as follows:-

(i) all modes of the controlled system are damped to at least 0.5 relative damping;

(ii) the elevator and DLC motivator rates and positions are limited to within practical values;

(iii) a representation of the actual hardware is included in the mathematical model.

In order to obtain an insight into some of the problem areas, the design was first treated using a simple model of the aircraft dynamics plus first-order filters representing the actuation systems, including both elevator and DLC. The design technique involved the use of parameter optimisation[6,8], optimal control[7,8], time response[8], frequency response[8,9] and root-locus programs, both digital and hybrid. This initial design approximated to pure state feedback and enabled a broad assessment to be achieved. These initial control laws were then applied, with some small modifications, to a more complete and realistic model of the aircraft plus control system, including representation of actuators, power controls, sensors with their associated noise filters, and various nonlinearities.

Two flight cases have been considered, one, a low-speed, high incidence case and the other a high Mach number case, both at low altitude. Normal accelerations at various positions along the fuselage have been calculated, although the optimisations were mainly done for normal accelerations at the centre of gravity. For the closed-loop systems the reduction in rms normal acceleration was relatively insensitive to position along the fuselage. Worthwhile theoretical reductions of the rms of normal acceleration have been achieved (>30%).

Comparisons are made between results obtained using three different types of turbulence model: band-limited white noise, the conventional Dryden spectrum, and families of discrete gusts[4,5]. Since the gust scale length of the Dryden spectrum is a function of height, this parameter has also been varied. Percentage reductions in rms of normal acceleration are shown to be proportional to the DLC actuator activity. The effects of design constraints due to actuator rate and position limits have been considered.

Since it has been suggested that an appropriate measure of 'bumpiness' should involve the number of peaks or exceedances in normal accelerations per unit time, a preliminary assessment in terms of this criterion has been included. It has been shown that, compared to the datum aircraft, for closed-loop ride-control systems the number of zero level crossings, or total number of bumps, will increase, although the number of g-exceedance levels will decrease above certain amplitudes. Thus although the rms of normal acceleration may have been reduced drastically, the number of g-exceedances below a certain level will have increased. In discrete gust terminology this means that the 'tuned' gust length has decreased relative to that of the basic aircraft. The correlation between variances of aircraft states derived from conventional statistical turbulence models and peak response amplitudes obtained using discrete 'worst-gust' theory[4] is demonstrated. The total number of bumps is shown to depend on the ratio between the rms of rate of change of normal acceleration and the rms of normal acceleration itself. Thus some on-line measure of the rate of change of normal acceleration would appear beneficial for reducing bumpiness. This possibility has been discussed and the associated use of phase-advance filters in the feedback path of the DLC loop and of nonlinear control have been considered.

In addition to various types of closed-loop control, this Report includes an investigation of the 'open-loop' solution. The latter necessitates the use of incidence sensors such as wind vanes, in addition to rate gyros and accelerometers, for a practical solution.

Comparisons are made between the improved ride due to DLC and that associated with an increase of wing-loading for several aircraft. The objective or performance function is subsequently discussed in detail. The possibility of designing a DLC system that not only reduces the rms of normal acceleration due to turbulence but also does not increase the g-exceedance rate at low amplitudes is considered. For linear closed-loop systems these two criteria are shown to be conflicting. More generally, the possibility of defining a 'g-exceedance level' curve that is governed by both structural and physiological constraints is discussed. Some limitations of the 'open-loop' solution are outlined and the influence of rate-limiting of the DLC actuator on performance and stability has been described. The relative merits of open- and closed-loop designs have been compared.

The study described deals with the rigid-body motion only and does not include effects of flexible modes of the aircraft. For a fighter-type aircraft, effects of structural flexibility would probably have relatively little direct

effect on the ride*, although there is a possible structural fatigue-load problem due to the decrease in the tuned gust length introduced by the ride-smoothing system. The principles and techniques involved are, however, applicable to a more complete model of the aircraft including flexible modes. The inclusion of such modes would allow possible instabilities due to coupling between the control system and the flexible structure to be monitored. In addition, a logical extension planned for future work is to investigate gust-load control. Nevertheless, it is concluded from the present study that whilst possible instabilities associated with flexible characteristics may impose constraints on the degree of control in the case of combat aircraft, much can be achieved through the modification of the rigid-body modes to alleviate ride problems.

2 DEFINITION OF AIRCRAFT AND CONTROL SYSTEM MODELS

A mathematical model of a modern combat aircraft was used for the analysis. The small perturbation equations of motion are defined in Appendix A, and the aerodynamic data for the two flight cases considered, 0.3 and 0.9 Mach number, are defined in Table 1. Two motivators were assumed to be available: elevator and a form of direct lift control acting via split flaps. Closed-loop feedbacks, pitch rate to elevator and a variety of feedbacks to the DLC motivator, were considered.

For the initial investigation simple first-order approximations to the elevator and DLC (flap) actuators were used and a block schematic of the system is shown in Fig 1. This simple system is explored in depth and the results then applied to a more comprehensive simulation including sensors, noise filters, actuators, power controls, nonlinearities, etc.

The mathematical model of the aircraft contains only the rigid-body modes, and does not include any flexible modes, although the implications of possible structural coupling are discussed. There is clearly a need in the final design of any active control system to include a fully representative model of the aircraft[11-13] including at least the first few flexible modes at the lower frequencies.

3 ATMOSPHERIC TURBULENCE MODELS

Three different models of vertical turbulence were used. They were (i) band-limited white noise, (ii) the standard Dryden gust spectrum and (iii) a statistical discrete gust model. These are defined in Appendices B and C and a non-dimensional comparison of the power spectral density functions with the Von Karman spectrum is given in Fig 2.

* Subsequent work on a combat aircraft, however, has shown that flexibility can have an appreciable effect on the rms of normal acceleration.

It can be shown that the variance of a state output to white noise can be calculated analytically from an impulse or initial condition disturbance. Similarly the variances due to band-limited white noise (BLWN) can also be found from a single time response, by shaping the initial impulse[14,6,8]. This is equivalent to adding another first order differential equation to the system model. The equivalent Dryden type turbulence model can be defined by the addition of two first-order differential equations[14]. Thus, the variance or rms of any output state to either BLWN or Dryden type input can be calculated analytically in the time plane. The Dryden model was preferred to the Von Karman model simply on the grounds of analytical expediency, the Dryden power spectra being amenable in particular to the inverse Fourier transform for use in the state space domain (see Appendix B).

The statistical discrete gust approach[3-5] has been proposed as an alternative method for the assessment of aircraft systems. The more intense energy concentrations in atmospheric turbulence are modelled by equi-probable families of discrete ramp gusts covering a wide range of gradient distance and intensities (Appendix C). The method has been applied in this Report to the analysis and assessment of ride-smoothing systems and has also been included in an optimising procedure as part of a digital computer program (involving minimising the maximum response to the worst gust). Although slightly unwieldy for digital computer optimisations the technique has proved useful for nonlinear systems, where the standard techniques for minimising variances cannot be applied.

4 INITIAL RIDE-COMFORT OBJECTIVE FUNCTION

For the initial phase of this work ride improvement is defined as a reduction of the normal acceleration response of the aircraft to vertical turbulence at specified positions along the fuselage. This may be quantified in two ways, (i) statistically, by reducing the rms of normal acceleration response to the standard power spectral representation of turbulence, and (ii) deterministically, by reducing the peak amplitude of the normal acceleration response to discrete gusts. The second method involves the use of a set of discrete ramp gusts, as described in Appendix C, such that the response to the worst gust can be investigated. Both methods were employed and the results compared.

A further objective, pertinent to all systems investigated, was that all modes of the system should have damping greater than a prescribed minimum level. The value used in this study was 0.5 relative damping. As will be seen later, the achievable 'ride' improvement is a function of this damping constraint.

Alternative objective functions, other than merely reducing normal-acceleration response, are discussed and analysed in sections 8 and 9.

5 DESCRIPTION OF DESIGN METHODS

The mathematical model used has been outlined in section 2. It is defined by the equations

$$\dot{\underline{x}} = [A]\underline{x} + [B]\underline{u} + [C]\underline{w}_g \qquad (1)$$

$$\underline{y} = [D]\underline{x} + [E]\underline{w}_g$$

where $\underline{x}$, $\underline{u}$ and $\underline{w}_g$ are respectively state-space, control, and input vectors and $\underline{y}$ is the output vector.

Extensive use has been made of an existing suite of digital and hybrid (analogue/digital) computer programs to design the feedback control laws of Fig.1. These programs include matrix-Riccati optimal control[7], parameter optimisation[6,8], frequency responses[9,8] Bode plots[8], root locus[8], eigenvalues[8], time responses[8] to deterministic inputs and variances to statistical inputs[8]. The parameter optimisation was the dominant program used. Given a form of control law, this program automatically selects the set of parameters (feedback coefficients, time constants etc) which will minimise a chosen performance function. The program allows for constraints to be put both on parameters and on cost function elements. The variances of all aircraft states, control displacements and rates, due to the various turbulence inputs, were calculated. The cost or performance function was a weighted sum of these variances, together with a damping constraint from all the eigenvalues. In choosing the cost function, most weight was placed on the variances of normal acceleration, pitch rate, and DLC motivator rate.

Another design method was to calculate the normal acceleration responses to a family of discrete gusts (Appendix C) and to minimise the maximum amplitude due to the worst gust.

Further optimisations were performed in which the variances of elevator and flap rate were constrained to within prescribed values.

These methods were used to determine the 'optimum' state feedbacks and gain values for the reduced or simple model (Fig 1). This set the scene and guide-lines for the more practical solutions subsequently applied to specific aircraft. A block schematic of the design procedure is given in Fig 3.

A typical output of the parameter-optimisation program is given in Table 2. The aerodynamic data is followed by the initial parameter array including cost-function weights and state constraints. The variances of all states are then given for this parameter set, $\theta(i)$; i = 1(1)n , where n equals the number of parameters, usually the initial $\theta(i) = 0.0$. The variances for the derivatives of the states, *eg* $\dot{u}$, $\dot{w}$, $\dot{q}$, $\dot{\theta}$, $\dot{n}$, $\dot{\delta}$ may be included. The system eigenvalues follow, demonstrating the basic aircraft short period and phugoid modes, the two actuator poles, and finally the inverse of the input time constant (1.0 second). Each of the N-stages of the optimisation procedure (Table 2b), gives the iteration number the value of the total cost, and the M-parameters' values. The optimisation hill climbing procedure[15,16] finishes either as a function of the error between succeeding cost values or on the number of iterations. The end product (Table 2c), comprising the optimal parameters with associated variances, constraints and eigenvalues are then listed. In this purely typical example of a three parameter optimisation, the variances of aircraft states have been equally weighted with a unity factor, and the state combination $(\dot{\theta} - \hat{\dot{w}})$ by a factor of 10.0. Here $\hat{\dot{w}} = \dot{w}/V$, and thus $(\dot{\theta} - \hat{\dot{w}})$ is a non-dimensional measure of normal acceleration. No weights have been attached to the variances of the derivatives of the states, *ie* these are not included in the cost function, and there are no constraints on any of the state variances. If a constraint had been used, associated variances would have been included in the cost function if the current value was greater than the constraint. In this way, for example, the control activity $(\sigma_{\dot{\delta}})$ can be kept within prescribed limits.

All variances are in non-dimensional units with respect to unit variance input $(\hat{w}_g)$. It should be noted that each variance is factored by the square of the weight associated with it.

For the 'optimum' in Table 2c all modes are damped to 0.5 relative damping or greater. All variances have been reduced, some more than others, *eg* pitch rate variance has dropped from 0.5373 to 0.1041 and normal acceleration from 0.2931 to 0.2018. This relatively small reduction in normal acceleration variance is due to the choice of weighting vector; in this particular case the weights on speed (u) and attitude (θ) were such as to put more emphasis on the phugoid mode than necessary.

6 RESULTS FOR SIMPLE SYSTEM

6.1 Pitch-rate feedback to elevator

Without the direct-lift motivator operative, and using only elevator to alleviate normal acceleration, it soon became clear that large reductions

in rms normal acceleration at the pilot station could be achieved by feeding back only pitch-rate to the elevator. Since the centre of rotation of the aircraft's short period mode is usually well forward of the nose, the pilot will sense an acceleration due to rate of change of pitch, *ie* $a_z + \dot{q}/g$. Both terms are reduced by the pitch autostabiliser, due to the increased damping of the system. Clearly, the less stable the short period mode, the larger the effect an elevator loop can have on the ride performance.

Some results are shown in Table 3 giving percentage reductions in rms pitch rate of 71.6 and 73.6, and in normal acceleration of 17.9 and 7.4 for the two heights of 200 and 1000 feet respectively.

Thus, use of elevator alone can produce a significant element of ride improvement*. The system eigenvalues and rms values of the other states in response to band-limited white noise (BLWN) are also given in Table 3.

A root-locus of G_q (pitch-rate to elevator feedback gain) and frequency-response functions (Bode plots) for vertical turbulence input are given in Figs 4, 5a&b. From the Bode plot of pitch-rate, Fig 5a, it can be seen why the autostabiliser reduces the rms pitch rate so drastically. In the case of the normal acceleration Bode plot, Fig 5b, the main peak has been reduced at the expense of a slight increase in response at the lower frequencies.

6.2 Normal acceleration feedback to direct-lift motivator

Rearranging the second equation of Appendix A

$$-\dot{\hat{h}} = \dot{\hat{w}} - q = z_w \frac{\hat{w}}{\hat{t}} + z_\eta \frac{\eta}{\hat{t}} + z_\delta \frac{\delta}{\hat{t}} + z_u \frac{\hat{u}}{\hat{t}} \qquad (2)$$

where $a_z = v/g(\dot{\hat{w}} - q) = -\frac{v}{g}\ddot{\hat{h}}$,

and substituting

$$\delta = \frac{1}{(1 + \tau_2 S)} B_{a_z} \ddot{\hat{h}}$$

gives

$$\ddot{\hat{h}}\hat{t} = -(z_w \hat{w} + z_\eta \eta + z_u \hat{u}) \Big/ \left[1 + \frac{z_\delta B_{a_z}}{\hat{t}(1 + \tau_2 S)}\right] . \qquad (3)$$

Thus for fixed τ_2 , increasing B_{a_z} will always decrease $\ddot{h}(a_z)$ (see Fig 1). Normal acceleration feedback to the DLC motivator can thus be likened to a change in wing-loading (W/S), since $\hat{t} = m/\rho SV = W/S/\rho gV$. It should be noted

* Further reductions in the rms of normal acceleration can be achieved by feeding back incidence to the elevator, but at the expense of increases in the rms of pitch rate and attitude.

that this is not quite the same as reducing the aerodynamic derivative z_w, due to the influence of the other term in the numerator z_η when the elevator loop is closed.

Values for the two feedback parameters G_q and B_{a_z} (Fig 1) were obtained for a speed of 1000 ft/s (M = 0.9), with turbulence inputs applicable to 1000 feet and 200 feet height, using both Dryden and BLWN turbulence models with cut-off frequencies appropriate to height and speed[2].

A weighted sum of the variances of aircraft states was minimised, with a relative damping constraint of 0.5. Neither actuator rates or position were used in the cost function for this initial exercise.

A root-locus of B_{a_z} with fixed G_q(0.464) is given in Fig 6a. Large values of B_{a_z} can be employed without running into stability problems. The elevator/pitch pole remains invariant with B_{a_z}, whereas the heave pole (real root) due to the DLC loop increases with B_{a_z}. Thus the pitching and heaving components of the aircraft motion have become de-coupled. (An assumption made here is that the pitching moment due to the DLC motivator has been eliminated.) For the analysis of this Report it has been assumed that this pitching effect can be effectively cancelled by feeding a signal across from the DLC loop to the elevator loop with a gain of $-M_\delta/M_\eta$; *ie* $\eta = -M_\delta/M_\eta \delta$.)

The pole associated with the DLC feedback loop is equivalent to a rapidly damped exponential ($e^{-\lambda t}$). The eigenvalues for various values of B_{a_z} are given in Table 4a. A typical set of eigenvalues with and without control are given in Table 5, together with the rms values of all states and motivators. For example, comparing the basic and controlled aircraft, the rms values for pitch-rate (q) and normal acceleration (a_z) have dropped from 2.404 and 1.127 to 0.772 and 0.254 respectively. However, the large value of feedback gain $B_{a_z} = -63.5$ has also resulted in large motivator rate activity: rms flap deflection of 0.122 rad, and flap rate of 2.644 rad/s; *ie* small displacements but large rates.

The results show that, subject to the mathematical model assumed, without any constraints on the actuator rate rms the reduction in normal acceleration rms is effectively limitless. This is clearly shown in Fig 7 where the rms of normal acceleration is plotted against B_{a_z}. The rms of flap rate is shown in Fig 8, also against B_{a_z}. The rms of rate of change of normal acceleration is shown in Fig 9. This is effectively the only aircraft state rms that increases as a function of the feedback gain B_{a_z}. The significance of this will be discussed later (sections 8 and 9).

Figs 7, 8 and 9 also show the effect of varying the actuator time constant (τ_2)

where $\delta = \frac{B_{a_z}}{1 + \tau_2 S} a_z$,

and from these it would appear that large reductions in rms σ_{a_z} can be achieved despite large actuator lags and with small actuator rates, but with different values of the feedback gain (B_{a_z}), *eg* 30% reduction in rms normal acceleration can apparently be achieved with time constant and B_{a_z} values of 0.01 and 5.0, and 0.3 and 12.1 respectively. Unfortunately, however, with a more realistic representation of the actuation system, when the rate limit is taken to be a function of the actuator natural frequency, the above idealised result does not hold. This is described more fully in section 7. Fig 7 also shows that with a fixed gain the improvement in ride is a direct function of the speed of response of the actuator (τ_2).

The two Figs 10 and 11 show the variation of σ_q, σ_{a_z}, $\sigma_{\dot{a}_z}$ and $\sigma_{\dot{\delta}}$ for two different heights, namely 1000 feet and 200 feet. Both sets of results incorporate a fixed elevator loop gain of 0.464, *ie* the zero B_{a_z} values include the elevator/pitch rate closed loop. The dotted lines give the 30, 40 and 50% reduction levels for rms of normal acceleration. It is interesting to compare the results at the two heights, the difference being associated with the standard turbulence models, both Dryden and Von Karman spectrum forms predicting increased energy at higher frequencies closer to the ground.

The pitch rate to elevator loop has a bigger effect on the rms of normal acceleration at the low altitude, *ie* a 17% reduction as compared with an 8% reduction at 1000 feet. For comparison the variations of rms normal acceleration for both heights are plotted against wing-loading in Fig 13. The effect is more marked for the low altitude case. However, an associated difference between the two heights is the much larger flap rate ($\sigma_{\dot{\delta}}$) needed to achieve the same reduction in rms normal acceleration at the lower altitude. The two Figs 10 and 11 give an indication of the actuator characteristics needed to achieve a significant reduction in rms normal acceleration (say 30%). It appears that a minimum rms of about 10 deg/s (actuator rate) is required. Since the above graphs are for inputs of unity rms (1 m/s), then given an actuator rate limit of ±60 deg/s, 95% of the response to turbulence (±3σ) would be within the actuation rate limits for rms input values up to 2 m/s.

Thus it is clear that the rate limit of the DLC actuator imposes an important constraint on the achievable ride improvement. The size of the

feedback loop gain (Ba_zZ_δ) has a similar effect. This gain emphasises the significance of the motivator effectiveness (Z_δ), since for large values of Z_δ, the equivalent reduction in rms σ_{a_z} could be achieved with lower feedback gain B_{a_z}, and hence inferior actuators. Thus the system performance is constrained by a combination of the DLC surface effectiveness and the actuation characteristics.

Fig 12 shows the rms normal acceleration response for various positions along the fuselage for three cases, basic aircraft, elevator loop only and ride-smoothing system using DLC. Clearly, with this aircraft, in order to improve the response at all stations along the fuselage, it is perfectly adequate to minimise the normal acceleration at the centre of gravity.

The effect of changing the wing loading of the basic aircraft is shown in Table 6 and Fig 13. It can be seen that increasing the wing loading decreases the rms of normal acceleration for both heights.

6.3 Incidence feedback to direct-lift motivator

Rearranging the second equation of Appendix A

$$-\dot{\hat{h}} = \dot{\hat{w}} - q = z_u \frac{\hat{u}}{\hat{t}} + z_w \frac{\hat{w}}{\hat{t}} + z_\eta \frac{\eta}{\hat{t}} + z_\delta \frac{\delta}{\hat{t}} \qquad (4)$$

and substituting $\delta = (1/1 + \tau_2 S)B_\alpha \hat{w}$ gives

$$\ddot{\hat{h}}\hat{t} = -\left[z_w + \frac{z_\delta B_\alpha}{(1 + \tau_2 S)}\right]\hat{w} - z_u\hat{u} - z_\eta\eta \quad . \qquad (5)$$

Thus, for small values of τ_2, incidence feedback is effectively equivalent to changing the lift-curve slope z_w.

The eigenvalues for the system with incidence feedback are shown in Table 4b for a fixed elevator/pitch-rate loop gain. As will be seen, the short-period oscillatory mode remains invariant with DLC loop gain. Unfortunately, in contrast to the normal acceleration feedback, there is now a stability problem for larger DLC loop gains, the phugoid mode going unstable at a gain value between -20 and -30. The root locus of the poles is closely akin to changing z_w as shown by the Table 4c. The problem of phugoid instability is not serious since it can be solved by either a throttle/speed control or a pitch attitude/elevator control. Roughly equivalent results to those obtained with normal acceleration feedback can be obtained as demonstrated in Table 5 which shows rms

values due to Dryden turbulence. A plot of the aircraft and control state rms values against B_α is given in Fig 14 for two values of DLC actuator time constant (τ_2 = 0.1, 0.2). The trends are the same as for normal acceleration feedback, except for the stability boundary at $G_\alpha \triangleq 27.0$.

Although the theoretical results indicate that a normal accelerometer should give slightly superior 'ride' control than an incidence vane, the sensor imperfections, noise levels, sensitivity to damage, etc should all be considered in deciding the choice of method in practice.

6.4 Discrete gust input

This method involved the use of a family of discrete gust inputs[4] to obtain the parameters of the system giving the best performance. The largest amplitude normal-acceleration response to the worst gust was minimised. The main parameters associated with this discrete-gust approach are H , the gust length, $\gamma(H)$, the amplitude of the peak response and λ , the gust length sensitivity, as outlined in Appendix C. $\bar{H}$ and $\bar{\gamma}$ are designated the 'tuned' gust length and the 'tuned' response respectively. Including a damping constraint meant that only isolated ramp gusts need be used in this analysis, since there were effectively no significant overswings in the transient responses.

For the linear systems involved the optimum feedback gains were approximately the same as for the minimising variances method. However, the method, although rather unwieldy as a design technique, proved extremely useful not only for nonlinear systems where eigenvalues, etc cannot be calculated, but as a means of explanation and interface between different disciplines.

Fig 15 shows the maximum amplitude response $\gamma(H)$ of normal acceleration to a set of discrete gusts if variable length ($\bar{H}$). The tuned gust length $\bar{H}$ for the basic aircraft and also for the elevator-controlled system is about 70 metres. It may be seen from Fig 15 that the DLC loop reduces the peak normal acceleration response $\gamma(\bar{H})$, and that in addition the tuned or worst gust length $\bar{H}$ reduces as the feedback gain increases. A comparison between power-spectral-density (PSD) and statistical discrete gust (SDG) methods shows that a close relationship exists between zero crossing rate N_0 , evaluated using the PSD method, and the quantity $1/\lambda\bar{H}$ derived from the SDG method. If the tuned gust length decreases N_0 increases.

The 'ideal' control system would be one that reduced the amplitude of response $\gamma(\bar{H})$ without at the same time reducing the 'tuned' gust length $\bar{H}$. The problem of the changing tuned gust length is discussed more fully later in

the paper. As there is some uncertainty as to the practical importance of this effect, there is a need for further experimental work to determine what ride characteristics the pilot prefers.

7 EFFECT OF ACTUATOR CHARACTERISTICS, NATURAL FREQUENCY, RATE AND POSITION LIMITS

It has been shown previously (section 6.2) that the actuator rate limit plays an important part in determining how much improvement in ride can be achieved. Fig 16 demonstrates the effect of constraints on the maximum rms DLC actuator rate ($\sigma_{\dot{\delta}}$) for the system as defined in Fig 1, *ie* normal acceleration feedback and a first-order actuator. Values for actuator time constant are given along each curve of constant $\sigma_{\dot{\delta}}$. It should be noted that these are rms values of motivator rate per unity (1 m/s) rms amplitude of vertical turbulence. Thus assuming a Gaussian distribution for the turbulence, (with a desired physical limit of $3\sigma_{\dot{\delta}}$), 95% of the actuator rate would be within the linear range.

It can be seen that for a fixed $\sigma_{\dot{\delta}}$, higher attenuation in rms normal acceleration is achieved with more sluggish actuators (larger τ_2) and corresponding increases in the magnitude of the loop gain B_{a_z}.

For a fixed loop gain (B_{a_z}), further reduction in rms normal acceleration can be achieved by increasing the allowable rms actuator rate. It would appear that the optimal configuration would be an actuator with a large allowable rms actuator rate, together with a large actuation lag. This implies large feedback gains, which when using a more realistic representation of the actuator, is not possible due to stability constraints.

In order to elaborate this point, the actuation system has been modelled as a first order lag (representing the power control) followed by a second-order lag of natural frequency ω_n and damping 0.7, *ie*

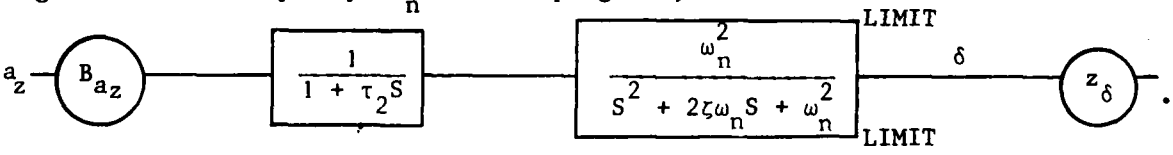

A root locus for fixed values of $\tau_2 = 0.04$ second, $\omega_n = 50$ rad, $\zeta = 0.7$, is given in Fig 6b. Again, the pitching and heave motions are decoupled, the elevator-pitch pole remaining invariant with B_{a_z} at approximately $-10.5 \pm 18.0i$. However the interaction between poles in the DLC loop causes the high frequency mode to go unstable at a gain modulus of just over 50. Similar root locii occur for different values of ω_n and ζ. The elevator loop remained fixed to give a damping of 0.5 for the pitching mode. A typical set of eigenvalues for $\omega_n = 50$ are given in Table 4d.

Fig 17 gives the rms of normal acceleration to unit rms vertical gust input plotted against the natural undamped frequency of the actuator ω_n. With this system the DLC loop gain is constrained by stability. The full line gives the 0.5 relative damping boundary, the figures in brackets giving the relative damping of the least damped mode in the system. As the actuators improve (faster acting, *ie* higher undamped natural frequency) larger reductions in rms normal acceleration can be achieved in association with the larger gains, B_{a_z}. With increasing gain, the variance for fixed ω_n drops until the system approaches the stability boundary when the variance increases rapidly.

The dotted lines in Fig 17 show the 30, 40 and 50% reductions in rms normal acceleration. Thus, to achieve a 30% reduction at ω_n = 25.0 rad the closed-loop gain would need to be about -12.0. However, the damping of the loop would be reduced to 0.34 relative damping. If a damping constraint of at least 0.5 is to be upheld then the minimum actuator natural frequency would need to be about 60.0 rad/s (10 cps).

Fig 18 shows the rms values of actuator rate plotted against the loop gain, B_{a_z}. The rms values are fairly consistent for different values of natural frequency, except at large loop gains when the system with low ω_n tend to be lightly damped.

It must be emphasised that these results are for a fixed value of flap effectiveness, z_δ, *ie* the coefficient of lift obtainable from a deflection of the DLC motivator. The more effective the surface, the lower are the closed loop gains necessary to achieve the desired improvement in ride, and hence the less actuator rate.

8 RE-CONSIDERATION OF RIDE-COMFORT OBJECTIVE FUNCTION

It is appropriate here to introduce the concept of exceedance-level curves. These are simply plots of the frequency of occurrence $N(x)$ of a given output state exceeding or crossing a particular level x.

It can be shown[18,19] using power spectral techniques that within a turbulence patch modelled by a Gaussian distribution

$$N(x) = \frac{N_0}{2} e^{-x^2/2\sigma_x^2} \qquad (6)$$

where
$$N_0^2 = \frac{1}{\pi^2}\left[\frac{\int_0^\infty \omega^2 \Phi_{xx}(\omega)\,d\omega}{\int_0^\infty \Phi_{xx}(\omega)\,d\omega}\right] . \tag{7}$$

Now
$$\sigma_x^2 = \frac{1}{2\pi}\int_0^\infty \Phi_{xx}(\omega)\,d\omega$$

and
$$\sigma_{\dot{x}}^2 = \frac{1}{2\pi}\int_0^\infty \omega^2 \Phi(\omega)\,d\omega .$$

Thus equation (7) becomes
$$N_0^2 = \frac{1}{\pi^2}\frac{\sigma_{\dot{x}}^2}{\sigma_x^2} . \tag{8}$$

Similar results are available using statistical discrete gust theory[3] (Appendix C), and the exceedance rate is given by
$$N(x) = \frac{\alpha}{\lambda \bar{H}} \exp\left(-\frac{x}{\beta\gamma(\bar{H})}\right) \tag{9}$$

where the term $\alpha/\lambda\bar{H}$ is effectively the zero crossing rate. This latter approach is particularly useful for investigating the response of nonlinear systems[22].

Fig 19 shows a normal acceleration exceedance curve for an assumed Gaussian patch of turbulence input of unity rms. It can be seen that N_0 has increased with increase in DLC normal acceleration feedback, whereas the variance represented by the slope of the curves has decreased. N_0 also increases as the actuator lag decreases. In contrast, with an increase of wing-loading, both rms and N_0 decrease (see also Table 6).

With the 'ride' systems designed so far, the rms of normal acceleration has been reduced but the rms of rate of change of normal acceleration has always increased. Thus N_0 has automatically increased (equation (8)), being a function of the ratio of the two rms values. However, it should be noted from the frequency response curve of Fig 5b that the amplitude of the normal acceleration response to turbulence at high frequencies is not increased by the ride-smoothing system in comparison to that of the basic aircraft. Above about 80 rad/s (for this particular example), the response amplitudes for both controlled and basic aircraft are effectively the same. Thus the increase in N_0 is not due to an increase in high frequency energy, it is due rather to an increase in the ratio in equation (8), with rms normal acceleration (σ_x) decreasing and at the same time rms rate of change of acceleration ($\sigma_{\dot{x}}$) increasing.

The combination of reduced rms normal acceleration and increased N_0 have been described qualitatively by pilots as giving a 'cobblestone ride'. Little is known of the effect of the associated increase in rate of change of acceleration or 'jerkiness' on the pilot. However, an increase in N_0 implies an increase in the rate of occurrence of sign reversals in normal acceleration fluctuation about 1g, and may be expected to have some adverse effect on the pilot. Also any increase in N_0 could well have structural implications associated with effects on airframe fatigue life.

Previous designs of 'ride' control systems, do not appear to have considered these 'jerk' effects.

In order to have some control over the 'jerkiness' without changing the structure of the feedback system, the possibility has been investigated of including N_0 in the cost or performance function to be minimised. Thus the cost function takes the form $\left(N_0 + \lambda\sigma_x^2\right)$, where λ is an arbitrary constant. Such a system would not only be required to reduce the variance of normal acceleration but also N_0. However, since $N_0 = \frac{1}{\pi}\frac{\sigma_{\dot{x}}}{\sigma_x}$, the cost function would effectively be:-

$$V = \frac{\sigma_{\dot{x}}^2}{\sigma_x^2} + \lambda\sigma_x^2 \qquad (10)$$

[where x is taken to be normal acceleration].

The two elements of the cost function are clearly conflicting since minimising σ_x^2 will decrease the second term but increase the first ($\omega > 1.0$). An

alternative solution would be to minimise the variance of x (normal acceleration) plus a heavily constrained N_0, *eg*

$$\sigma_x^2 + C\delta(N_0 - N_{0_C}) \tag{11}$$

where C is a large constant and δ is 0 or 1, depending upon whether N_0 is less than or greater than N_{0_C}. N_{0_C} is thus the prescribed limit N_0 should be allowed to achieve, set from other practical considerations.

On the basis of the cost function, equation (10), however, and using only normal acceleration or incidence feedbacks, clearly a compromise must be reached between reduction of rms normal acceleration and allowing N_0 to increase. The two elements of the cost function are plotted in Fig 20a&b for different values of actuator time constant. Thus $\lambda \triangleq 6$ gives a 30% reduction in rms normal acceleration ($\tau_2 = 0.04$) with an increase in N_0 from 1.5 (basic aircraft) to 2.5. Exploitation of this cost function in a parameter optimisation procedure requires additional flexibility (for example use of complex filters or extra motion feedbacks) in the control laws. Two possible alternative solutions are discussed in section 9.

9 ALTERNATIVE RIDE-CONTROL SYSTEMS

9.1 Shaping of feedback signal

It was thought that in order to control 'jerkiness' some measure of the rate of change of normal acceleration should be used in the feedback loop. Clearly no sensor measures 'jerkiness' but a possible solution could be:-

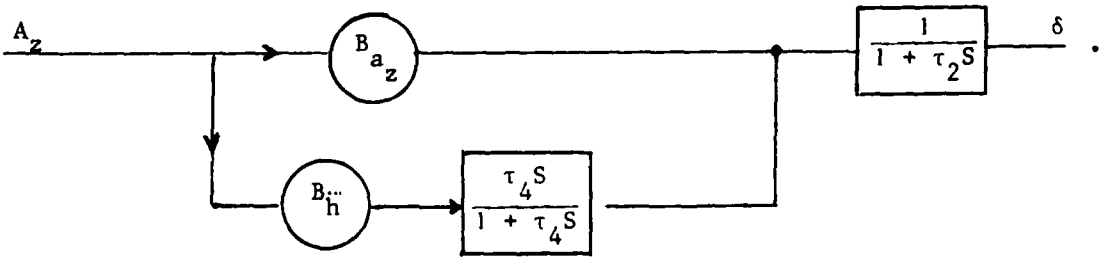

This is equivalent to filtering the normal acceleration signal, *ie*

$$\delta = B_{a_z}\left[1 + \frac{B_{a_z} + B_{\dddot{h}}}{B_{a_z}}\tau_4 S\right] \Big/ (1 + \tau_4 S)(1 + \tau_2 S) \tag{12}$$

where τ_4 is a wash-out time constant, and τ_2 represents the actuator lag. Equation (12) may be written in the form

$$\delta = B_{a_z}(1 + \tau_3 S)/(1 + \tau_4 S)(1 + \tau_2 S) \quad . \tag{13}$$

In order to give a direct comparison with the normal-acceleration feedback only case (Fig 10) variances for the relevant states are given in Fig 21 for fixed values of $\tau_3 = 0.01$, $\tau_4 = 0.1$, $\tau_2 = 0.05$ and varying B_{a_z}. Comparing the 50% reduction in rms of normal acceleration, for the non-filtered and filtered feedback cases the following rms values of significant parameters were obtained.

σ_{a_z}	0.048	(0.048)	g's/m/s($\hat{\omega}_g$)
$\sigma_{\dddot{h}}$	8.3	(7.0)	m/s^3/m/s($\hat{\omega}_g$)
$\sigma_{\dot{\delta}}$	16.0	(10.7)	deg/s/m/s($\hat{\omega}_g$) .

Thus, although N_0 has only been reduced from 5.62 to 4.74, the DLC motivator rate rms has decreased from 16.0 deg/s per unit rms gust to 10.7. Since B_{a_z}, $B_{\dddot{h}}$, τ_4 (wash-out time constant) and τ_2 (actuator time constant) were all considered important parameters, a series of optimisations were carried out with the following cost function:-

$$k_1\sigma^2_{a_z} + k_2\sigma^2_{\dddot{h}} + k_3\left(\sigma^2_{\dot{\delta}} - \sigma^2_{\dot{\delta}_C}\right) \tag{14}$$

where $\sigma_{\dot{\delta}_C}$ is a constraint on the rms of motivator rate, k_3 being operative only if the variance of actuator rate exceeded the constraint value and is otherwise zero. k_1 was fixed at 1.0, and k_2 varied through 0.01, 0.02, 0.03 for three optimisations.

Table 7 gives the results of the optimisations with the values for the case of normal-acceleration feedback only given as a comparison, *ie* for a comparable reduction in rms of normal acceleration. From the table it can be seen that for the 42% reduction in rms normal acceleration (0.055), the addition of a phase-advance network reduces N_0 from 4.07 to 3.27 and rms surface rate from 12.3 deg/s to 6.86 deg/s. The rms of surface position has, however, increased to 1.33 deg/m/s rms gust input. Nevertheless, for even heavy

turbulence (3 m/s rms) the surface movement would still be less than 12^{o} for 95% of the time. The interesting point about the optimisations is that the gain $B_{\ddot{h}}$ in the wash-out loop always turned out to be opposite in sign to B_{a_z}. This indicates that in fact a composite lag/lead filter and not a lead/lag is the desired filter for this particular cost function and system.

Optimisation 1 reduces to a filter equivalent to $-27.4\ (1+0.16S)/(1+0.25S)$ and an actuator time constant of 0.273 second, thus recommending a fairly sluggish actuator. This result may be seen in Fig 17 where the same attenuation in normal acceleration is achieved either with a low gain, fast actuator or a high gain, slow actuator. However, a fast actuator is still desirable since a 'slow' actuator would have relatively low rate limits which would constrain the degree of reduction in normal acceleration (Fig 16). Thus the optimum would appear to be a fast actuator system, but with suitable lags in the feedback loop.

As a further illustration of this phenomenon, Figs 22 and 23 show conflict curves of var(a_z) against var($\ddot{h}$) and var(a_z) against var($\dot{\delta}$). The dotted line shows the performance for normal-acceleration feedback only; the other curves are for various wash-out time constants and varying the $B_{\ddot{h}}$ gain (fixed actuator time constant of 0.04 second). Thus all the points to the left of the dashed line and below the 30% reduction in rms a_z line show an improvement compared with the system with pure normal acceleration feedback.

As stated above, the studies indicate the desirability of using a fast acting actuator, but with fairly large lags in the loop, and with high gains. However, with a more realistic simulation of an actuation system (Fig 6b), stability problems arise with large gains (see Fig 6b).

Since the filtered normal-acceleration signal appeared to give beneficial effects for the simple actuator system, it was considered worth assessing with a more realistic actuator model, *ie*

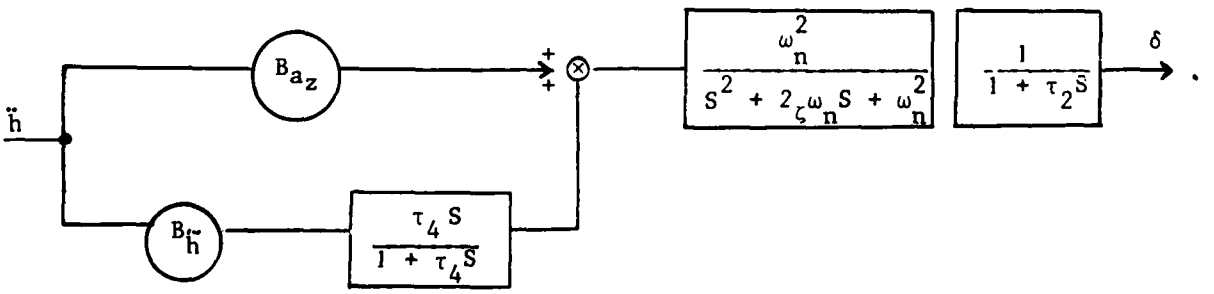

As a baseline for comparison, Fig 24 shows a root locus for B_{a_z} ($B_{\dddot{h}} = 0.0$), and varying actuator natural frequency ω_n ($\tau_2 = 0.05$). Table 8 gives the variances for the particular set of parameters: $\omega_n = 120$, $\zeta = 0.7$, $\tau_2 = 0.05$, $B_{a_z} = -12.0$, $B_{\dddot{h}} = 0.0$, $G_q = 0.464$. With these parameter values, it can be seen that $\sigma_{a_z} = 0.056$, which is a 40% reduction in rms normal acceleration. In order to see what improvement could be achieved for the same attenuation in normal acceleration response and constant values for the DLC actuation parameters, a search on three parameters (B_{a_z}, $B_{\dddot{h}}$ and τ_4) was performed, minimising N_0 with a constraint of 0.056 g on σ_{a_z} and 14.36 deg/s on $\sigma_{\dot{\delta}}$. Table 8 gives the final values of the optimised parameters ($B_{a_z} = -20.5$, $B_{\dddot{h}} = 12.8$, $\tau_{\omega_0} = 2.77$) together with appropriate rms values. As seen in this table, addition of such filtering enables the system to be tuned so that for identical rms normal acceleration there are reductions in N_0 and $\sigma_{\dot{\delta}}$. Unfortunately, however, the root locus of the above system shows that a very small real root of the system is quite sensitive to $B_{\dddot{h}}$. This root can become positive, although it is not significant enough to show up in the time responses. Although this root can easily be stabilised by the addition of an attitude feedback to the elevator, this has the effect of somewhat reducing the damping of the 'pitch rate' mode, so a slight re-adjustment of the pitch-rate feedback is necessary. To illustrate this, a further optimisation of the five parameters G_q, G_θ, B_{a_z}, $B_{\dddot{h}}$, τ_4, again restraining the reduction in rms normal acceleration to 40%, gives the following results:

$G_q = 0.4$, $G_\theta = 0.53$, $B_{a_z} = -20$, $B_{\dddot{h}} = 13.6$, $\tau_4 = 3.2$,

with rms values as shown in Table 8. All real eigenvalues are now well removed from the axis (*ie* no stability sensitivity problem).

A similar argument for the minimisation of N_0 can be applied to the incidence feedback system. Fig 25 shows the effect on the state and control rms values of the incidence system with the addition of a feedback employing rate of change of incidence:

$$\delta = \frac{1}{(1 + \tau_2 S)} \left[- B_\alpha \alpha - B_{\dot{\alpha}} \dot{\alpha} \right] . \qquad (15)$$

It can be seen from Fig 25 that for a constant B_α (in this case $B_\alpha = 10$), increasing the magnitude of $B_{\dot{\alpha}}$ results in a reduction in N_0, $\sigma_{\dot{\delta}}$ and $\sigma_{\dddot{h}}$, together with an increase in σ_{a_z}. From this figure, and Fig 26, which illustrates the variation in performance with respect to a family of discrete

gusts, it can be seen that by including some rate of change of angle of attack in the DLC loop, it is possible to minimise any increase in N_0 and $\sigma_{\dot{\zeta}}$ for some given decrease in rms normal acceleration with respect to that of the basic aircraft. However, since these rate signals are obtained by differentiating or phase advancing a sensor signal, there is a potential problem with respect to sensor noise which could invalidate this particular solution.

9.2 Nonlinear control using dead-space

In this section the effect of a dead-space in the normal-acceleration feedback loop is considered. Since the number of zero level crossings of normal acceleration may well be a criterion in determining ride comfort, it was thought that attenuating only those 'g' responses greater than a particular value would improve the 'ride' in this respect. The discrete gust method[3-5] (Appendix C), was used to assess the different nonlinear control systems. Fig 15 shows the maximum amplitude response of $a_z(\gamma(H))$ plotted against the gust length H for the following linear systems: basic aircraft, basic plus pitch autostabiliser, basic plus pitch autostabiliser and ride control system. It can be seen that $\bar{H}$, the tuned gust length at which maximum response occurs, decreases as the feedback gain B_{a_z} is increased. This is associated with an increase in N_0.

The effects of three values of dead-space ±0.1g, ±0.2g and ±0.3g are shown in Figs 27 and 28, for a fixed value of $B_{a_z} = -12.0$ and actuator lag $\tau_2 = 0.05$ second. Fig 27 shows the rms of normal acceleration plotted as a function of the rms of gust input (σ_{w_g}). For large levels of input the system tends to the linear case from above, but for σ_{w_g} less than 1 m/s, the ride control system has less effect, especially for large dead-space. Fig 28 shows that for the lower levels of input there is a correspondingly marked reduction in motivator activity. Thus for lower levels of turbulence, when the system is unnecessary, there is little flap activity, but for large levels of input the full flap activity (linear) comes into play. There is an associated reduction in N_0 at the lower levels of input. Since the system is nonlinear these rms values have been calculated via integration of a time response.

9.3 Nonlinear control using square law

In the previous section, a nonlinear control law that separated the potentially conflicting constituent elements of the ride qualities criteria into those desirable for low levels of turbulence intensity, and those desirable for the higher levels, was illustrated. This system, however, used a dead zone which could render the results sensitive to steady or slowly varying offsets in the

feedback loop. A simpler alternative is to use a square law filter[22,23] whose output $x_0(t)$ is related to an input $x_i(t)$ through the differential equation:

$$\dot{x}_0(t) = |x_i(t) - x_0(t)|(x_i(t) - x_0(t))\tau_f \quad .$$

The overall system is illustrated in Fig 29. The system's response characteristics (measured in rms quantities in response to a 150 second BLWN input) for a range of turbulence intensities are shown in Fig 30a&b, together with characteristics of a comparable linear system. In addition Figs 31 and 32 illustrate variation in discrete gust response parameters with turbulence intensity. As seen, for low levels of turbulence intensity, the aircraft response is identical to that of an elevator only system, with virtually no DLC activity. As the intensity increases, more weighting is placed on the normal acceleration response magnitude. It has been shown in earlier sections for linear ride smoothing systems that, for a given level of turbulence, as σ_{a_z} is decreased both $\sigma_{\dot{\delta}}$ and $\sigma_{\dot{h}}$ tend to increase, giving consequently an increase in N_0 . For the nonlinear system described above, the tuned gust length $\bar{H}$ will tend towards that of the basic aircraft for small levels of turbulence input and towards the linear control case for large levels of input. Thus the 'cobblestone' ride effect would not become so apparent at the lower levels of turbulence.

Typical time responses of gust input, normal acceleration and motivator rate are shown in Figs 36, 37 and 38. These show a comparison between the linear and nonlinear ride control systems for an identical turbulence input. As can be seen, the motivator rate has been reduced without much adverse effect on the normal acceleration. This type of system also has the advantage of attenuating the effects of sensor noise.

10 'OPEN'-LOOP RIDE CONTROL SYSTEMS

The principle of an open-loop ride-smoothing system is to generate some estimate of the vertical component of turbulence, and to move the DLC as a function of that estimated signal. Through this approach, the handling characteristics are unchanged, unlike those of the closed-loop systems described previously (although any handling deficiencies associated with such closed-loop systems can be removed through appropriate filtering of the pilot stick input).

However, practical difficulties arise in the implementation of open-loop systems as adequate gust sensors are difficult to mechanise. Wind vanes or

incidence probes measure not only turbulence but also components of the aircraft motion, and it is necessary to correct the vane output with aircraft state outputs. Furthermore, the integrity of the incidence vane type of sensor is in doubt, particularly under, say, icing conditions.

An estimate of the gust (w_{g_e}) can be written in terms of three sensor outputs[10], for a given speed, as

$$w_{g_e} = w_v - \int (qV - \ddot{h})dt \qquad (16)$$

where w_v is the output of the vane (m/s)

q is the output of a pitch rate gyro (rad/s)

$\ddot{h}$ is the output of a vertical accelerometer placed at the CG (m/s^2).

A block schematic of a ride-control system using such open-loop control is shown in Fig 33. A detailed analysis of this system is given in Ref 10 which describes how an open-loop direct-lift system could be integrated into an existing fly-by-wire aircraft.

Analysis shows that the open-loop controller becomes slightly more complex than the closed-loop, and with much the same characteristics. In fact, the theoretical benefits of 'open' loop become lost in the practical implementation. Figs 34 and 35 show 'ride' $\left(\sigma^2_{a_z}\right)$ against jerkiness (section 8) $\left(\sigma^2_{\dddot{h}}\right)$ and 'ride' against surface rate activity ($\sigma^2_{\dot{\delta}}$), for varying actuator lags and loop gain B_{w_g}. There is clearly an optimum value for this gain where the system is equivalent to the closed loop normal acceleration feedback system.

11 DISCUSSION OF HANDLING CHARACTERISTICS

It has been shown that closed-loop direct-lift control systems have an effect approximately equivalent to increasing the wing loading (normal acceleration feedback) or decreasing the lift curve slope (incidence feedback). In both cases the dynamic characteristics of the aircraft are changed (different poles and zeros). The short period pitching and normal acceleration response to both turbulence and pilot's stick input are changed. In the absence of additional pilot-command stick shaping, the aircraft having a reduced sensitivity to gusts has consequently a more sluggish normal acceleration response to stick input.

045

However, if the stick is connected to both the elevator and DLC motivator, then by the use of stick command shaping filters practically any desired transient

response in pitch, pitch rate, incidence and normal acceleration can be achieved. The effect of such command stick shaping is that the zeros of the transfer function of the stick to aircraft state output are changed, but not the poles.

The theory and design of such systems are discussed in other papers[20,21]. It is suggested that, although DLC can be used to improve the ride of an aircraft, the benefits due to improved handling could well be even more important, *eg* for air-to-ground aiming, weapon delivery etc. Thus, using DLC motivators, an aircraft designed primarily for good air-to-air performance, (low wing-loading, large lift-curve slope) could both achieve good turbulence performance (ride), at low altitude and have handling characteristics optimised for specific tasks.

12 DISCUSSION OF RESULTS

A comparison has been made between three types of ride control system, normal acceleration feedback, incidence feedback, and the so-called open-loop system. It has been shown that approximately the same reduction in rms of normal acceleration can be achieved with all three systems, a theoretical reduction of at least 30% being the target level. Similar problems arise with all three systems and involve basic stability and actuator characteristics including natural frequency, damping and rate limits, increase in surface rate activity and associated ride-jerkiness. Thus, choice of system would appear to depend on other factors, such as complexity, sensors, reliability, susceptibility to damage etc. On this overall basis it would appear that the use of accelerometers is slightly superior.

It has been shown that N_0, the zero level exceedance rate of normal acceleration, increases with feedback control, giving the so-called cobblestone ride. However, there is some evidence (from a survey of Service pilots) that pilots prefer a 'hard' ride to a softer response with fluctuation of larger amplitude. This survey also indicated that the ratio of $\frac{W}{S}\Big/\frac{\partial C_L}{\partial \alpha}$ is not the sole criterion for assessing ride quality and that aircraft handling characteristics and trimmability are also taken into account. Recent studies indicate in particular that 'clean' response of the control system and good stick characteristics, such as stick force per g, also play a part in the pilot's overall assessment of ride quality. The essential criterion is whether or not the pilot and crew can satisfactorily perform a task in turbulence.

The paper also indicates that a good pitch autostabiliser is always beneficial and in some cases can reduce the rms of normal acceleration by up to 20%. The effect of height variations on the frequency content and amplitude of the turbulence is also relevant to the design.

Most ride systems designed in the past, have used existing aerodynamic surfaces to generate the direct lift. Clearly, this is unsatisfactory, since they were not designed for this specific purpose, and more research is required with the objective of providing more effective direct-lift devices preferably with little or no pitching moment.

The effect of ride-control systems on the handling characteristics is also very important and is the subject of another paper. Suffice to say here, that advantage can be taken of the extra motivator to achieve any desired responses to pilot's stick in both pitch and heave.

One major limitation of the study presented in this paper has been the omission of consideration of the structural loading changes and possible instabilities due to coupling between the control system and the flexible aircraft structure. There is thus a need for continuing research into such effects.

The use of approximate mathematical models in the design process has proved very useful, particularly in the physical understanding of the different control systems. However, there are dangers in using simplified models, especially with respect to high feedback gains and general stability, as there may exist limitations not necessarily indicated by the simplified model. Also, the practical limitations of the actuation system should be included in the final assessment.

The optimisation of a ride-smoothing system using discrete-gust theory (Appendix C), *ie* minimising the maximum response to the worst gust, gave similar system parameters as optimisation using the more usual power-spectral methods (Appendix B). Although the discrete-gust method is rather lengthy and unwieldy, the present study indicated that the technique can be used for designing nonlinear control systems and in fact the theory is currently being extended for this purpose.

In order to give some time responses of state parameters the analogue model of the aircraft plus control system was excited by a record of actual turbulence, the results of which, for pitch rate and normal acceleration, are shown in Figs 36-38 for the uncontrolled and controlled aircraft (normal acceleration feedback). The two normal acceleration responses were subsequently used to drive a motion/vibration simulator for pilot assessment. This latter experiment in the human factors area is continuing.

13 FINAL COMMENTS

It has been shown that reasonable reductions in rms normal acceleration (≥30%) are potentially achievable using a properly designed ride-smoothing system with direct-lift control (DLC). The recommended system uses accelerometers to measure normal acceleration as the input signal to the DLC loop. This results in a system with comparatively fast motivator surface rates but relatively small displacements. Consequently, there is a need for fast (high natural frequency) actuators with wide rate limits. Although theory suggests that the same reduction in rms of normal acceleration can be achieved with either low loop gains and fast actuators or high loop gains and slow actuators, stability problems can occur with the higher loop gain systems. Consequently, a compromise has to be reached between stability, reduction in rms of normal acceleration and surface rate activity. The optimum system appears, paradoxically, to require fast actuators but with some lag inserted into the feedback loop.

A consequence of controlling the normal acceleration through the use of DLC is that the rms rate-of-change of normal acceleration increases. This leads to an associated increase in the 'zero crossing' parameter N_0 (which reflects the overall rate of sign reversal in the 'g' fluctuations). This 'jerkiness' or increase in N_0 could well have a significant effect on the quality of the ride, and although there is some evidence that pilots prefer this 'hard' or 'cobble-stone' ride, further human factors work is required to fully evaluate the implications. This paper suggests that N_0 can be constrained by appropriate design of the control system. In particular, work has indicated that nonlinear control systems have promising potential for this purpose.

Pilot surveys have indicated that ride quality associated with the basic airframe is not merely a function of the parameter $\frac{W}{S}/C_{L_\alpha}$, and that handling qualities, including the ability to control the aircraft response in pitch, are equally important.

The potential benefits of DLC are twofold: improvement of the ride and also, using the extra motivator, improvement of the handling qualities, particularly for target acquisition and tracking. Proposed future work includes the assessment of control systems employing aerodynamic surfaces (and/or deflected thrust) designed with this joint objective in mind.

Appendix A

EQUATIONS OF MOTION

$$D\hat{u} = -X'_u\hat{u} - X'_w\hat{w} - k\theta$$

$$D\hat{w} = q - Z'_u\hat{u} - Z'_w\hat{w} - Z'_\eta\eta - Z'_\delta\delta$$

$$Dq = -M'_u\hat{u} - M'_w\hat{w} - M'_{\dot{w}}Dw - M'_q q - M'_\eta\eta - M'_\delta\delta$$

$$D\theta = q$$

$$D^2\hat{h} = q - \dot{\hat{w}}$$

where $X'_u = -x_u/\hat{t}$

$X'_w = -x_w/\hat{t}$

$k = C_L/2\hat{t}$

$Z'_u = -z_u/\hat{t}$

$Z'_w = -z_w/\hat{t}$

$Z'_\eta = -z_\eta/\hat{t}$

$Z'_\delta = -z_\delta/\hat{t}$

$M'_u = -\mu_1 m_u/i_B\hat{t}^2$

$M'_w = -\mu_1 m_w/i_B\hat{t}^2$

$M'_{\dot{w}} = -\mu_1 m_{\dot{w}}/i_B\hat{t}$

$M'_q = -mq/i_B\hat{t}$

$M'_\eta = -\mu_1 m_\eta/i_B\hat{t}^2$

$M'_\delta = -\mu_1 m_\delta/i_B\hat{t}^2$

$\hat{t} = m/\rho SV$

$$\eta = \left(\frac{1}{1+\tau_1 S}\right)(G_q q + G_\theta\theta)$$

$$\delta = \left(\frac{1}{1+\tau_2 S}\right)(B_{a_z} a_z + B_\alpha\alpha \ldots.)$$

where $D = d/dt$

$\hat{w} = w/V$

$\hat{h} = h/V$.

Appendix B

SPECTRAL TURBULENCE MODELS

B.1 Band limited white noise (BLWN)

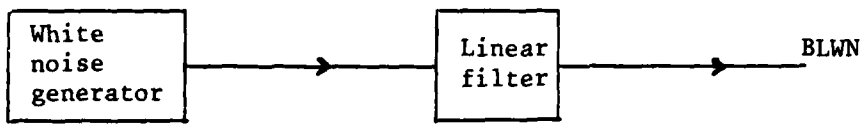

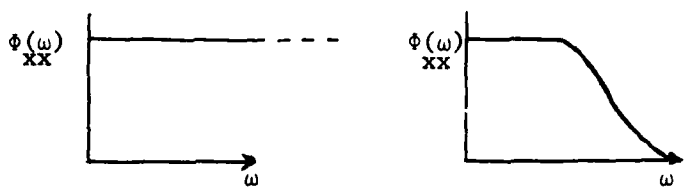

ie BLWN can be obtained by passing white noise through a linear filter, or if variances of the output signal are required:-

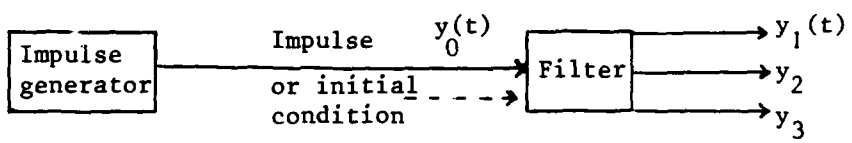

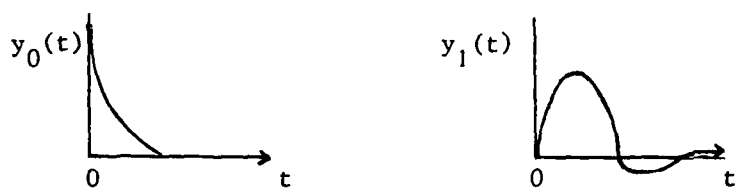

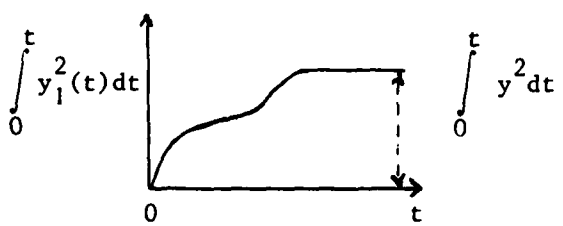

ie variances of state outputs can be obtained by using an impulse or putting an initial condition on a linear filter. This can be expressed as a first order differential equation by:-

$$\dot{x} = -\frac{1}{\tau} x \tag{B-1}$$

where τ determines the cut-off frequency of the power spectral function and the initial condition is of magnitude $\sqrt{2/\tau}$ to give unity variance of the input.

B.2 Dryden spectrum

Dryden gives the power spectral function for vertical turbulence as:

$$\Phi_{w_g w_g}(\omega) = \frac{1}{\pi} \sigma_{w_g}^2 \frac{L}{V} \frac{1 + 3\frac{\omega^2 L^2}{V^2}}{\left(1 + \frac{\omega^2 L^2}{V^2}\right)^2} \tag{B-2}$$

where L = gust length
V = aircraft velocity.

By using the inverse Fourier transform equation (B-2) gives:-

$$y_{w_g}(t) = \sigma_{w_g}\sqrt{\frac{L}{V}}\, e^{-Vt/L} \left\{\sqrt{3} + (1 - \sqrt{3})\frac{Vt}{L}\right\} . \tag{B-3}$$

In a similar way to BLWN, $y_{w_g}(t)$ can be expressed as the solution to two differential equations

$$\left.\begin{aligned} \dot{y}_1 &= y_2 \\ \dot{y}_2 &= -\frac{V^2}{L^2} y_1 - 2\frac{V}{L} y_2 \end{aligned}\right\} \tag{B-4}$$

the initial conditions being:-

$$\left.\begin{aligned} y_1(0) &= y_{w_g}(0) = \sigma_{w_g}\sqrt{\frac{3V}{L}} \\ y_2(0) &= \dot{y}_{w_g}(0) = (1 - 2\sqrt{3})\sigma_{w_g}\sqrt{\left(\frac{V}{L}\right)^3} \end{aligned}\right\} \quad \text{(B-5)}$$

These equations can be used as an extension of the system [A] matrix in order to generate the system variances to Dryden type turbulence.

B.3 Von Karman spectrum

The power spectral function for vertical turbulence is given as:-

$$\Phi_{xx}(\omega) = \frac{1}{\pi}\sigma_{w_g}^2 \frac{\left\{1 + \frac{8}{3}\left(1.339\,\frac{\omega L}{V}\right)^2\right\}}{\left\{1 + \left(1.339\,\frac{\omega L}{V}\right)^2\right\}^{11/6}} \quad . \quad \text{(B-6)}$$

Unfortunately this equation is not easily amenable to inverse Fourier transform so cannot be used in a comparable way to both BLWN and Dryden for direct calculation of variances. Comparisons of the three power spectral functions are given in Fig 2.

Appendix C

STATISTICAL DISCRETE GUST RESPONSE ANALYSIS

The following description of a family of discrete ramp gusts, and the definition of aircraft performance in terms of the response to these gusts, are based on Ref 5.

The family of discrete gust is illustrated in Fig 39, and is defined through equations (B-1) and (B-2):

$$w_g = \left\{ \begin{array}{ll} 0 & , \quad h < 0 \\ \frac{W_{g_m}}{2}\left(1 - \cos\frac{\pi h}{H}\right) & , \quad 0 \leqslant h \leqslant H \\ W_{g_m} & , \quad h > H \ , \end{array} \right\} \tag{C-1}$$

$$W_{g_m} = \left\{ \begin{array}{ll} u_0 H^{\frac{1}{3}} & , \quad H \leqslant L_w \\ u_0 L_w^{\frac{1}{3}} & , \quad H \geqslant L_w \end{array} \right\} \tag{C-2}$$

where h is the penetration distance through the gust,

H is the gust length or gradient distance,

u_0 is a gust intensity parameter

and L_w is the turbulence scale length.

For well-damped systems, such as those investigated in the present study, the normal-acceleration response to the above family of ramp gusts is generally such that there is a one-to-one correspondence between significant response peaks and individual gusts[5] (for less well-damped systems, gust patterns involving interacting ramp components need to be considered).

The responses may be assessed in terms of the scaled magnitude

$$\gamma_{a_z}(H,u_0) = \frac{a_z(H,u_0)}{u_0} \tag{C-3}$$

of the amplitude $a_z(H,u_0)$ of the largest peak in the normal-acceleration response to an isolated ramp gust of length H as defined by equation (C-2). In the case of a linear system, $\gamma_{a_z}(H,u_0)$ becomes independent of u_0 and we have

$$\gamma_{a_z}(H) = \gamma_{a_z}(H,u_0) \quad . \tag{C-4}$$

Examples of the functions $\gamma_{a_z}(H)$ for a linear system and $\gamma_{a_z}(H,u_0)$ for a nonlinear system are illustrated in Figs 15 and 31 respectively.

By varying the gust length H it is possible to find a tuning condition corresponding to a peak in the curves $\gamma_{a_z}(H)$ or $\gamma_{a_z}(H,u_0)$. We denote these peak values by

$$\bar{\gamma}_{a_z} = \bar{\gamma}_{a_z}(\bar{H})$$

or

$$\gamma_{a_z}(u_0) = \gamma_{a_z}\{\bar{H}(u_0),u_0\}$$

and the associated tuned gust lengths by $\bar{H}$ or $\bar{H}(u_0)$. In addition, a gust length sensitivity λ, which is a measure of the 'breadth' of the peak in a $\gamma(H)$ curve, may be defined[5]. For most practical applications the variations in λ are relatively insignificant and for the purposes of the present work a nominal value of $\lambda = 0.2$ may be assumed.

The discrete-gust response assessment is then based on the performance measures

$$\bar{\gamma}_{a_z}, \bar{H} \qquad \text{(linear system)}$$

or

$$\gamma_{a_z}(u_0), \bar{H}(u_0) \qquad \text{(nonlinear system).}$$

In statistical terms, the rate of occurrence, per unit distance travelled, of response peaks greater than magnitude y is given by

$$N_y = \frac{\alpha}{\lambda\bar{H}} \exp\left\{-\frac{y}{\beta\bar{\gamma}}\right\} \quad , \tag{C-5}$$

where α and β are turbulence-dependent parameters. In Ref 5 the values

$$\alpha = 0.38$$

$$\beta = \begin{cases} 0.07\bar{\sigma} & \text{(ft/s, units)} \\ 0.10\bar{\sigma} & \text{(m/s units)} \end{cases}$$

proposed for 5 mile patch lengths at low altitude, where $\bar{\sigma}$ is a turbulence reference intensity. Thus α is assumed to be a constant and β is a constant for each turbulence patch but varies from patch to patch in proportion to $\bar{\sigma}$.

In the case of a nonlinear system it is convenient to take u_0 as an independent variable. From equation (C-3) it then follows using the tuning condition that the corresponding value of y is given by

$$y = \frac{u_0 a_z}{u_\beta}(u_0) \quad . \tag{C-6}$$

Also, equation (C-5) may be written in the form

$$N_y = \frac{\alpha}{\gamma \bar{H}(u_0)} \exp\left\{-\frac{u_0}{\beta}\right\} \quad . \tag{C-7}$$

From equations (C-6) and (C-7) we thus obtain a functional relationship between N_y and y with u_0 as a parametric variable.

By letting u_0 tend to zero we obtain a quantity

$$N_0 = \frac{\alpha}{\lambda \bar{H}} \quad . \tag{C-8}$$

Analogous to the 'zero-crossing frequency' N_0 (equation (7) in main text) of the power-spectral method.

Table 1

AERODYNAMIC DATA FOR THE TWO DATUM CASES

	Flight case 1 M = 0.3	Flight case 2 M = 0.9
V	103.1 m/s	307.7 m/s
X'_u	0.055	0.040
X'_w	0.143	0.002
k	0.104	0.032
X'_δ	0.0	0.0
Z'_u	0.208	0.045
Z'_w	0.674	1.696
Z'_Q	0.012	0.002
Z'_η	0.137	0.246
Z'_δ	0.02	0.082
M'_u	0.0	0.281
M'_w	1.882	21.066
$M'_{\dot{w}}$	0.141	0.670
M'_q	0.539	1.27
M'_η	6.381	42.134
M'_δ	0.50	3.652

Mass	10000 kg
Wing area	24.06 m^2
Span	8.49 m
W/S	4078 N m^{-2}

Table 2a

A TYPICAL PARAMETER OPTIMISATION OUTPUT
INITIAL PARAMETER ARRAY

Optimise G_q, G_θ, B_α

Flight case 1

$X'_u = 0.055$, $Z'_w = 0.674$, $M'_w = 1.882$,
$X'_w = 0.143$, $Z'_Q = 0.012$, $M'_{\dot{w}} = 0.141$,
$X_\theta = 0.104$, $Z'_\eta = 0.137$, $M'_q = 0.539$,
$X'_\delta = 0.0$, $Z'_\delta = 0.02$, $M_\eta = 6.381$,
$Z'_u = 0.208$, $M'_u = 0.00$, $M_\delta = 0.50$.

State	Weight	Variance*	Constraint
u	1.0	0.2005	0.0
w	1.0	0.9178	0.0
q	1.0	0.5373	0.0
θ	1.0	0.8829	0.0
η	1.0	0.00	0.0
δ	1.0	0.00	0.0
w_g	1.0	1.00	0.0
$\dot{\theta} - \dot{w}$	10.0	29.3148	0.0

System poles (eigenvalues)

Damping	Frequency	Relative damping	
-0.6846	1.3145	0.4619	} short period
-0.6846	-1.3145	0.4619	
-0.0191	0.1348	0.1403	} phugoid
-0.0191	-0.1348	0.1403	
-20.0	0.0	1.0	elevator actuator
-25.0	0.0	1.0	DLC actuator
-1.0	0.0	1.0	turbulence input

045

* Non-dimensional units.

Table 2b

TYPICAL SEARCH PROCEDURE

	Cost value	Parameters G_q	G_θ	B_α
0	2.420777E 01	2.000000	0.000000	0.000000
0	2.313220E 01	1.000000	1.732051	0.000000
0	2.426833E 01	1.000000	0.577350	1.632993
0	3.285332E 01	0.000000	0.000000	0.000000
SMALLEST COST=		23.132201		
1	2.446655E 01	2.666667	1.539601	1.088662
2	2.397088E 01	2.000000	1.154701	0.816497
SMALLEST COST=		23.132201		
3	2.475312E 01	2.333333	1.347151	-1.088662
4	2.364007E 01	1.333333	0.769800	0.952579
SMALLEST COST=		23.132201		
5	2.398765E 01	0.888889	2.437701	1.179384
6	2.365747E 01	1.166667	1.828276	0.884538
SMALLEST COST=		23.132201		
7	2.269598E 01	0.333333	1.732051	0.408248
8	1.000000E 05	-0.500000	2.020726	0.204124
SMALLEST COST=		22.695985		
9	2.234427E 01	0.611111	0.994325	0.022680
10	2.186945E 01	0.333333	0.577350	-0.408248
SMALLEST COST=		21.869454		
11	1.000000E 05	-0.222222	1.924501	-0.952579
12	2.294269E 01	0.944444	1.058475	0.476290
SMALLEST COST=		21.869454		
13	2.247502E 01	0.074074	0.513200	0.317526
SMALLEST COST=		21.869454		
14	1.000000E 05	-0.450617	0.823259	-0.264605
15	2.238345E 01	0.595679	0.999671	0.291066
SMALLEST COST=		21.869454		
16	1.000000E 05	0.335391	-0.338570	-0.274686
17	2.221826E 01	0.333848	1.214396	0.237515
SMALLEST COST=		21.869454		
18	2.275418E 01	0.767833	1.347745	-0.237305
19	2.177888E 01	0.247514	0.721836	0.178819
SMALLEST COST=		21.778879		
20	2.458962E 01	0.014118	0.676050	-0.285676
21	2.208664E 01	0.450289	0.918766	0.146880
SMALLEST COST=		21.778879		
22	2.220949E 01	0.353576	0.264239	-0.292548
23	2.181530E 01	0.348644	0.501778	-0.160032
SMALLEST COST=		21.778879		
24	2.263796E 01	0.169372	0.281877	-0.406522
25	2.188108E 01	0.380059	0.759544	0.008530
SMALLEST COST=		21.778879		
26	2.188695E 01	0.239601	0.441100	-0.268171
27	2.180596E 01	0.344945	0.679933	-0.060645
SMALLEST COST=		21.778879		
28	2.182776E 01	0.294068	0.691681	0.380343
29	2.177169E 01	0.303885	0.663099	0.183195
SMALLEST COST=		21.771687		
30	2.192830E 01	0.248918	0.874800	0.360944
31	21.815296	21.805961	21.778879	21.771687

Table 2c

FINAL PARAMETER ARRAY

State	Weight	Variance	Constraint
u	1.0	0.0073	0.0
w	1.0	0.3971	0.0
q	1.0	0.1041	0.0
θ	1.0	0.0397	0.0
η	1.0	0.0267	0.0
δ	1.0	0.0149	0.0
w_g	1.0	1.0	0.0
$\dot{\theta} - \dot{w}$	10.0	20.1819	

System poles (optimum)

Damping	Frequency	Relative damping
-25.0004	0.0	1.0
-1.4422	2.2193	0.5449
-1.4422	-2.2193	0.5449
-0.0209	0.0	1.0
-0.4526	0.0	1.0
-18.0491	0.0	1.0
-1.0	0.0	1.0

Optimal parameter values

G_q	G_θ	B_α
0.3034	0.6631	0.1832

Table 3

PITCH-RATE/ELEVATOR SYSTEM EIGENVALUES AND RMS VALUES TO BLWN INPUT

	Basic aircraft		Elevator-pitch-rate only	
	State rms values			
State	200 ft	1000 ft	200 ft	1000 ft
u	0.061	0.135	0.026	0.057
θ	0.145	0.166	0.040	0.058
q	0.532	0.367	0.151	0.097
a_z	0.167	0.095	0.137	0.088
η	0.0	0.0	0.062	0.042
$\dot{\eta}$	0.0	0.0	0.689	0.334
w_g	1.0	1.0	1.0	1.0
	System eigenvalues			
	-1.841 ± 4.46i -0.020 ± 0.0156i -20.0		-10.59 ± 18.02i -2.50 -0.032 -0.0087	

u	m/s			200 ft	1000 ft
θ	deg	% reduction in	σ_{a_z}	17.9	7.4
q	deg/s		σ_q	71.6	73.6
a_z	g				
η	deg				
$\dot{\eta}$	deg/s				
w_{gust}	m/s				

Table 4

SYSTEM EIGENVALUES FOR VARIOUS CASES

(a)

$\tau_1 = 0.05$, $\tau_2 = 0.04$, $G_q = 0.464$					
B_{a_z}	Poles				
0	-25.0	-2.5	-0.032	-10.6 ± 18.0i	-0.0087
-5	-35.9	-2.03	-0.033	-10.5 ± "	-0.0072
-12	-50.8	-1.72	-0.035	" " "	-0.0058
-20	-67.6	-1.53	-0.036	" " "	-0.0047
-50	-130.1	-1.26	-0.038	" " "	-0.0028

(b)

$\tau_1 = 0.05$, $\tau_2 = 0.04$, $G_q = 0.464$					
B_α	Poles				
0	-25.0	-2.50	-0.032	-10.6 ± 18.0i	-0.0087
-5	-25.4	-2.07	-0.02 ± 0.0012i	" "	
-10	-25.9	-1.65	-0.02 ± 0.014i	" "	
-15	-26.3	-1.24	-0.02 ± 0.023i	" "	
-20	-26.7	-0.85	-0.02 ± 0.034i	" "	
-30	-27.4	-0.17	+0.016 ± 0.095i	" "	

(c)

$\tau_1 = 0.05$, $G_q = 0.464$				
z_w	Poles			
1.71	-2.50	-0.032	-0.0087	-10.6 ± 18.0i
1.5	-2.30	-0.029	-0.0120	"
1.0	-1.82	-0.02	±0.0117i	"
0.5	-1.34	-0.02	±0.0220i	"
0.0	-0.86	-0.019	±0.0356i	"
-1.0	-0.11	+0.09	±0.087i	"

(d)

$\omega_n = 50.0$, $\tau_2 = 0.04$, $\tau_1 = 0.05$, $G_q = 0.464$						
B_{a_z}	Poles					
-8	-52.3	-1.85	-0.034	-0.006	-10.5 ± 18.0i	-21.7 ± 39.7i
-12	-59.3	-1.70	-0.035	-0.0058	"	-18.3 ± 42.8i
-20	-68.9	-1.52	-0.035	-0.0047	"	-13.6 ± 47.9i
-50	-88.7	-1.25	-0.038	-0.0028	"	-3.88 ± 60.7i
0	-25.0	-2.50	-0.032	-0.0087	-10.6 ± 18.0i	-35.0 ± 35.7i

Table 5

EIGENVALUES AND RMS VALUES FOR CONTROLLED AND UNCONTROLLED AIRCRAFT

BASIC AIRCRAFT M = 0.9 HEIGHT 1000 FT

Mode	Damping	Frequency	Relative damping	
1	-1.80	4.516	0.37	short period
2	-1.80	-4.516	0.37	
3	-0.022	0.086	0.248	phugoid
4	-0.022	-0.086	0.248	
5	-20.0	0.0	1.0	elevator actuator
6	-25.0	0.0	1.0	DLC actuator
7	-1.0	0.0	1.0	Dryden input
8	-0.997	0.0	1.0	

Rms value* (Dryden input)

State	Basic a/c	Normal acceleration feedback	Incidence feedback
u	0.094	0.0837	0.109
$\dot{h}$	0.356	0.162	0.159
q	2.404	0.772 (68%)	0.774 (68%)
θ	0.935	0.526	0.618
η	0.0	0.342	0.349
δ	0.0	0.122	0.141
$\dot{u}$	0.030	0.016	0.019
$\dot{h}$	1.127	0.254 (78%)	0.412 (64%)
$\dot{q}$	12.827	7.621	7.290
$\dot{\theta}$	2.404	0.772	0.774
$\dot{\eta}$	0.0	2.422	2.348
$\dot{\delta}$	0.0	2.644	1.135
w_g	1.0		

Eigenvalues controlled a/c (Normal acceleration feedback)

Mode	Damping	Frequency	Relative damping
1	-158.21	0.0	1.0
2	-10.468	18.132	0.5
3	-10.468	-18.132	0.5
4	-0.022	0.025	0.66
5	-0.022	-0.025	0.66
6	-1.213	0.0	1.0
7	-1.00	0.0	1.0
8	-0.997	0.0	1.0

* Rms values are in non-dimensional units for comparison only.

Table 6

EFFECT OF WING-LOADING ON RMS NORMAL ACCELERATION AND N_0

Basic aircraft varying wing loading.

(a) 1 second time constant (1000 ft), BLWN

% change with respect to basic aircraft	σ_{a_z} 'g's/1 m/s gust	N_0 s^{-1}
-20%	0.112	1.829
0%	0.094	1.746
+20%	0.082	1.694
+40%	0.072	1.659
+60%	0.065	1.634
+80%	0.059	1.615

(b) 0.2 second time constant (200 ft), BLWN

-20%	0.2	2.78
0%	0.167	2.633
+20%	0.144	2.539
+40%	0.126	2.467
+60%	0.113	2.415
+80%	0.102	2.374

Table 7

EFFECT OF VARIOUS OPTIMISATIONS ON SYSTEM RMS VALUES

	Parameters					Rms values to 1m/s gust					
						deg/s	g s	m/s^{-3}	deg	deg/s	
	G_q	B_{a_z}	$B_{\dddot{h}}$	τ_4	τ_2	$\dot{\delta}_c$	a_z	$\dddot{h}$	δ	$\dot{\delta}$	N_0
Basic aircraft	0	0	0	0	0.05	14.36	0.095	5.11	-	-	1.75
+ pitch autostab	0.464	0	0	0	0.05	14.36	0.088	3.71	-	-	1.37
+ pitch autostab + RCS	0.464	-11.0	0	0	0.05	14.36	0.055	6.93	0.99	12.32	4.07
Optimisation 1	0.464	-27.4	10.1	0.25	0.233	14.36	0.055	5.57	1.33	6.86	3.27
Optimisation 2	0.464	-18.51	9.26	0.505	0.228	14.36	0.065	4.81	0.98	4.26	2.40
Optimisation 3	0.464	-15.1	8.97	0.943	0.227	14.36	0.071	4.45	0.74	2.94	2.03

Cost function

Optimisation 1; $\sigma^2_{a_z} + k_2\sigma^2_{\dddot{h}} + k_3\left(\sigma^2_{\dot{\delta}} - \sigma^2_{\dot{\delta}_c}\right)$; $k_2 = 0.01$

Optimisation 2; $k_2 = 0.02$

Optimisation 3; $k_2 = 0.03$

045

Table 8

EFFECT OF FILTERING THE FEEDBACK ON SYSTEM RMS VALUES

	Parameters								Rms values						
	G_q	G_θ	B_{a_z}	$B_{\dddot{h}}$	τ_4	τ_2	ω_n	ζ	a_z	$\dddot{h}$	δ	$\dot{\delta}$	q	$\dot{h}$	N_0
Case 1	0.464	0	-12.0	0	0	0.05	120.0	0.7	0.056	6.8	1.04	11.57	0.11	0.365	3.93
Case 2	0.464	0	-20.5	12.8	2.77	0.05	120.0	0.7	0.056	6.0	1.17	8.66	0.11	0.305	3.49
Case 3	0.40	0.53	-20.0	13.6	3.2	0.05	120.0	0.7	0.056	5.77	1.12	7.77	0.11	0.466	3.35

Eigenvalues

Case 2	Case 3
-73.98 ± 79.11i	-76.51 ± 80.39i
-38.72	-32.63
-10.53 ± 17.95i	-9.98 ± 16.26i
-5.22	-6.628
-1.366	-0.042
-0.0387	-2.295
+0.016	-0.229

Case 1 Normal acceleration feedback only

Case 2 Filtered normal acceleration feedback

Case 3 Addition of attitude term to elevator control

LIST OF SYMBOLS

a_z	normal acceleration in g s
B_{a_z}	normal acceleration feedback gain (DLC loop)
B_α	incidence feedback gain (DLC loop)
$B_{\dot{\alpha}}$	rate of change of incidence feedback gain (DLC loop)
B_{wg}	incidence feedback gain, open loop system
BLWN	band limited white noise
d	gradient distance of discrete gust
DLC	direct-lift control
G_q, G_θ, G_α, $G_{\dot{\alpha}}$	feedback gains of elevator loop
G_{OL}	'open'-loop cross-feed gain to elevator
H	discrete gust length
$\bar{H}$	'tuned' gust length
$\hat{h} = \theta - \hat{w} = \theta - \alpha$	
$\hat{\dot{h}} = \dot{\theta} - \hat{\dot{w}} = q - \dot{\alpha}$	
k	arbitrary constant
L	gust length (Dryden spectrum)/scale length of discrete gust
M	Mach number
N(x)	$\left(N_0/2\right) e^{-x^2/2\sigma^2}$, exceedance frequency
N_0	zero-level exceedance frequency
q	rate of change of pitch attitude
rms	root-mean square
S	Laplace operator
$\hat{t}$	$m/\rho SV$
V	aircraft velocity (m/s)
W	aircraft weight
w_{g_e}	estimate of gust velocity
w_v	output of wind vane
w/s	wing loading
α	angle of incidence
$\dot{\alpha}$	rate of change of incidence; $d\alpha/dt$
$\gamma(H)$	amplitude of first overshoot of response
$\bar{\gamma}(H)$	'tuned' amplitude
δ	DLC motivator deflection
Φ_{xx}	power spectral density function

LIST OF SYMBOLS (concluded)

σ_i	rms of state 'i'
τ_1	time constant of elevator actuator
τ_2	time constant of DLC motivator actuator
τ_3	time constant of shaping filter
τ_4	time constant of shaping filter
τ	wash-out time constant
θ	pitch attitude
λ	weighting parameter in cost function /discrete gust sensitivity parameter
η	elevator angle
ζ	damping ratio
ω_n	undamped natural frequency

Aerodynamic symbols and derivatives

$\hat{u} = u/V$	forward speed
$\hat{w} = w/V$	vertical speed
q	pitch rate
θ	pitch attitude
$\hat{h} = \theta - \hat{w}$	non-dimensional rate of change of height
η	elevator angle
δ	flap (DLC) angle

$X'_u = -x_u/\hat{t}$; $M'_u = -\mu_1 m_u/i_B\hat{t}^2$

$X'_w = -x_w/\hat{t}$; $M'_w = -\mu_1 m_u/i_B\hat{t}^2$

$k = C_L/\hat{t}$; $M'_{\dot{w}} = -\mu_1 m_{\dot{w}}/i_B\hat{t}$

$Z'_u = -z_u/\hat{t}$; $M'_q = -m_q/i_B\hat{t}$

$Z_w = -z_w/\hat{t}$; $M'_\eta = -\mu_1 m_\eta/i_B\hat{t}^2$

$Z'_\eta = -z_\eta/\hat{t}$; $M'_\delta = -\mu_1 m_\delta/i_B\hat{t}^2$

$Z'_\delta = -z_\delta/\hat{t}$;

$\hat{t} = m/\rho SV$; $\mu_1 = m/\rho S\ell_t$

REFERENCES

No.	Author	Title, etc
1	NASA	1975 Ride Quality Symposium. NASA TM X-3295 (1975)
2	JAC	Flying Qualities Requirements. JAC 925 (1977)
3	J.G. Jones	Influence of atmospheric gusts and turbulence on aircraft flying qualities at low altitude. RAE Technical Memorandum FS 64 and FS 86 (1976)
4	J.G. Jones	Statistical discrete-gust theory for aircraft loads. RAE Technical Report 73167 (1973)
5	J.G. Jones	Aircraft longitudinal ride-bumpiness. An application of statistical discrete gust theory. RAE Technical Memorandum 77020 (1977)
6	D.E. Fry D.G. Ardron	A digital computer program for the parameter optimisation of aircraft control systems. RAE Technical Report 74053 (1974)
7	D.E. Fry D. Slatter	Design of aircraft flight control laws using the matrix Riccati equation. RAE Technical Report 75035 (1975)
8	M.J. Corbin J.S. Winter	A combined analysis package for the design of flight control systems (TSIM). RAE Technical Memorandum FS 185 (1978)
9	D.E. Fry D.G. Ardron	The determination of transfer functions and frequency response from state-space equations. RAE Technical Memorandum Avionics 159 (1973)
10	J.S. Winter	A preliminary design study of a ride control system for the ACT Hunter XE531. RAE Technical Memorandum FS 128 (1977)
11	G.C. Cohen R.L. Schoenman	Use of active control technology to improve ride qualities of large transport aircraft. AGARD Conference Proceedings, No.157 (1975)

REFERENCES (continued)

No.	Author	Title, etc
12	C.R. Stockdale R.D. Poyneer A.F. Barfield	Control configured vehicles ride control system. AFFDL TR-74-66 (1975)
13	J.H. Wykes L.U. Nardi A.S. Mori	XB-70 structural mode control system design and performance analysis. NASA CR 1557 (1970)
14	O.H. Gerlach G.A.J. van der Moesdijk J.C. van der Vaart	Progress in the mathematical modelling of flight in turbulence. AGARD Proceedings No.140 Flight in turbulence (1973)
15	D.E. Fry F.R. Gill	A geometric search procedure with particular application to optimisation of flight control systems. RAE Technical Report 70018 (1970)
16	M.J. Corbin	A comparison of search procedures for the parameter optimisation of flight control systems. RAE Technical Memorandum FS 53 (1975)
17	J.G. Jones D.E. Fry	Aircraft ride-bumpiness and the design of ride-smoothing systems. AGARD Guidance and Control Panel meeting. Dayton, Ohio (1977)
18	J. Taylor	Manual on aircraft loads. AGARDograph 83, Pergamon Press (1965)
19	S.O. Rice	Mathematical analysis of random noise. Bell System Technical Journal, Vol 23 (1944)
20	J.S. Winter	A preliminary study into the use of direct lift control for augmenting handling qualities of combat type aircraft. RAE Technical Report (in preparation)
21	D.E. Fry P. Verey J.S. Winter	A preliminary simulator assessment into the use of direct lift control for augmenting the handling qualities of a combat aircraft. RAE Technical Memorandum FS 205 (1977)

REFERENCES (concluded)

No.	Author	Title, etc
22	J.S. Winter	A non-linear control law for a ride-control system. RAE Technical Memorandum FS 238 (1979)
23	J.S. Winter	A non-linear control law for FBW aircraft and its use in target acquisition and tracking. RAE Technical Memorandum FS 177 (1978)

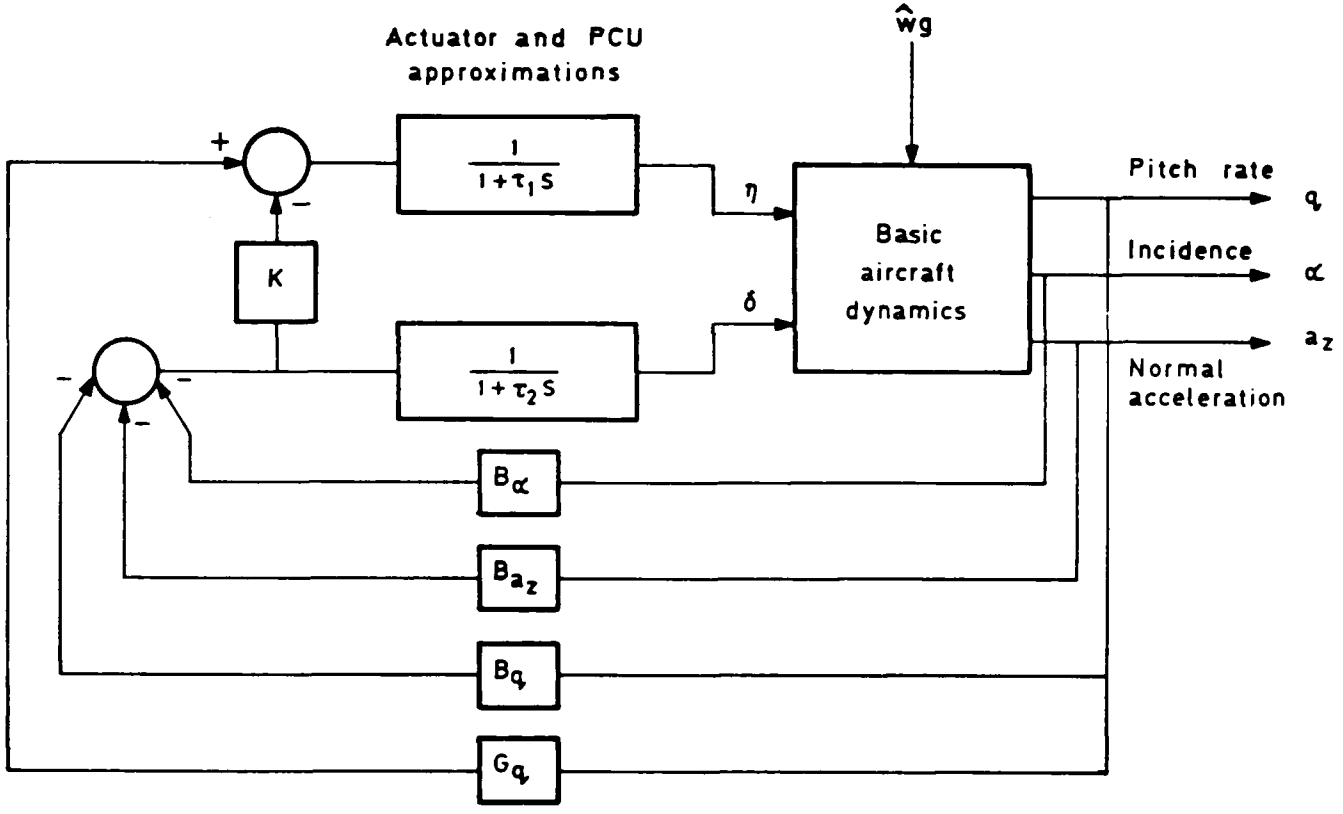

Fig 1 Block schematic of pure state feedback system

Fig 2

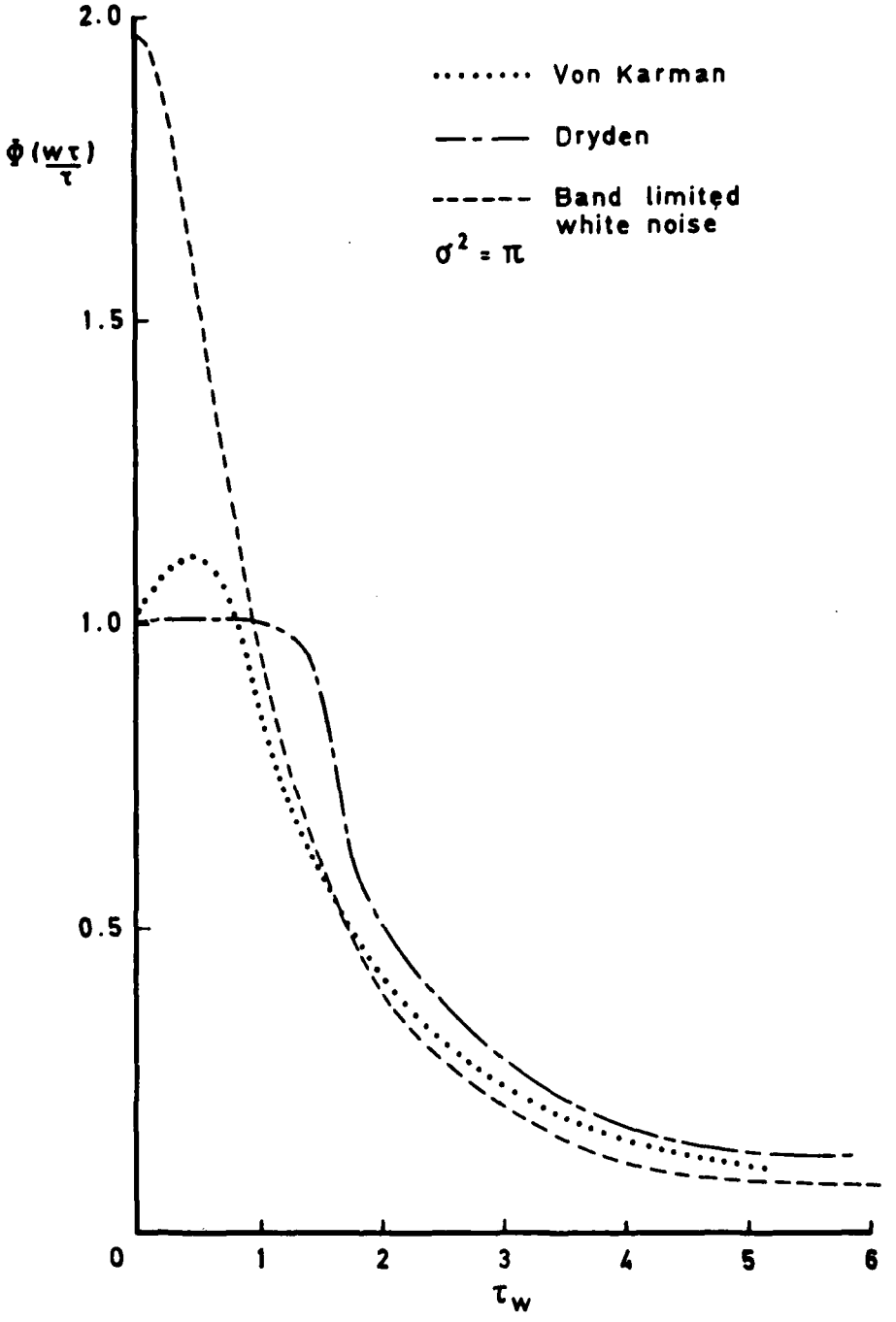

Fig 2 Comparison of power spectral density functions

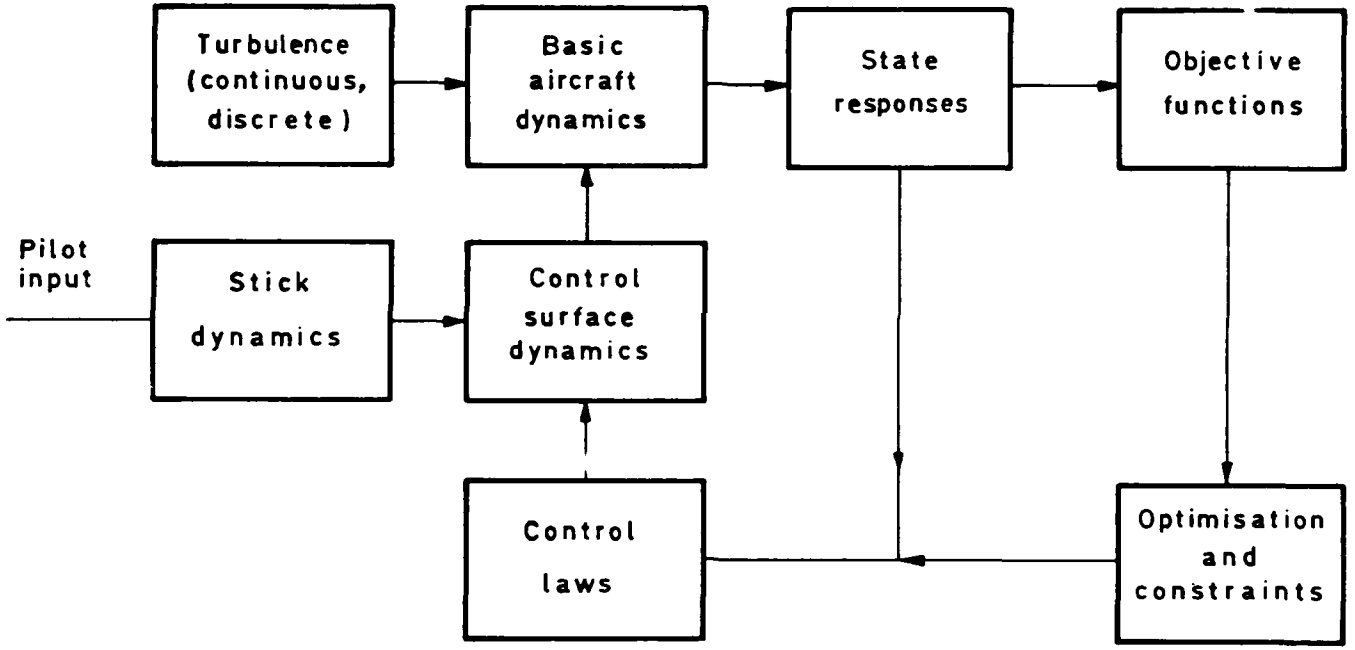

Fig 3 Block schematic of design procedure

Fig 4

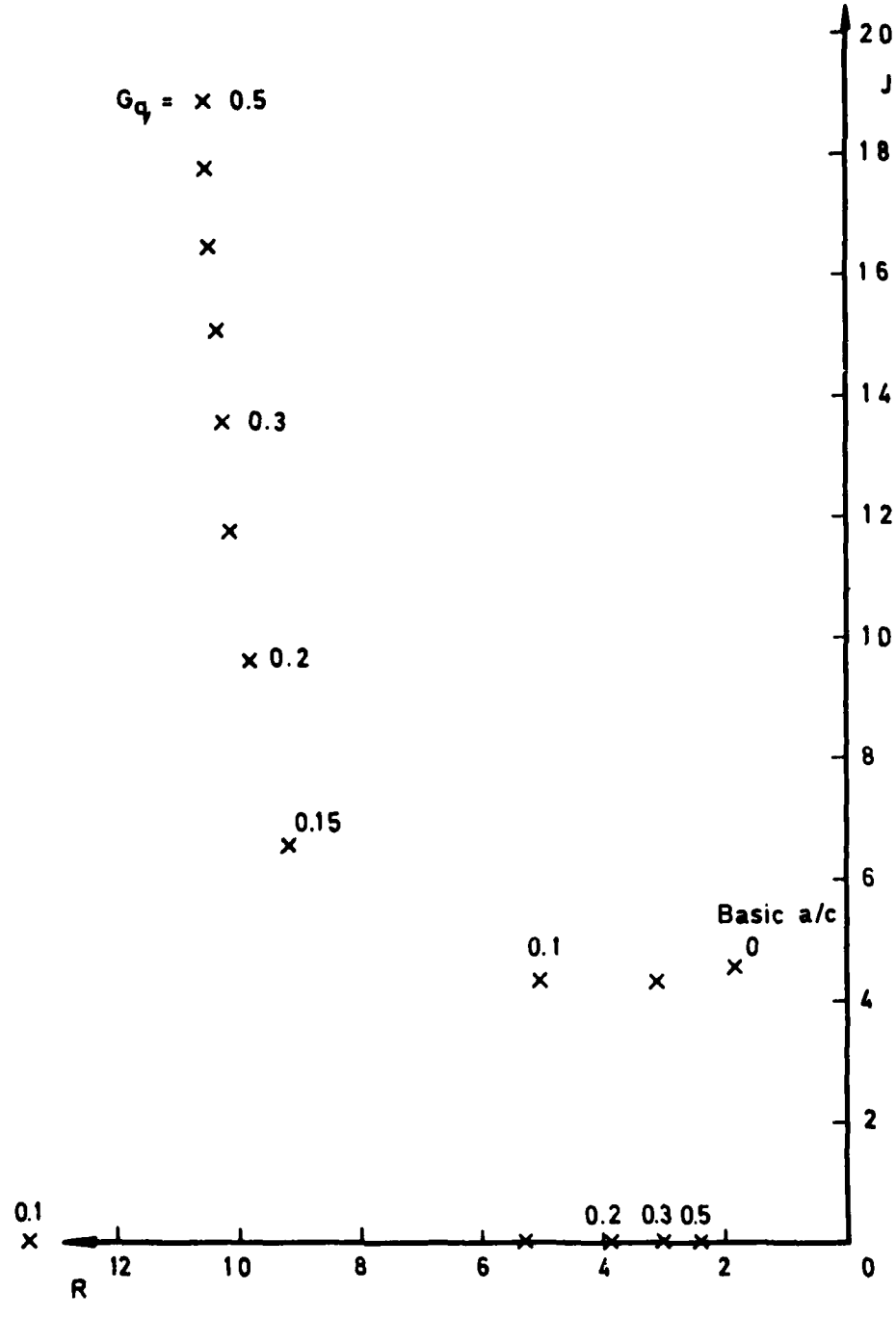

Fig 4 Root locus of elevator loop gain (G_q)

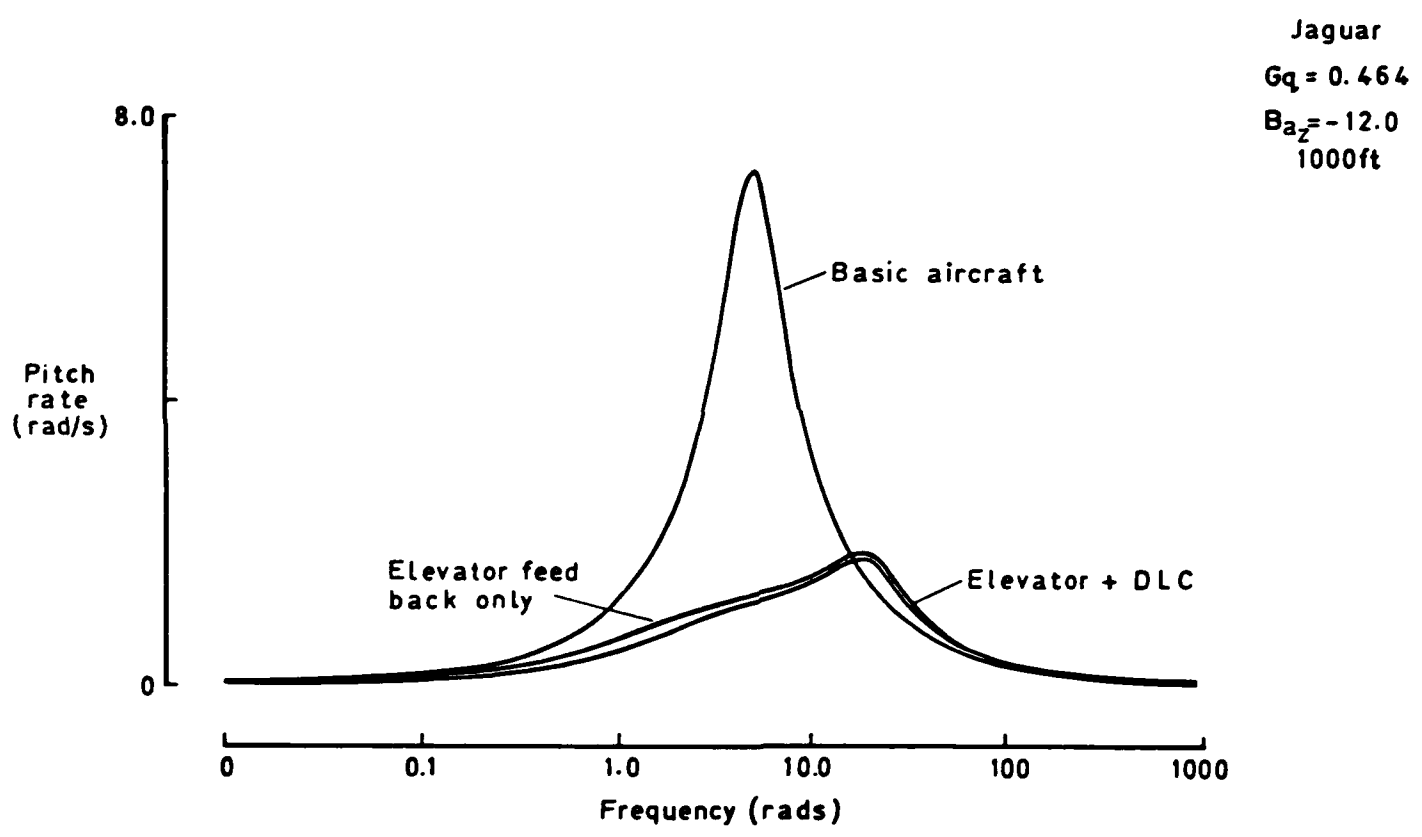

Fig 5a Frequency response of pitch rate to gust input

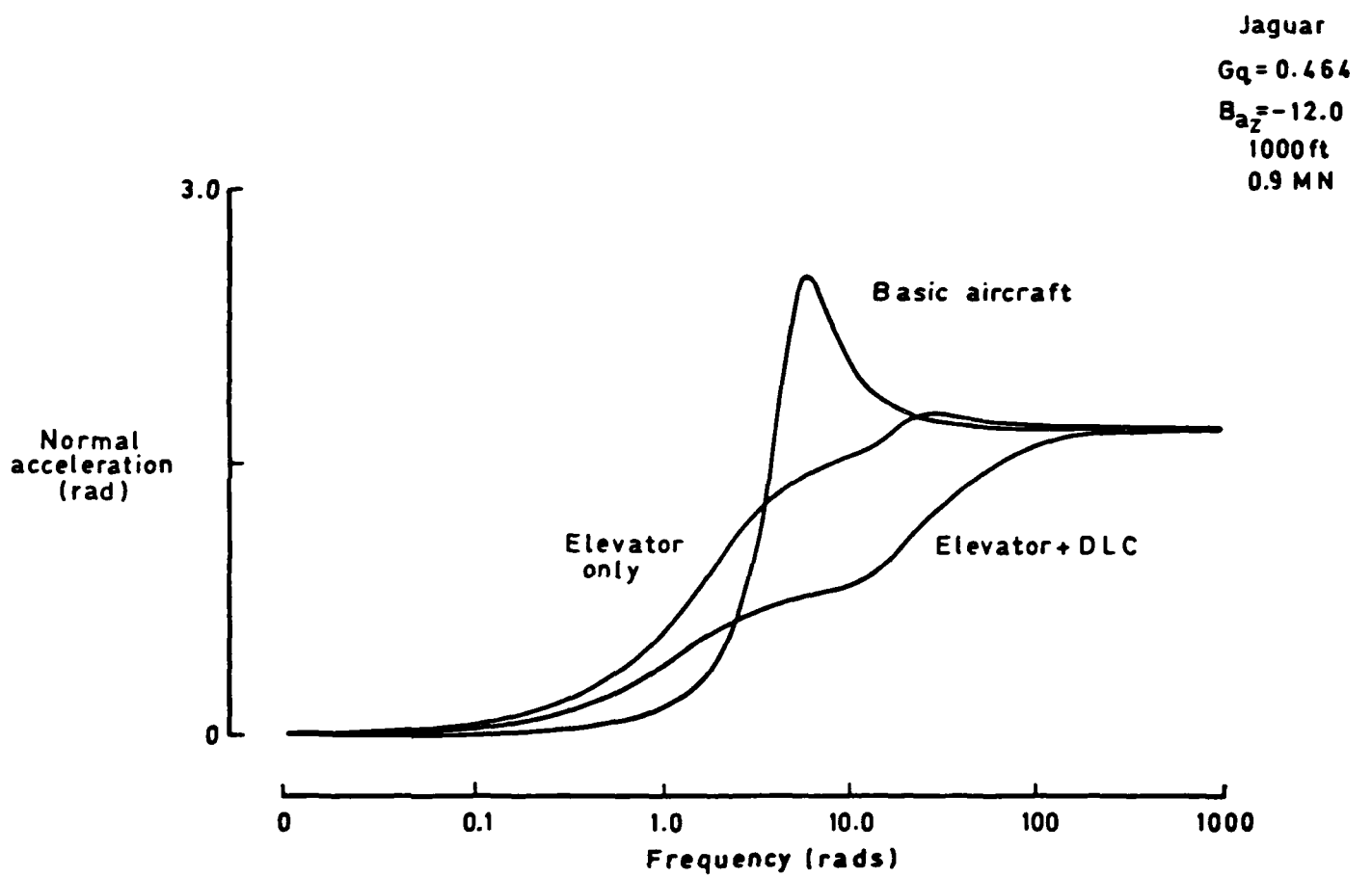

Fig 5b *Frequency response of normal acceleration to gust input*

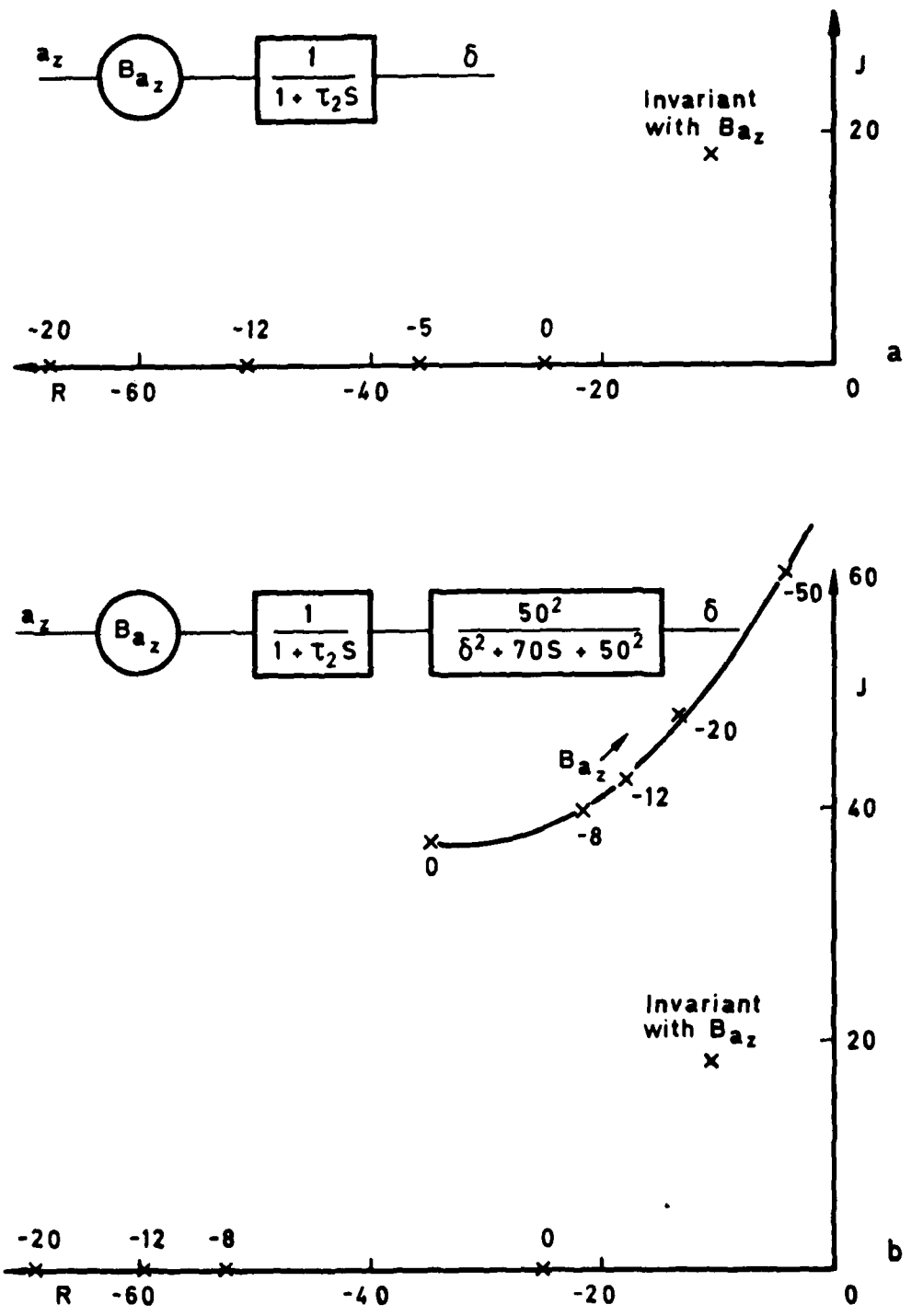

Fig 6 Root locus of B_{a_z}, systems (a) and (b)

Fig 7

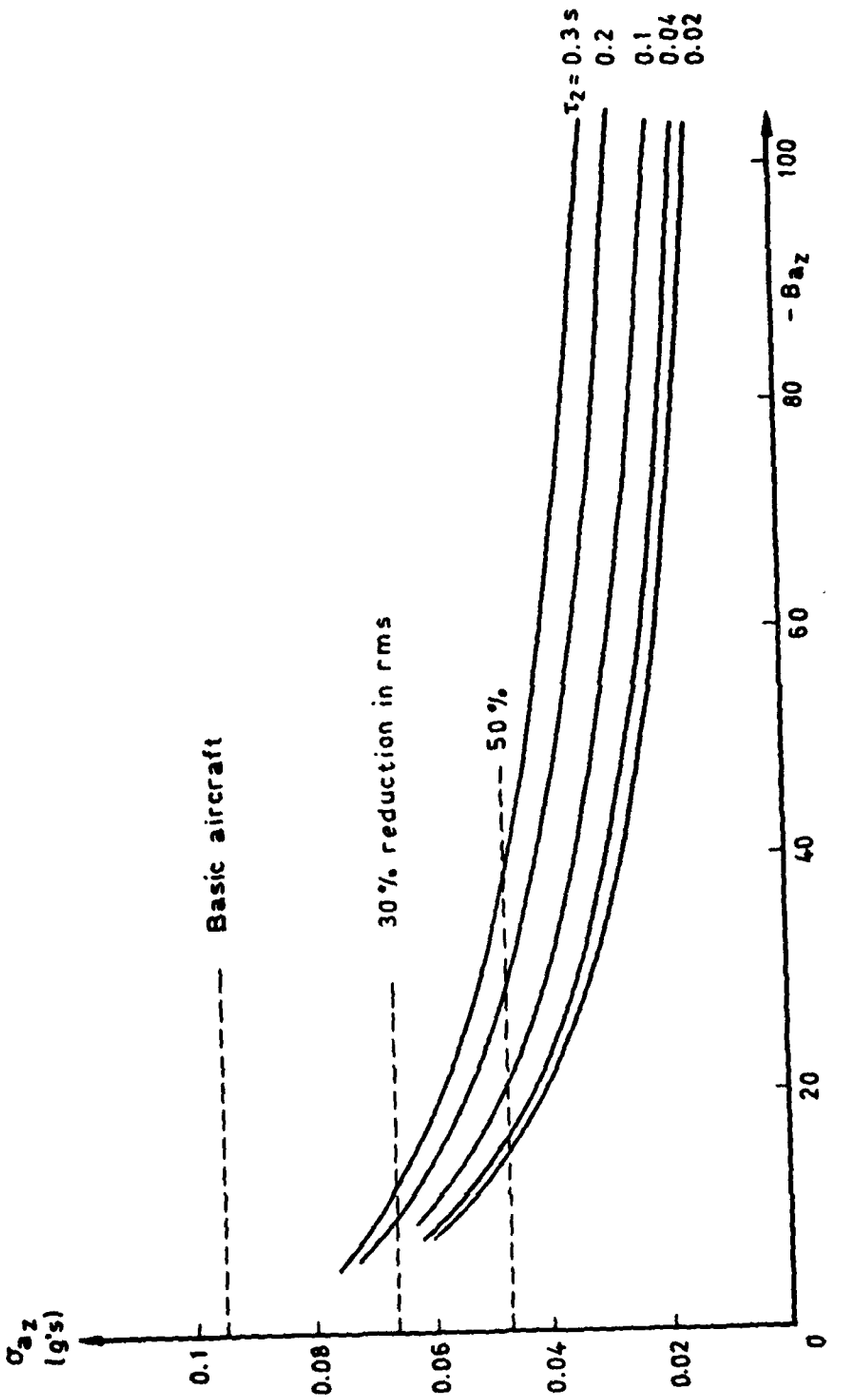

Fig 7 Effect of feedback gain and actuator time constant (τ_2) on rms of a_z

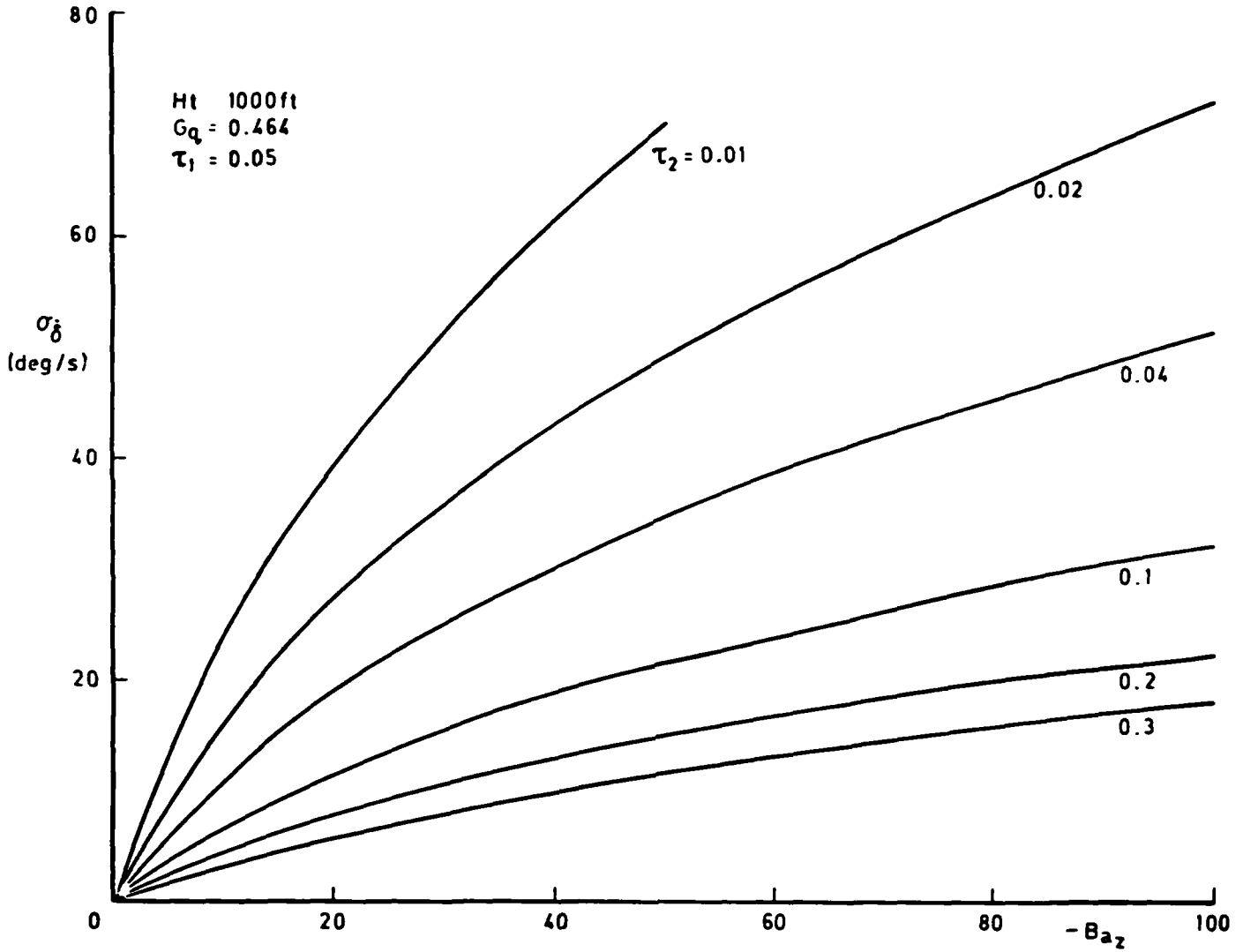

Fig 8 Effect of feedback gain and actuator time constant (τ_2) on rms of DLC motivator rate

Fig 8

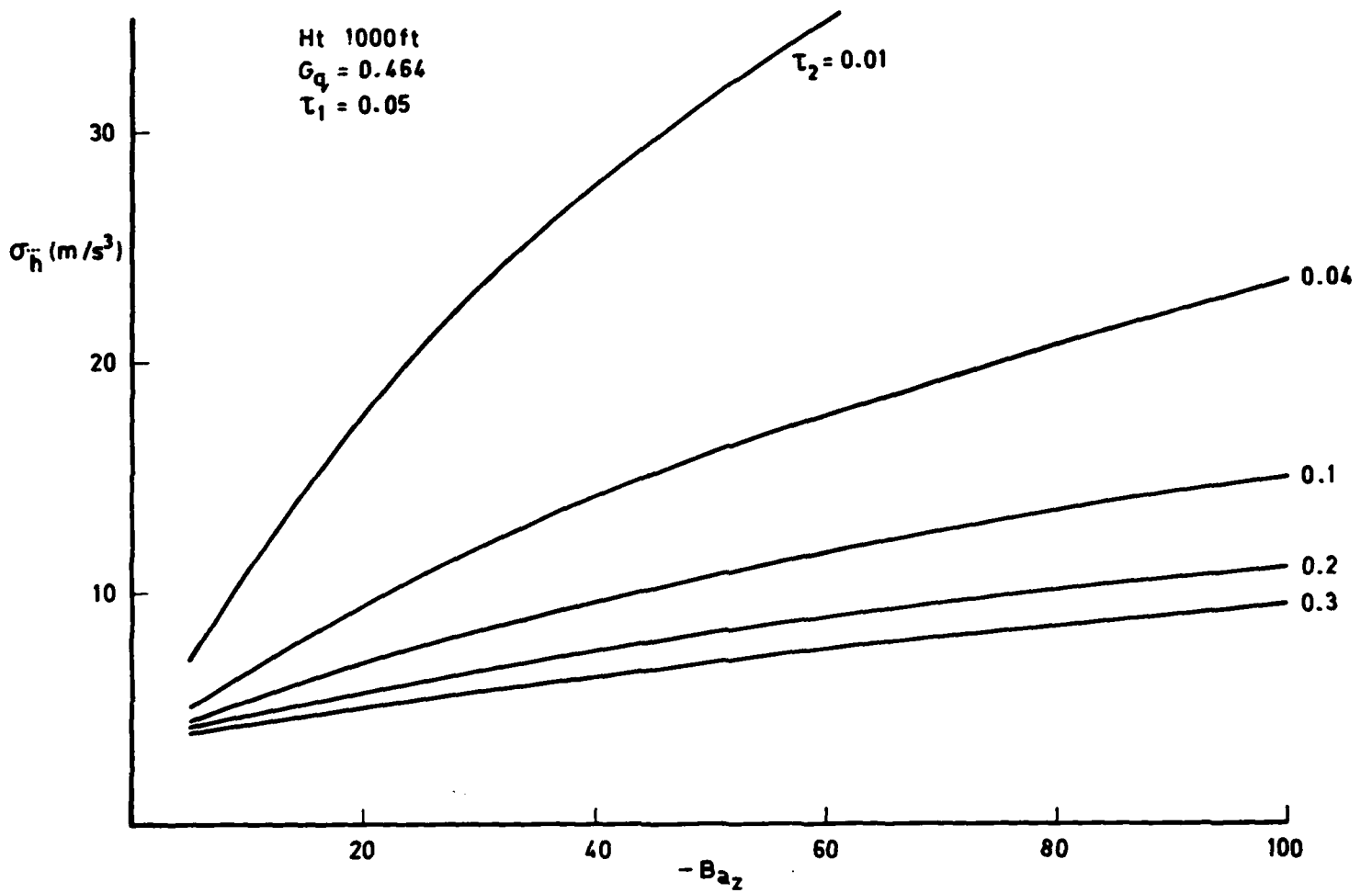

Fig 9 Effect of feedback gain and actuator time constant (τ_2) on rms of rate of change of normal acceleration

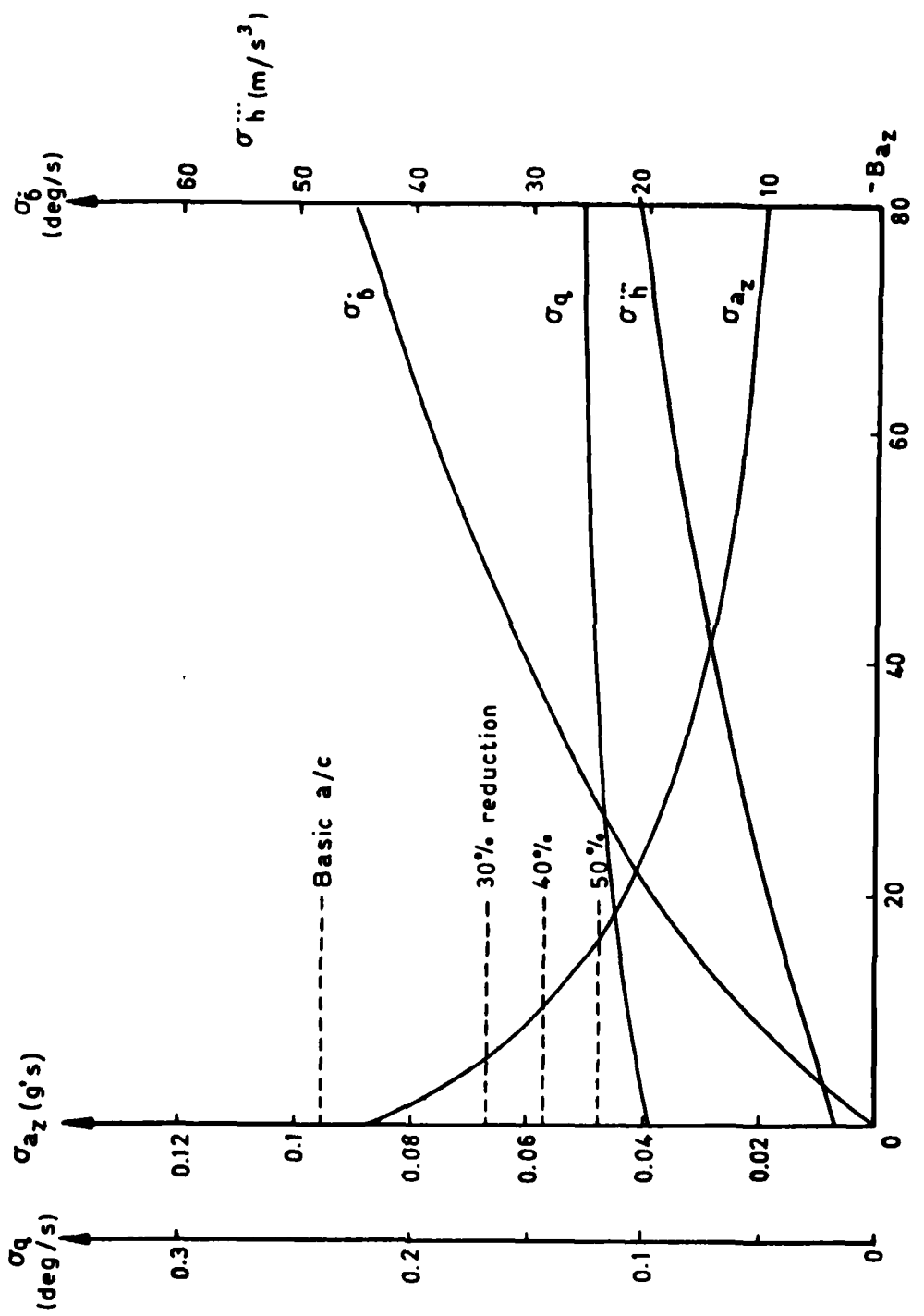

Fig 10 Effect of feedback gain $\left(B_{a_z}\right)$ on rms values. 1000 ft, $\tau_2 = 0.04$

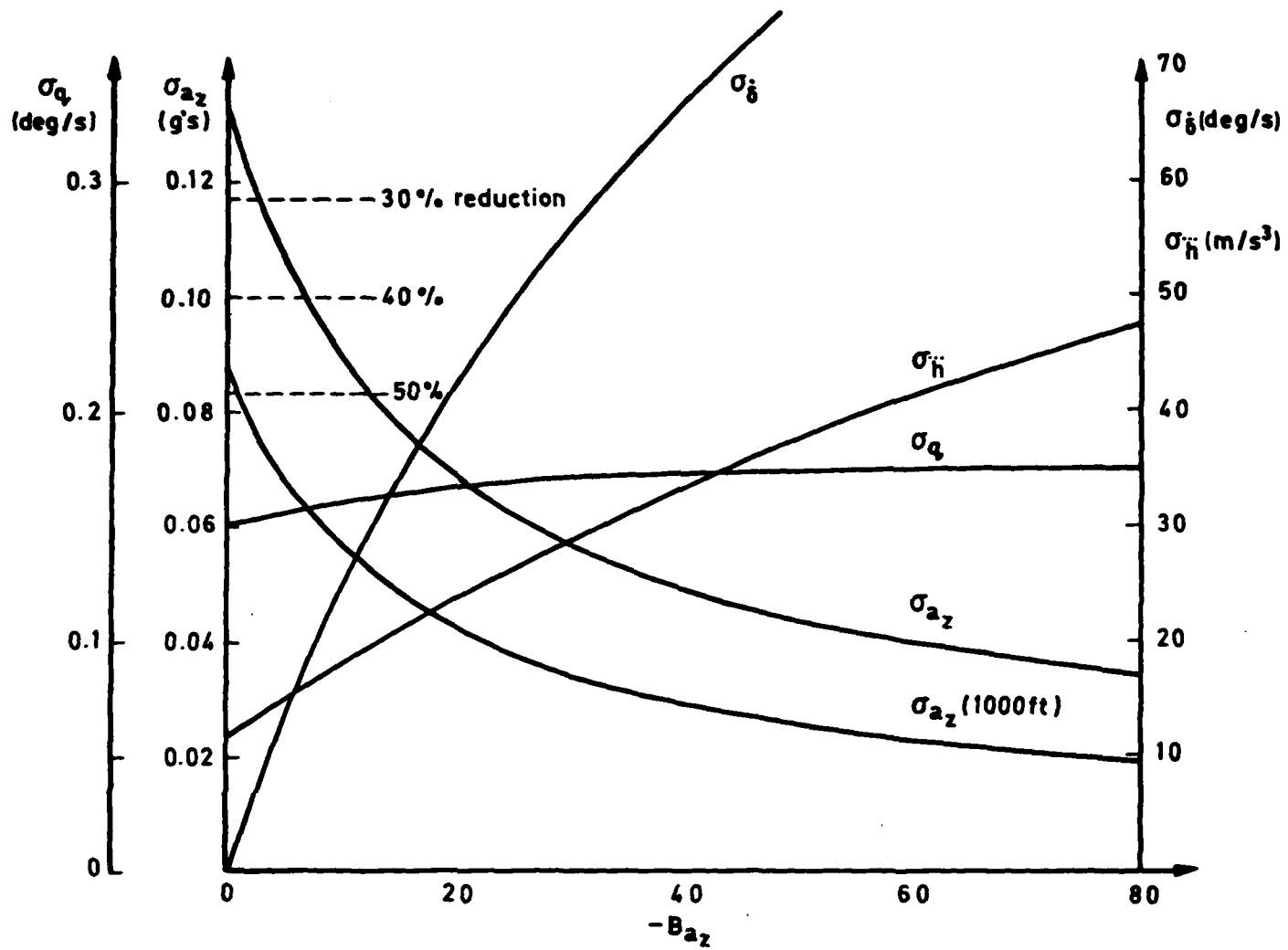

Fig 11 Effect of feedback gain $\left(B_{a_z}\right)$ on rms values. 200 ft, $\tau_2 = 0.04$

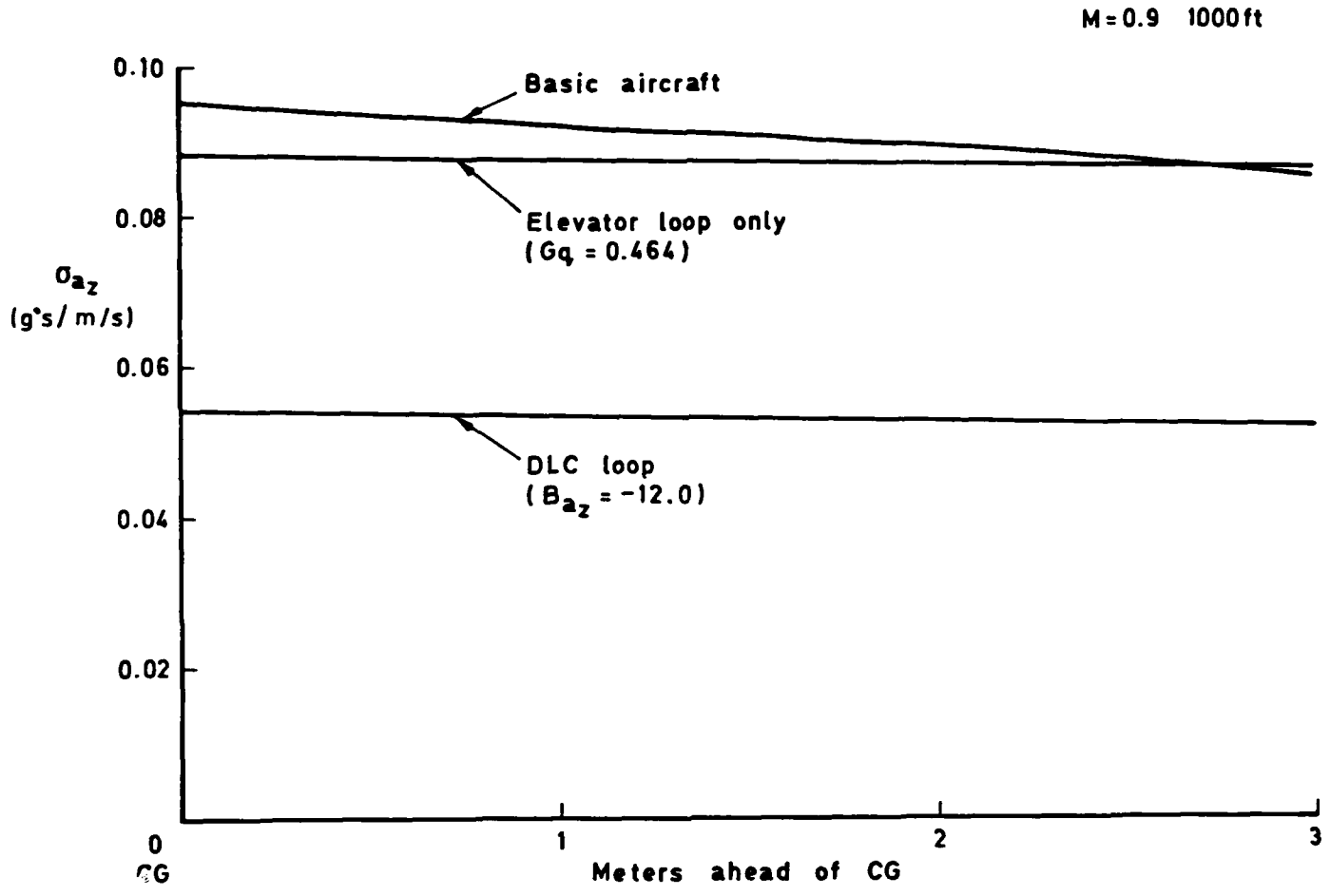

Fig 12 Rms normal acceleration along fuselage

Fig 13

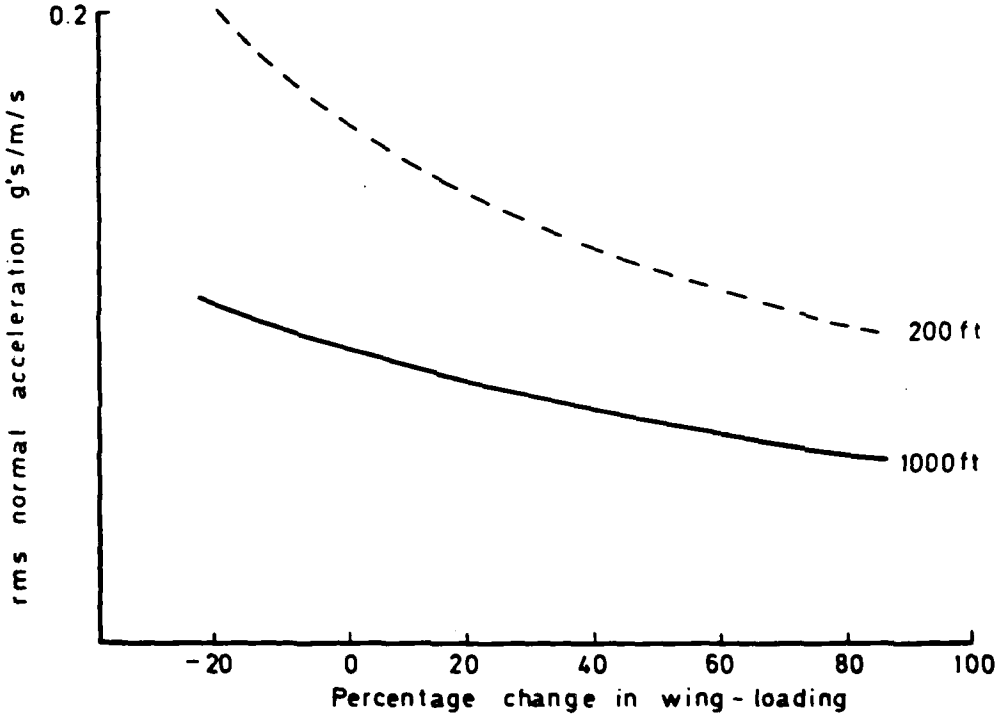

Fig 13 Effect of wing-loading on rms normal acceleration

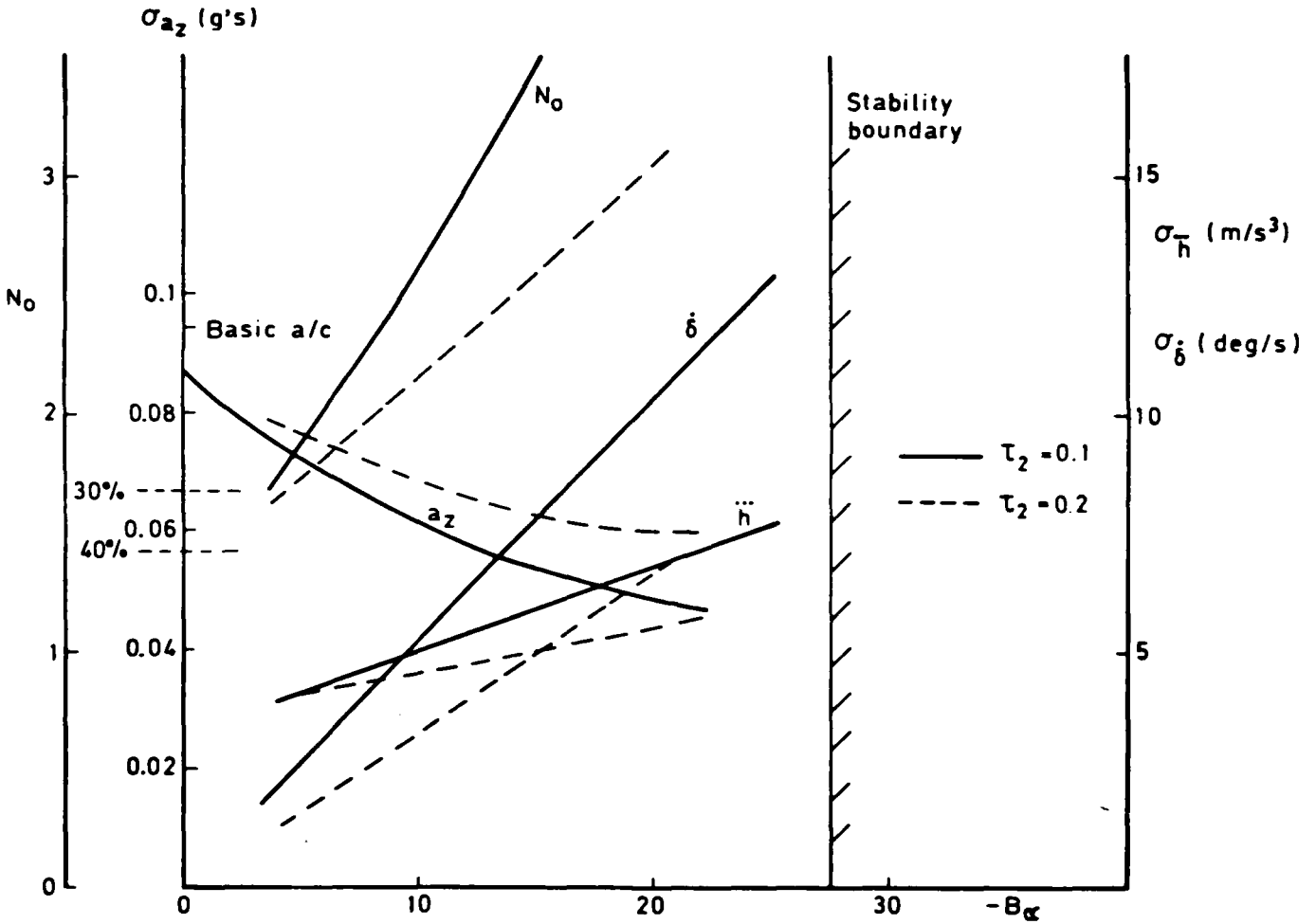

Fig 14 Effect of incidence feedback on rms values

Fig 14

Fig 15

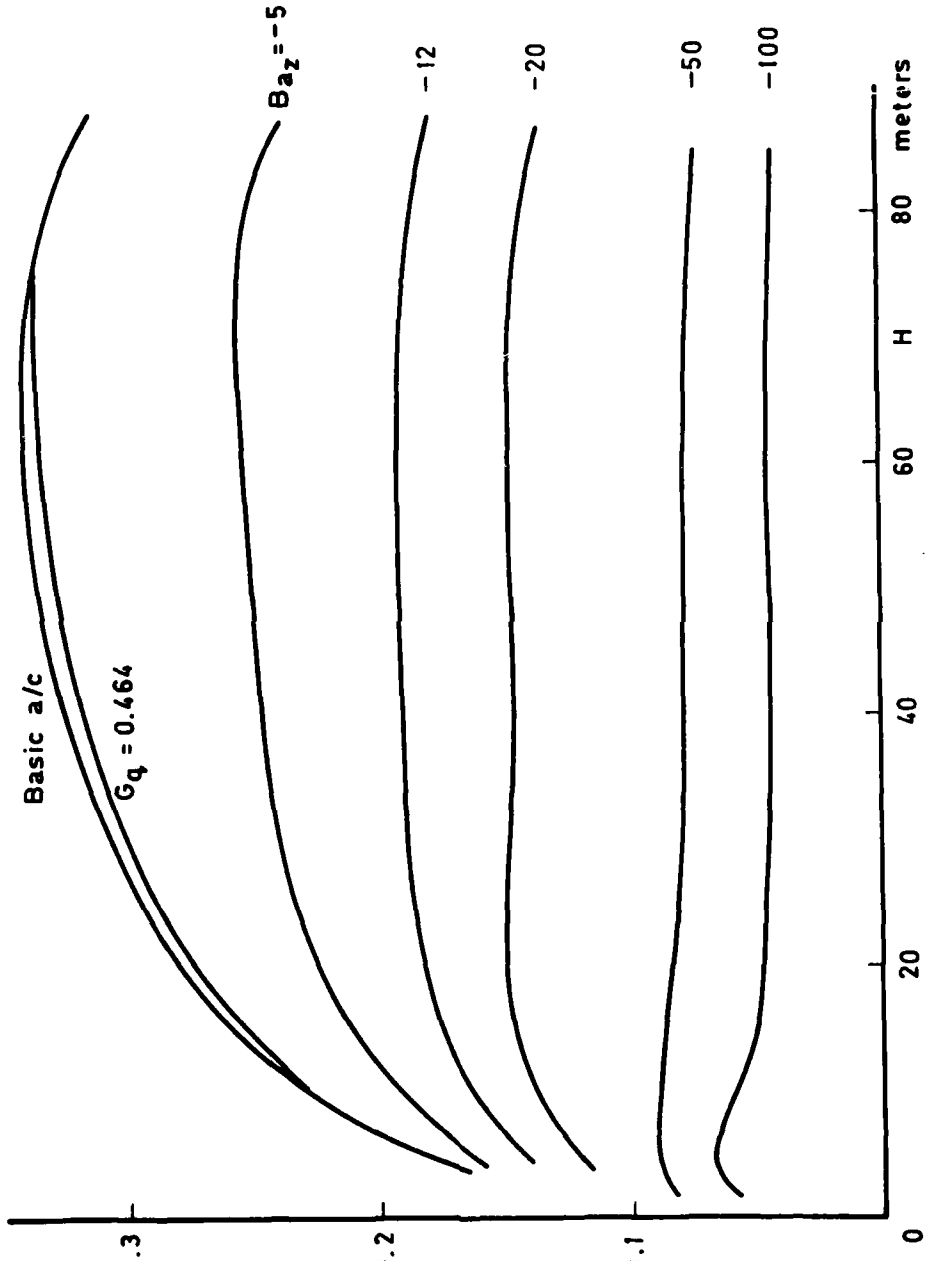

Fig 15 Normal acceleration maximum amplitude response to discrete gusts. Altitude 200 ft

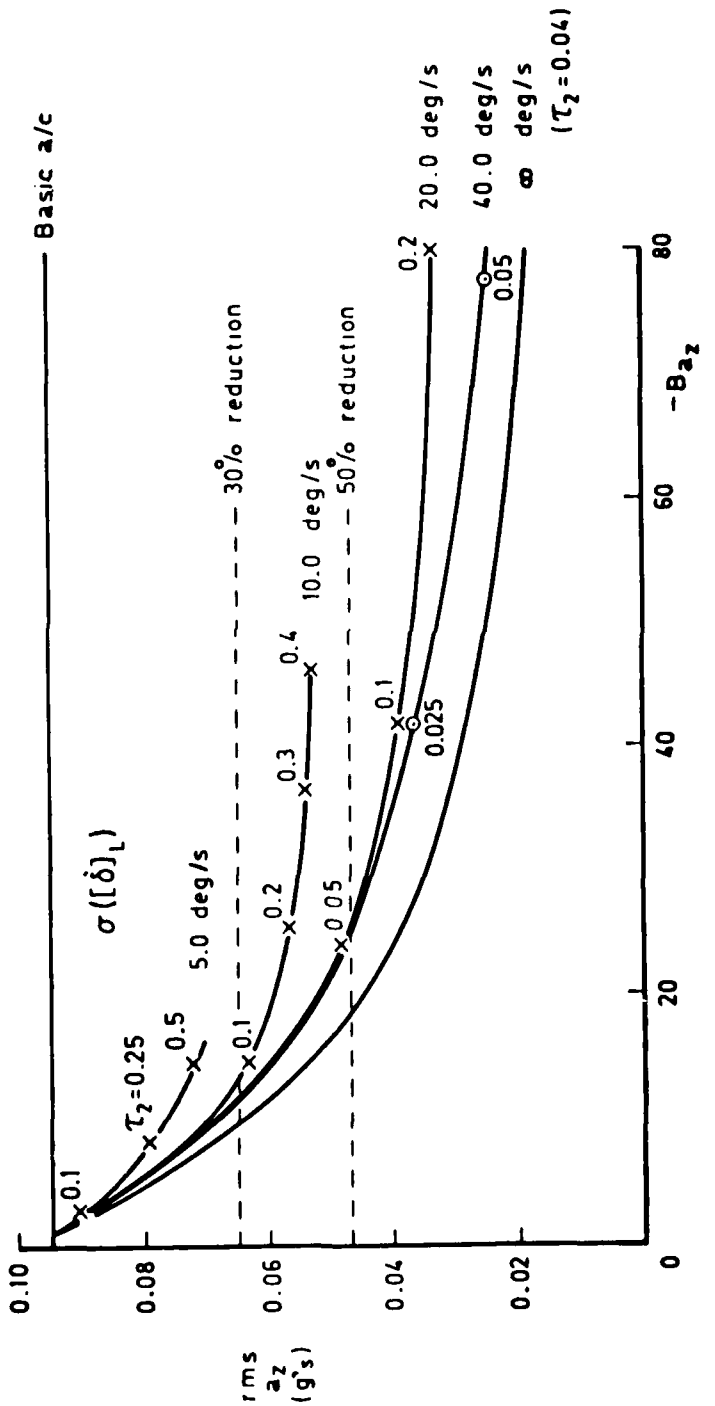

Fig 16 Effect of DLC rate limit on rms values (a_z feedback)

Fig 17

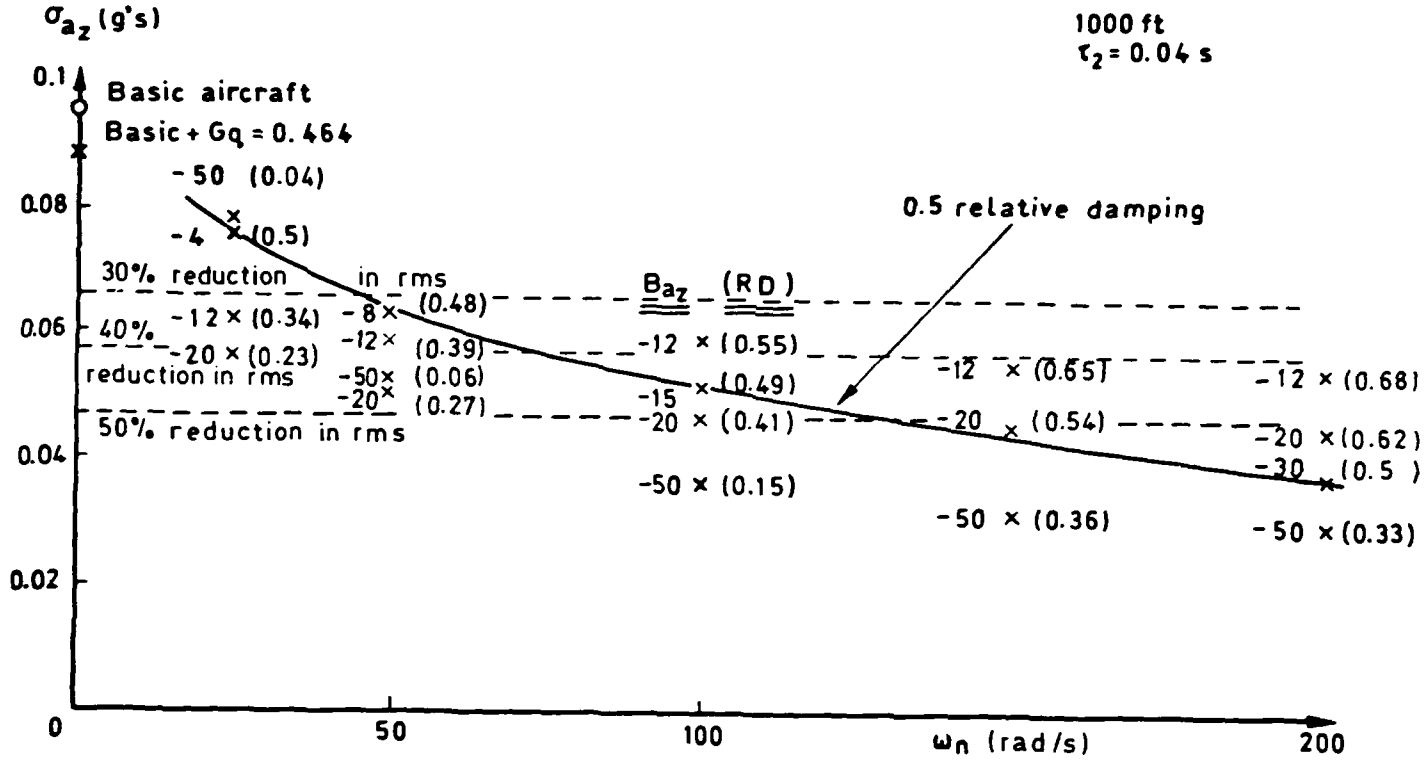

Fig 17 Effect of actuator natural frequency (ω_n) on stability and rms values (a_z feedback)

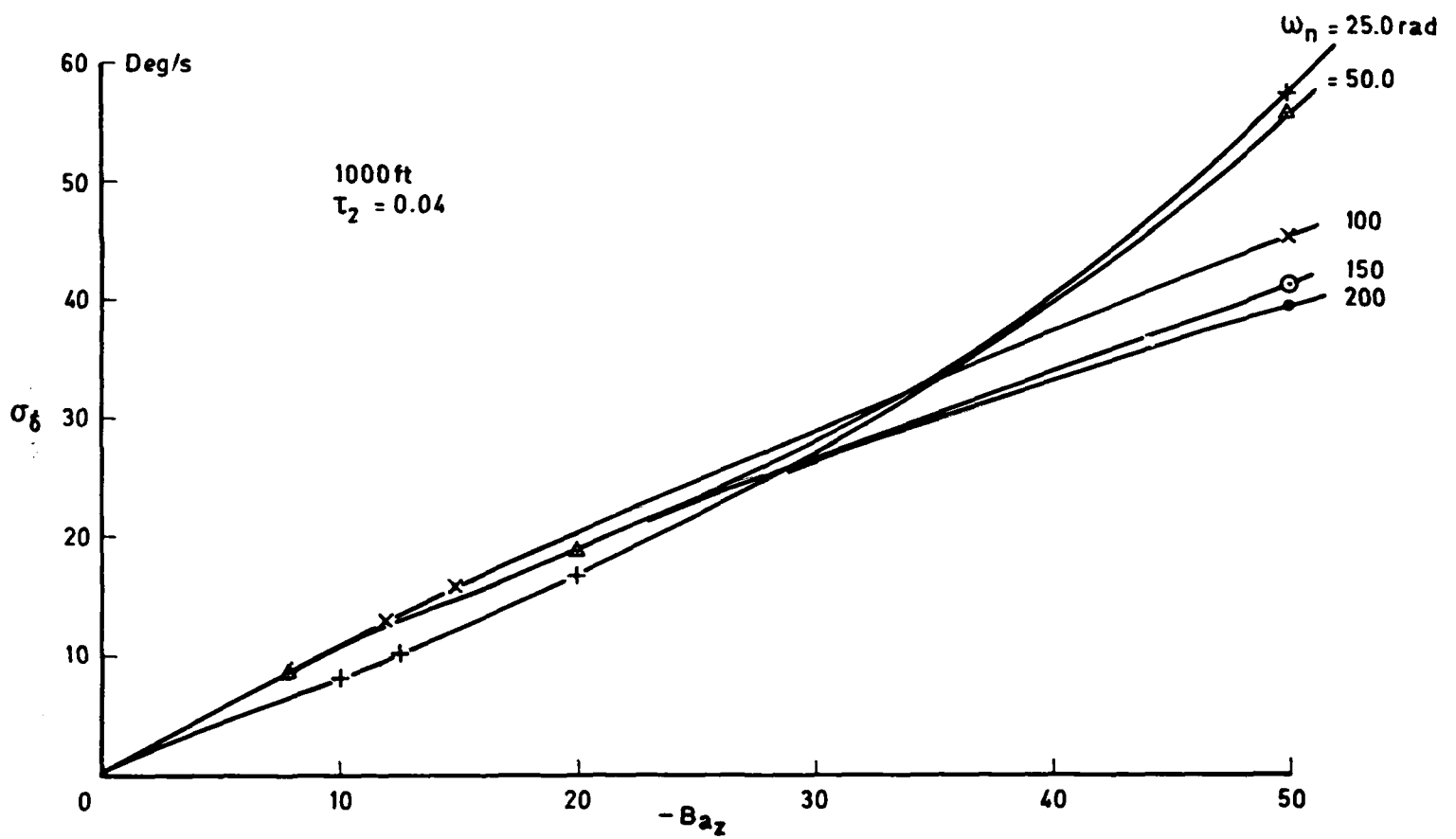

Fig 18 Effect of feedback gain $\left(B_{a_z}\right)$ on rms of actuator rate

Fig 19

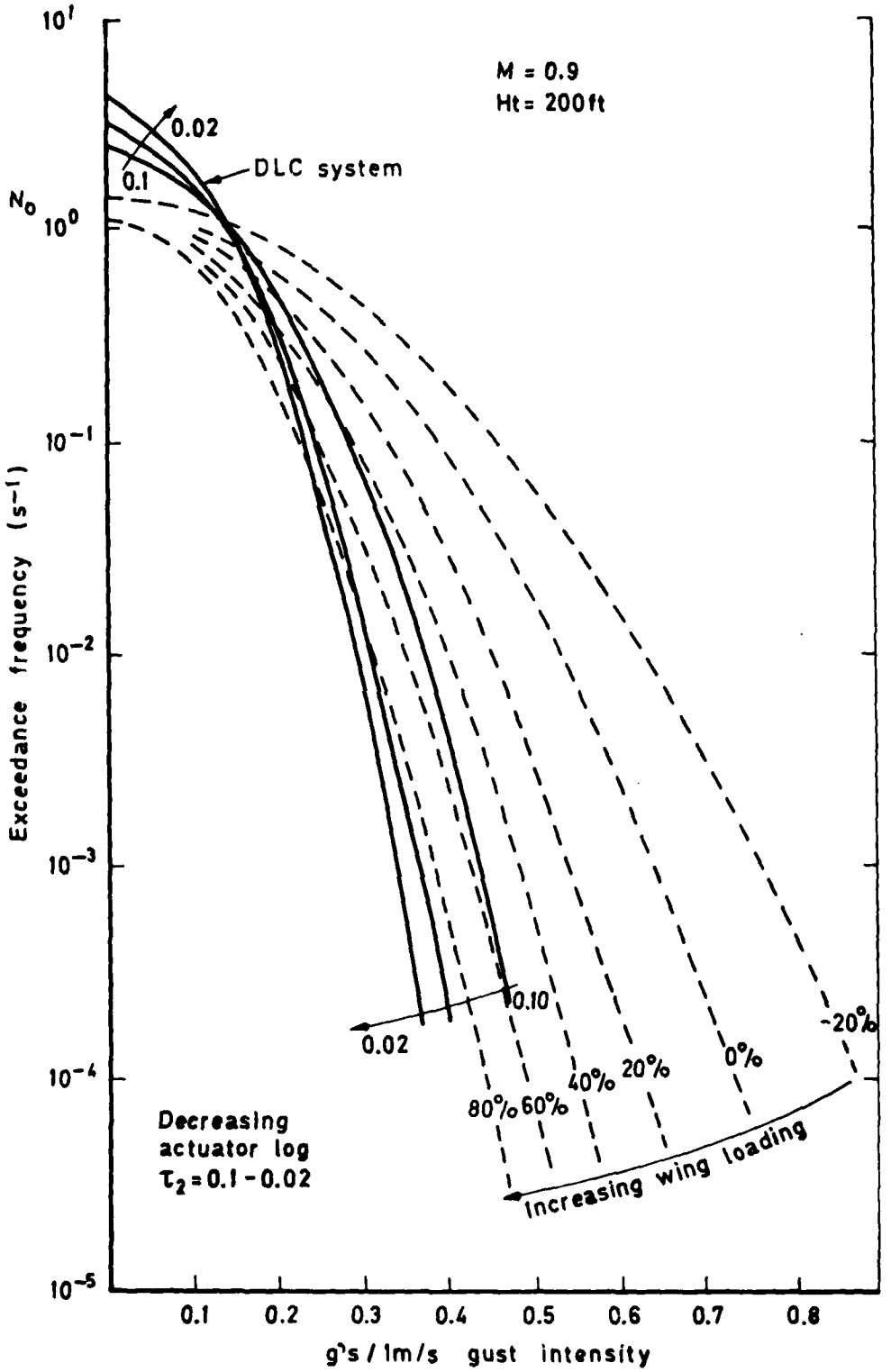

Fig 19 Normal acceleration exceedance frequency

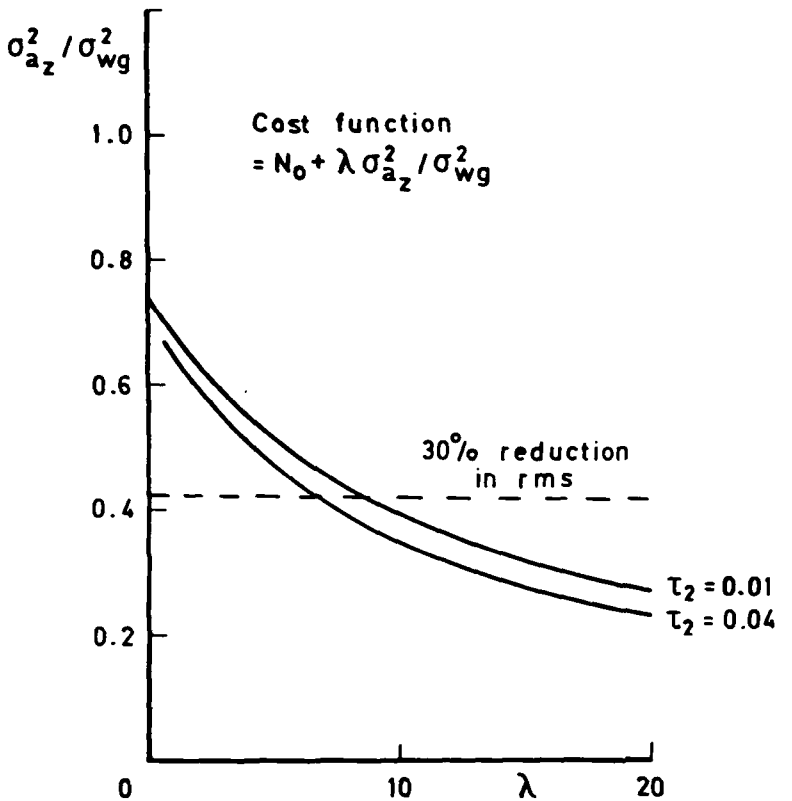

Fig 20a Effect of weighting factor (λ) on cost function minimisation $\left(\sigma^2_{a_z}\right)$

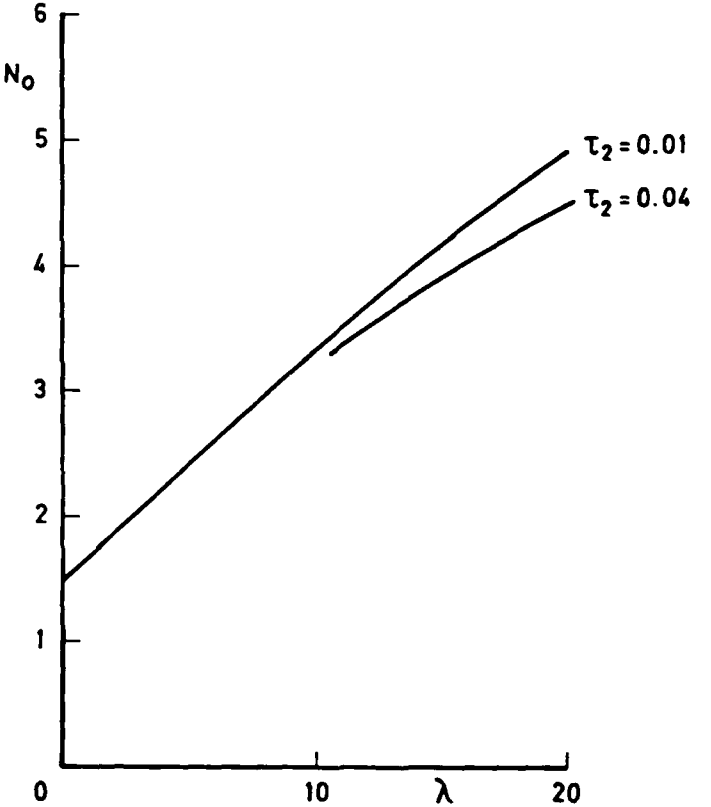

Fig 20b Effect of weighting factor (λ) on cost function minimisation (N_o)

Fig 20 a & b

Fig 21

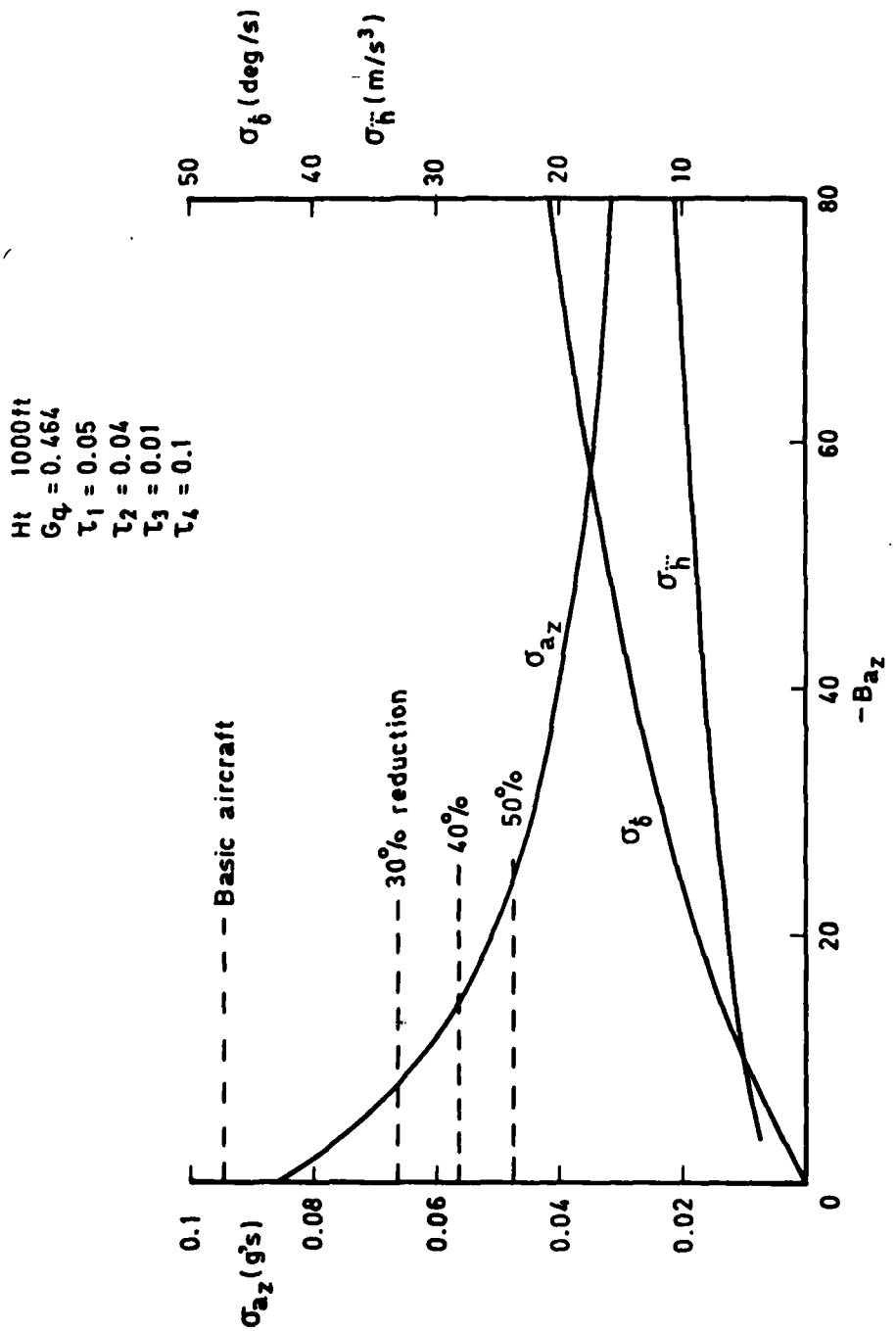

Fig 21 Effect of shaped feedback on rms values

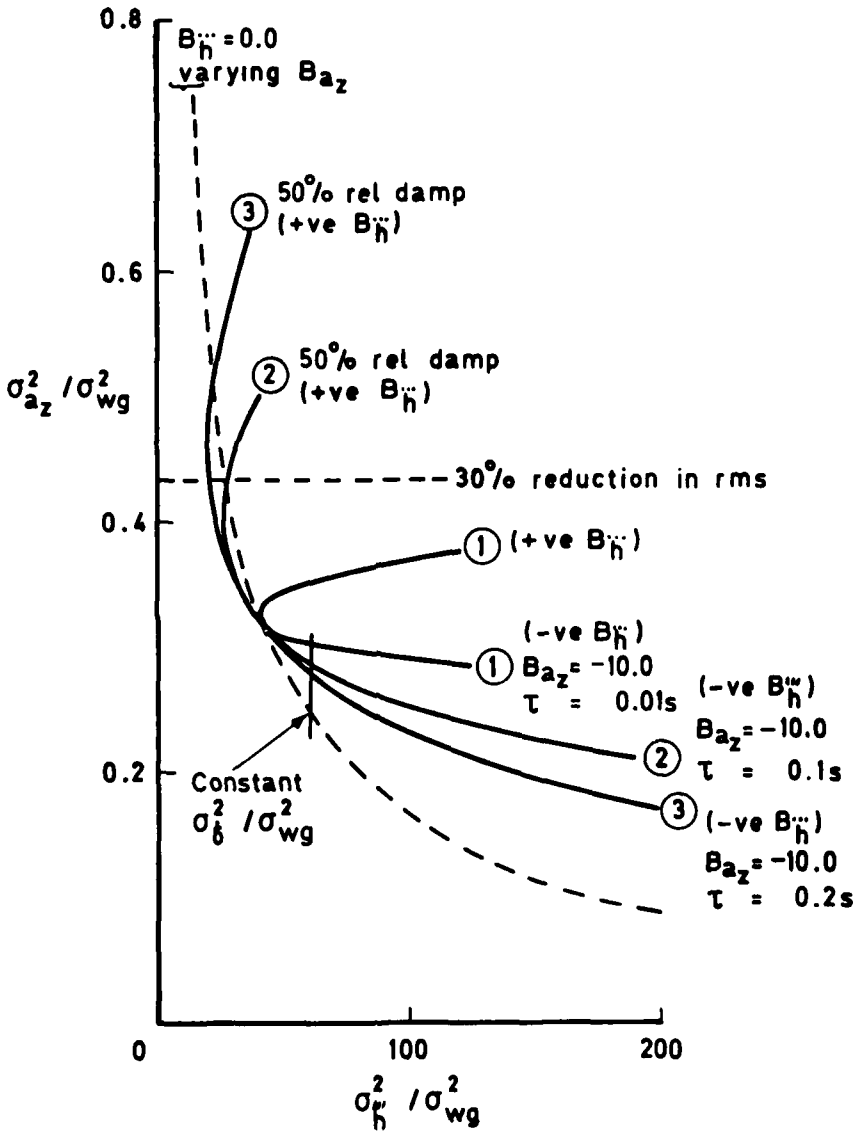

Fig 22 Conflict curve of $\sigma^2_{a_z}$ versus $\sigma^2_{\ddot{h}}$ ($B_{\ddot{h}}$)

Fig 23

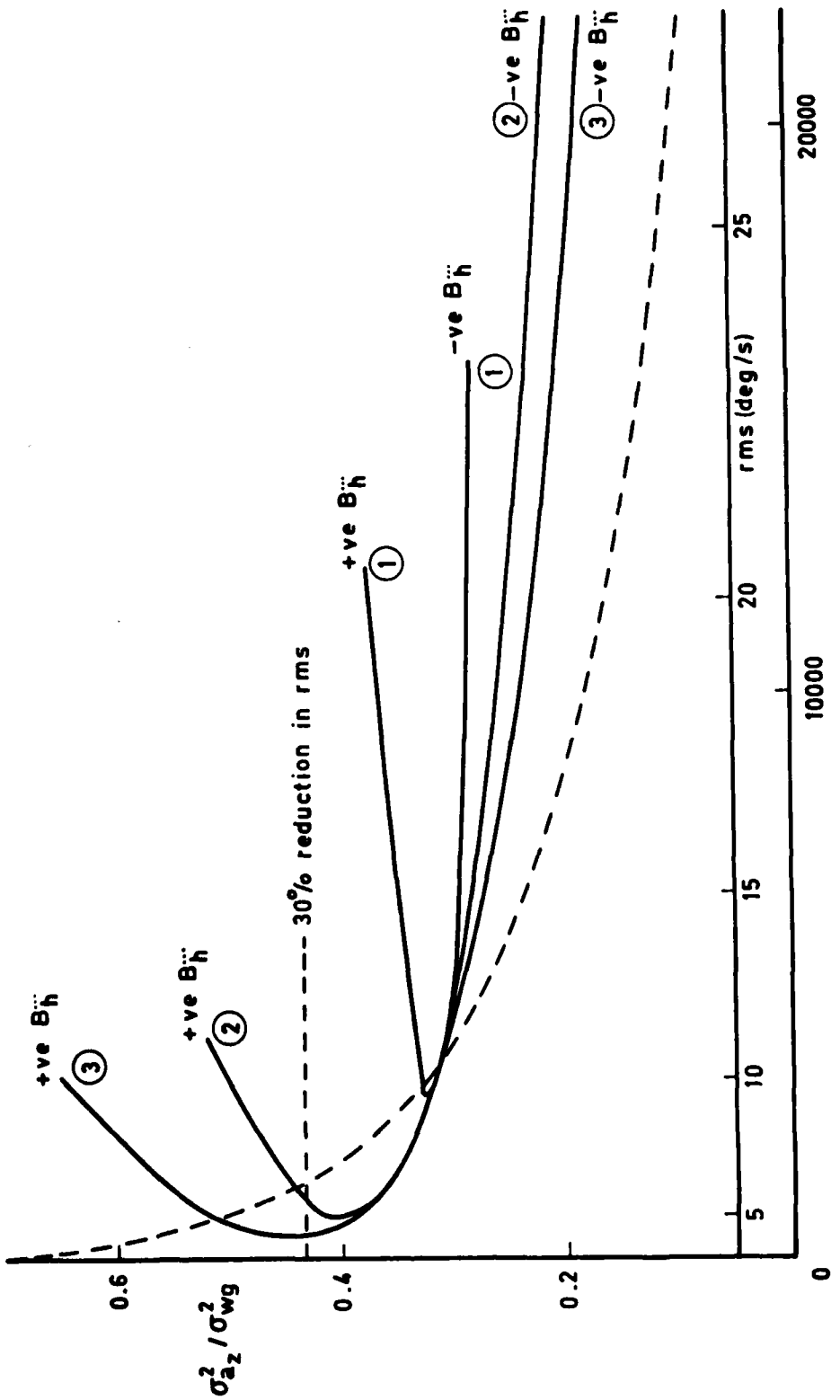

Fig 23 Conflict curve of $\sigma^2_{a_z}$ against σ^2_δ ($B_{\ddot{h}}$ feedback)

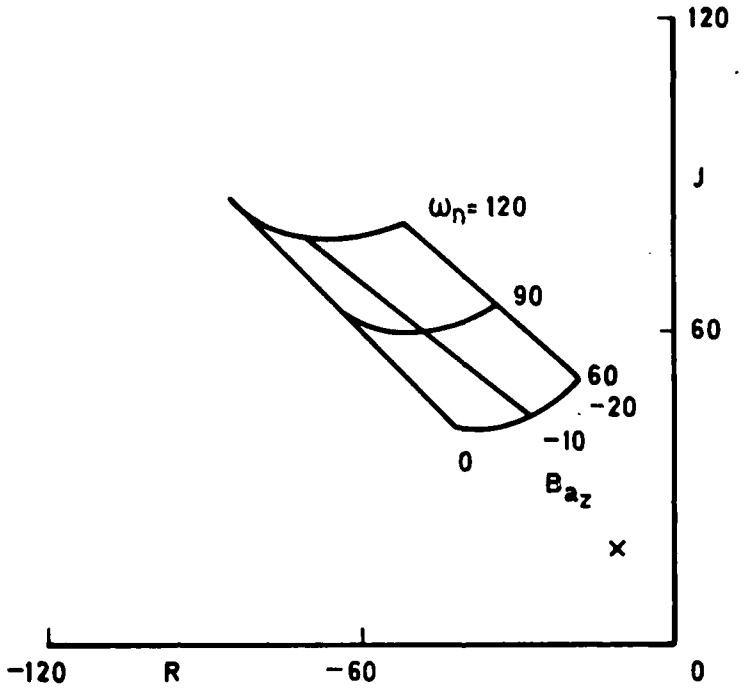

Fig 24 Root locus of feedback gain $\left(B_{a_z}\right)$ and actuator natural frequency (ω_n)

Fig 25

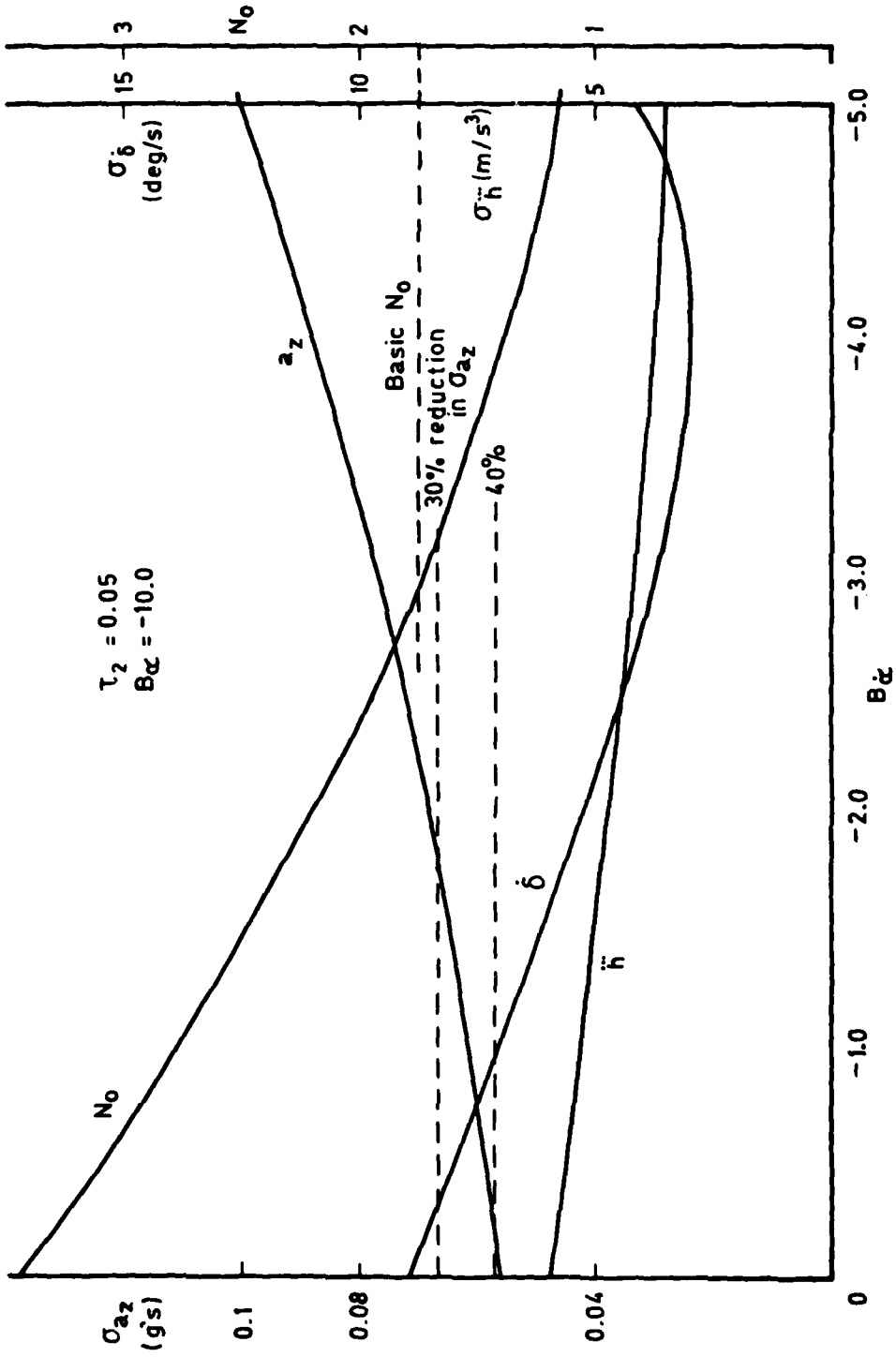

Fig 25 Effect of incidence and incidence rate feedback on rms values

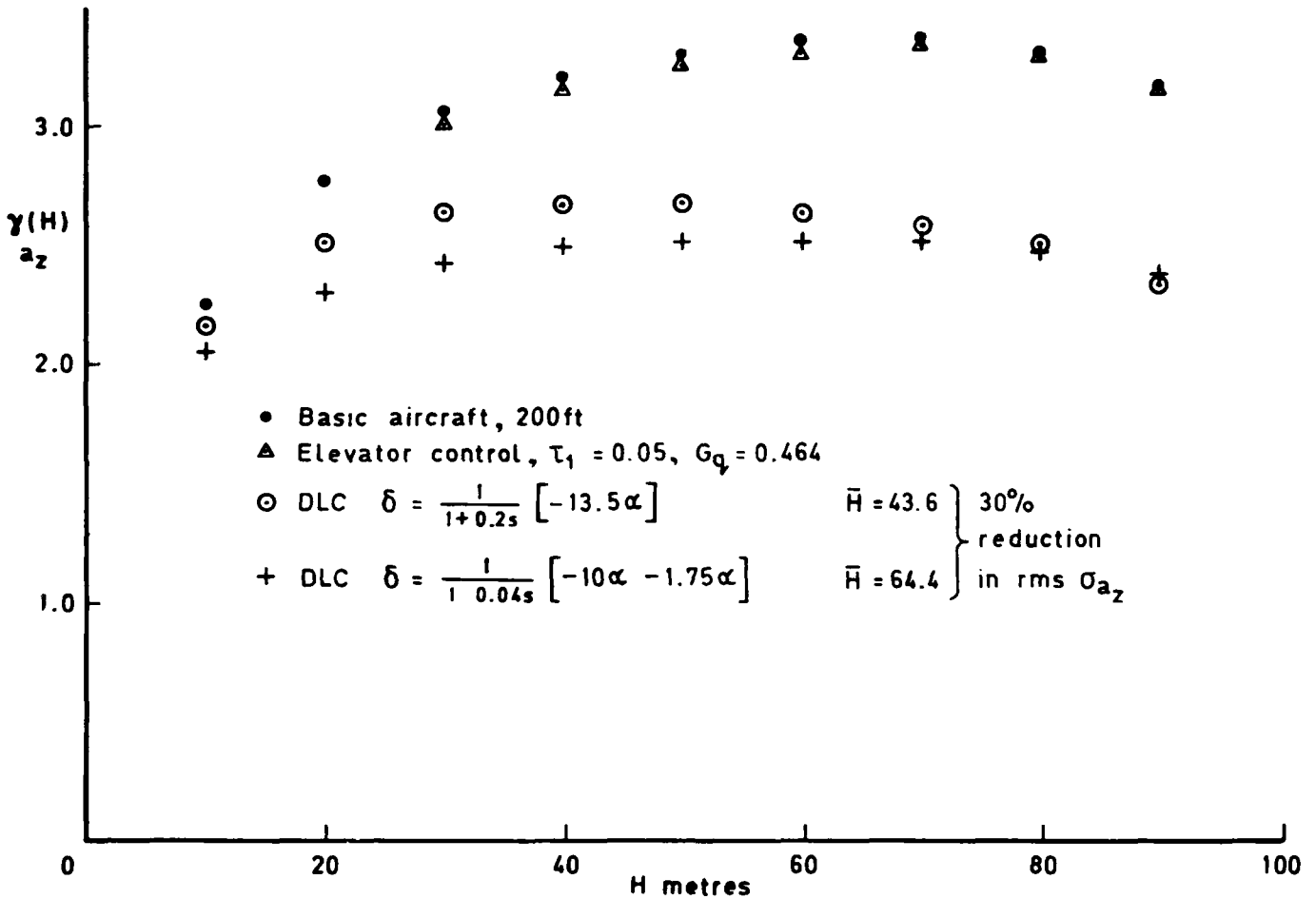

Fig 26 Discrete gust response, filtered incidence feedback

Fig 26

Fig 27

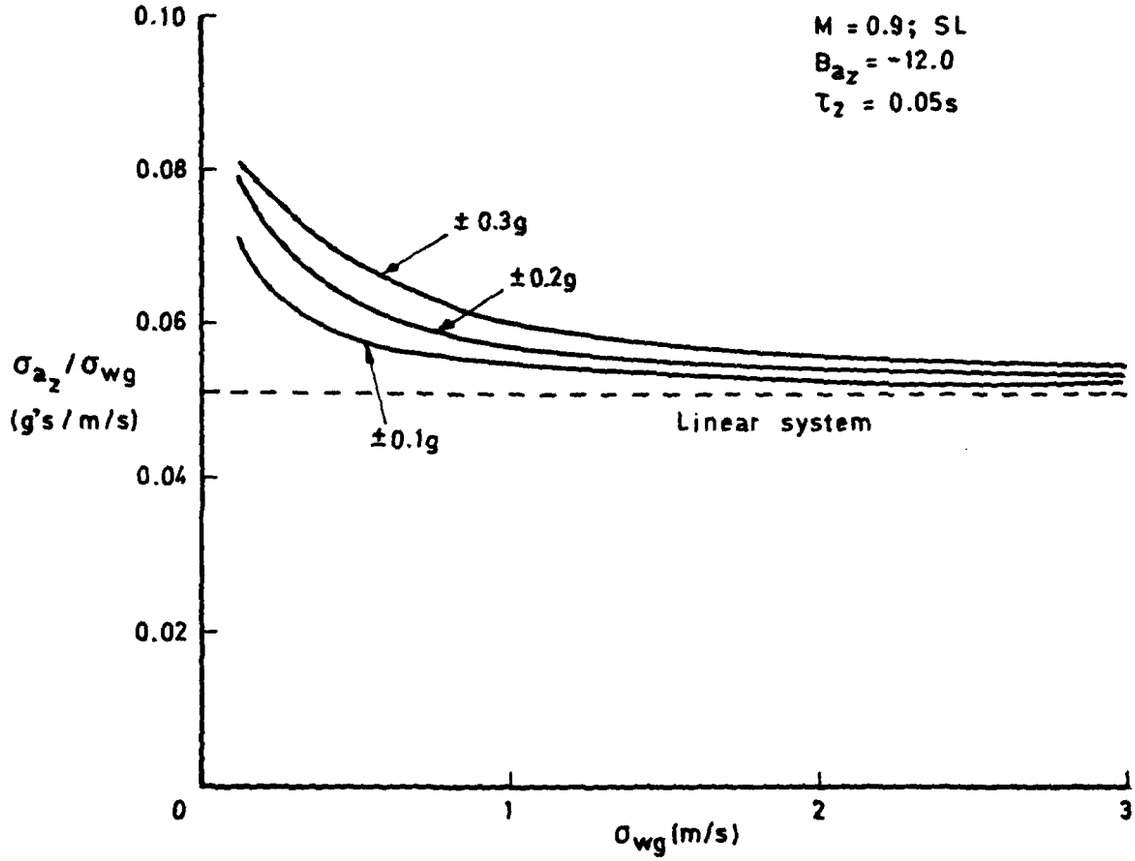

Fig 27 Effect of dead-zone on rms normal acceleration

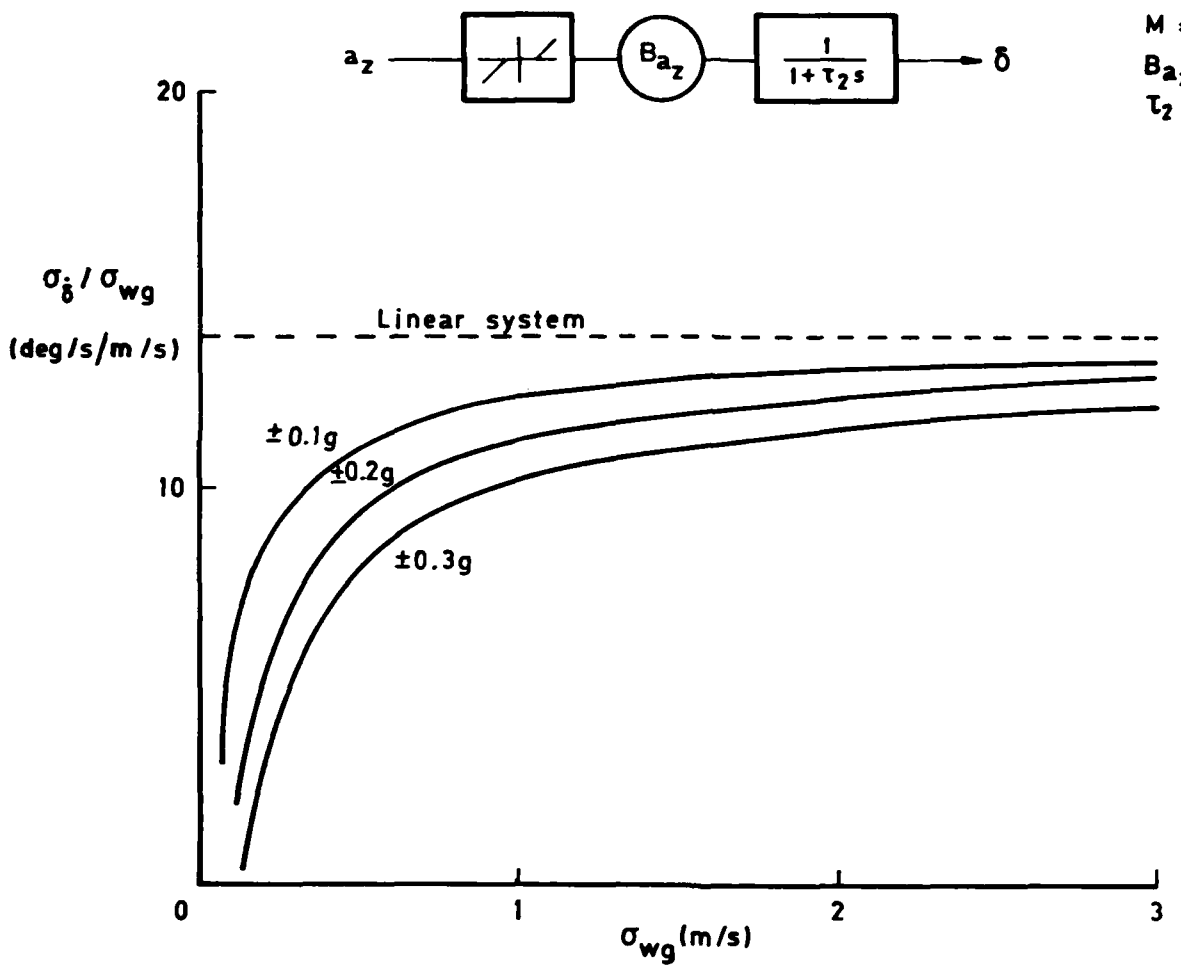

Fig 28 Effect of dead-zone on motivator rate, normal acceleration feedback

Fig 29

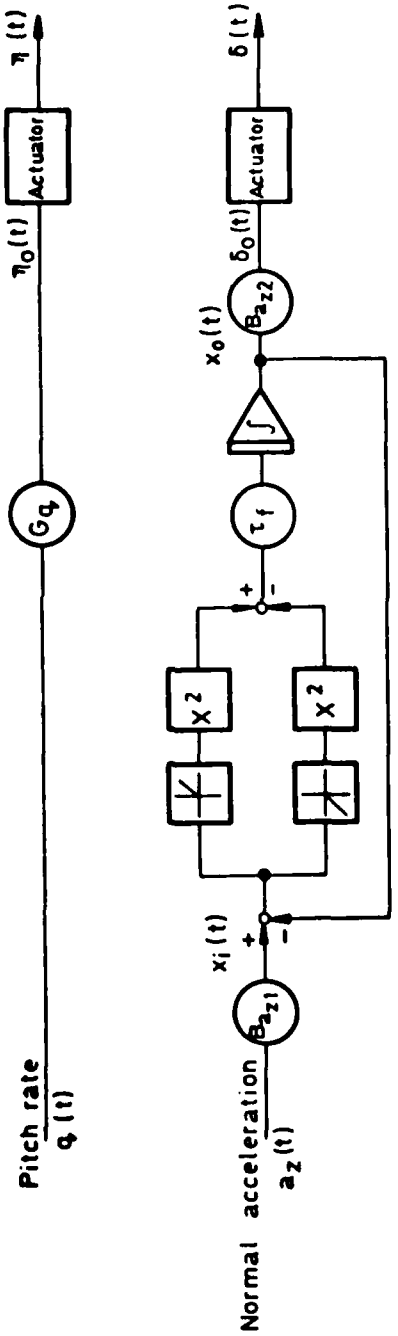

Fig 29 Block schematic of nonlinear controller using square law

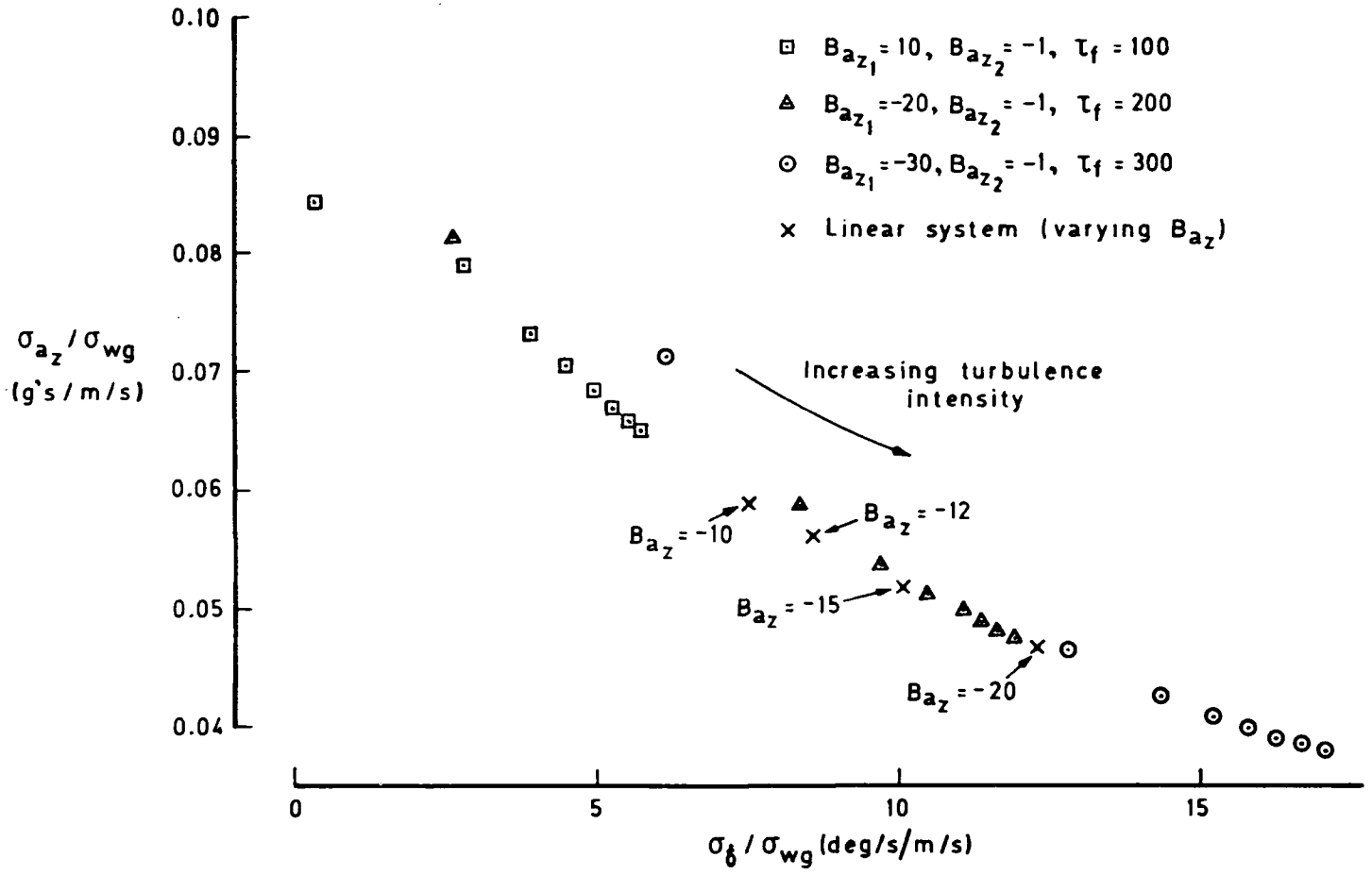

Fig 30a Relationship between normal acceleration and DLC actuator rate in response to varying levels of turbulence intensity for nonlinear RCS

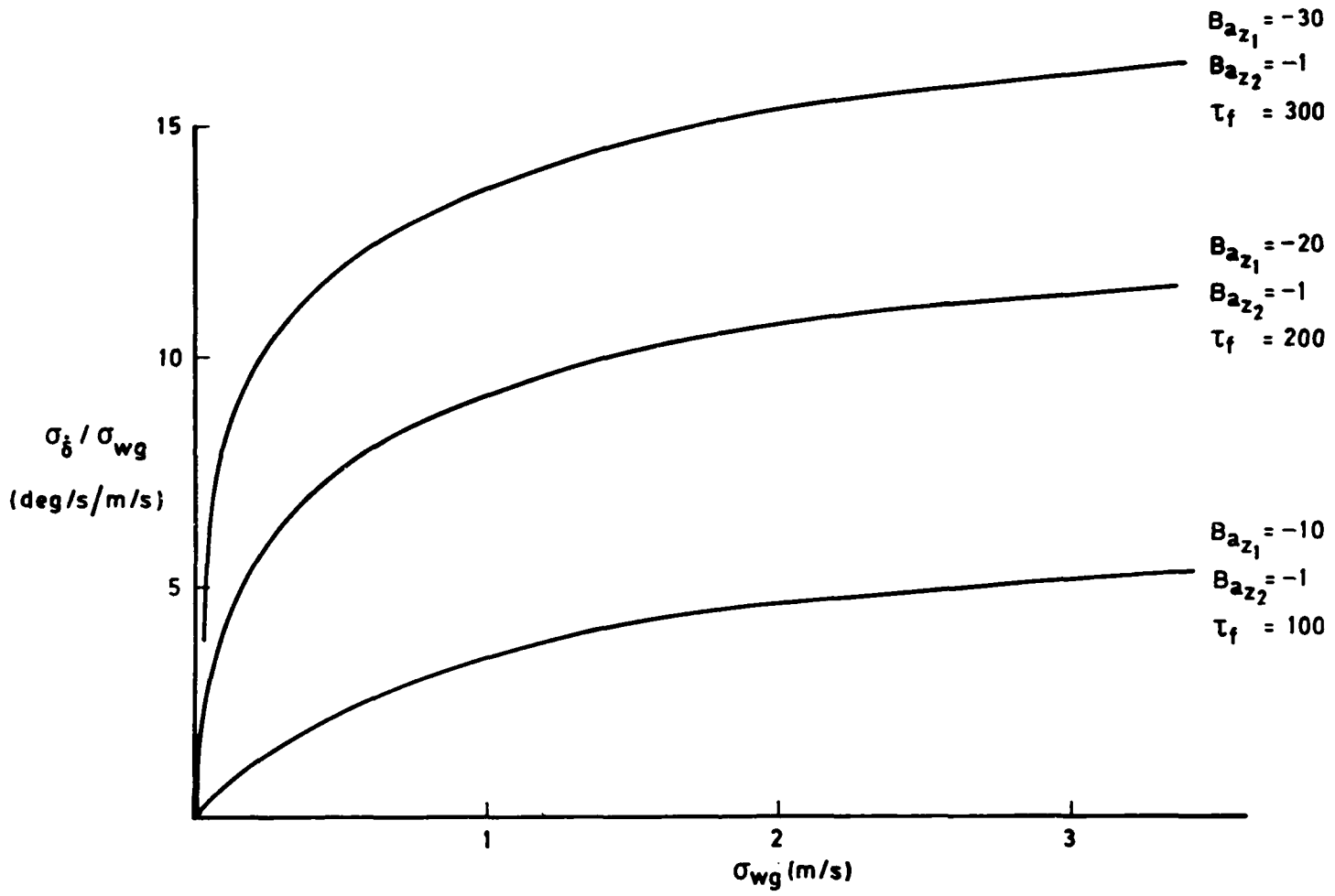

Fig 30b Relationship between turbulence intensity and DLC actuator rate for nonlinear RCS

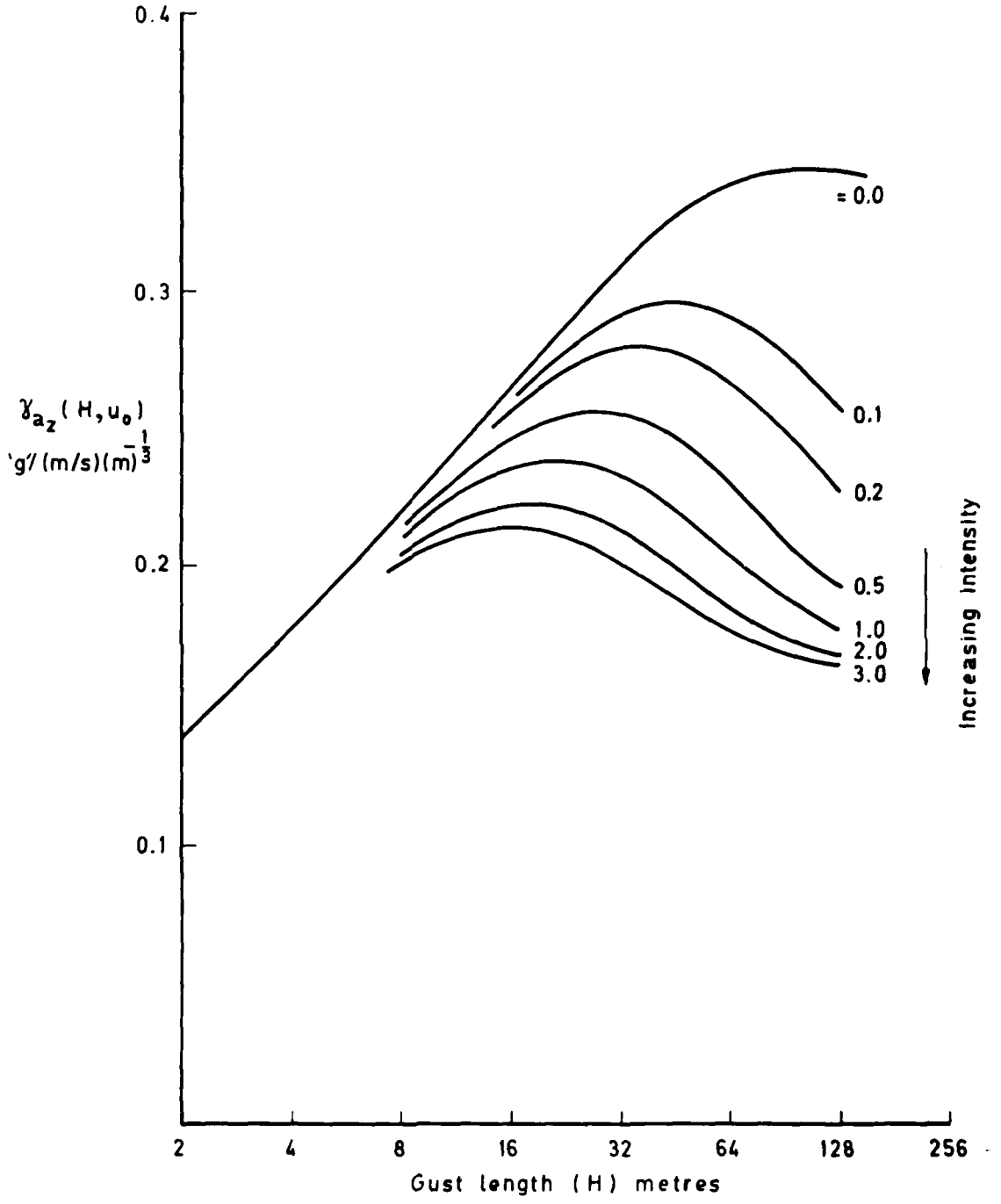

Fig 31 $\gamma_{a_z}(H,u_o) \sim H$ curves for nonlinear RCS with $B_{a_{z_1}} = 20$, $B_{a_{z_2}} = -1$, $\tau_f = 200$

Fig 32

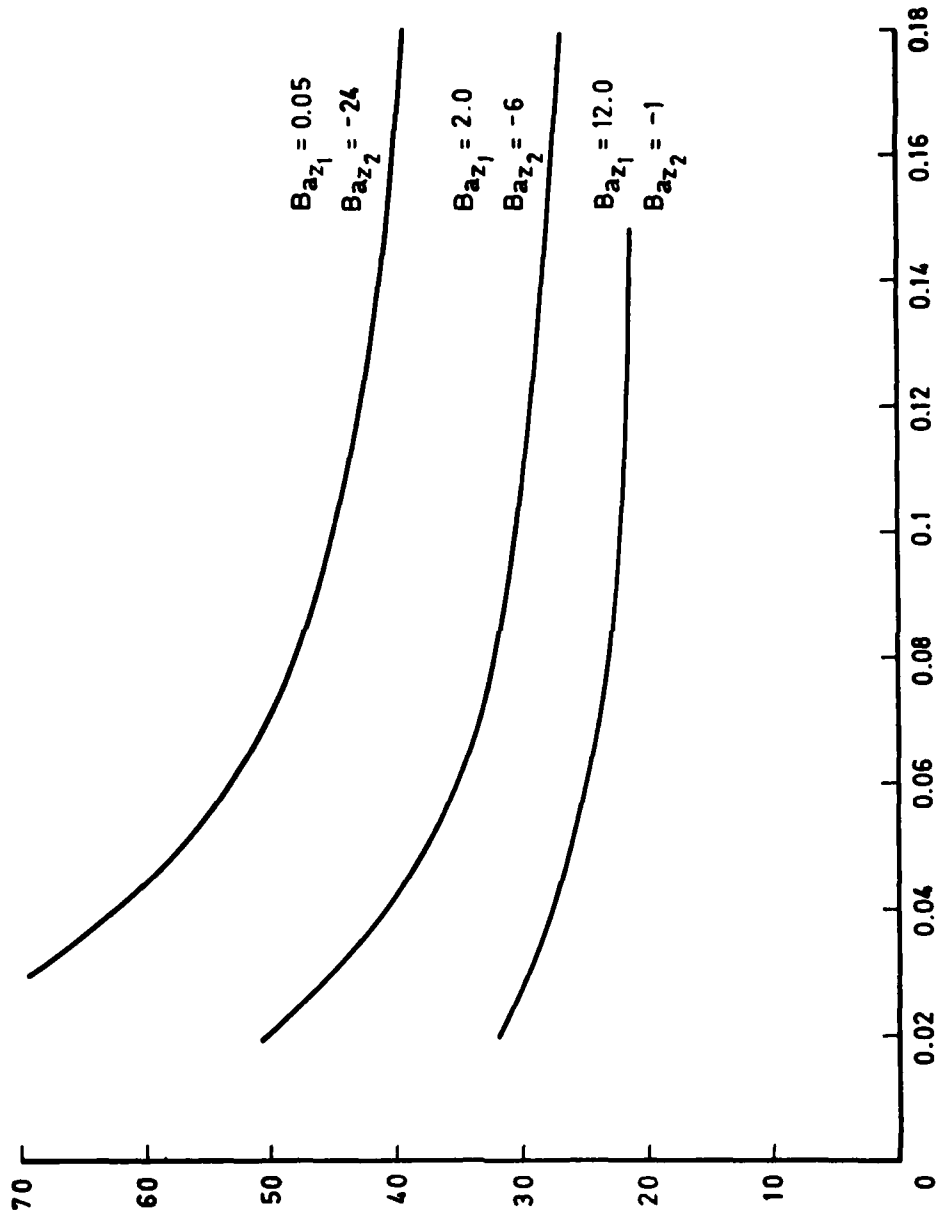

Fig 32 Effect of increasing turbulence intensity on $\bar{H}$ for nonlinear system $\tau_F = 25.0$

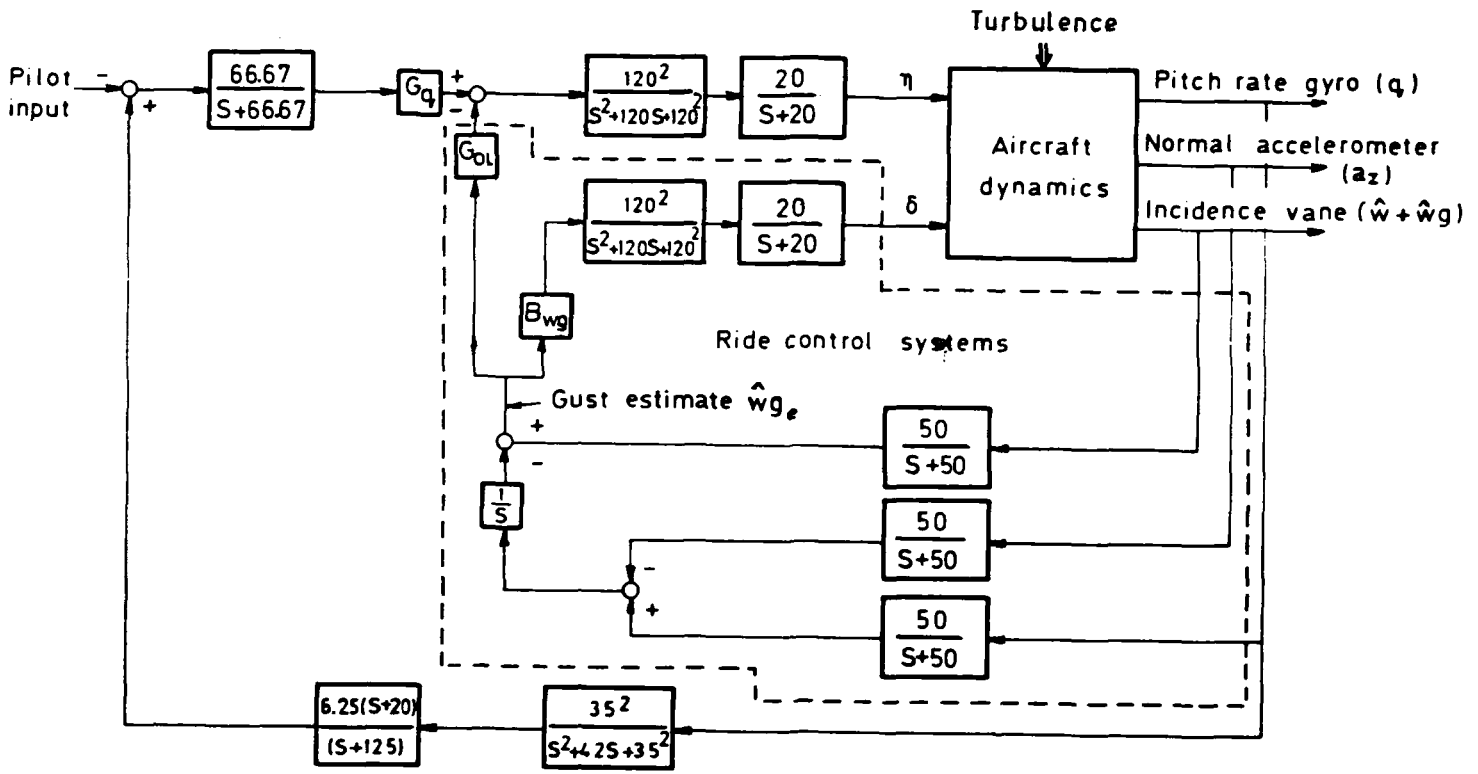

Fig 33 'Open-loop' RCS integrated with existing Hunter longitudinal control law

Fig 33

Fig 34

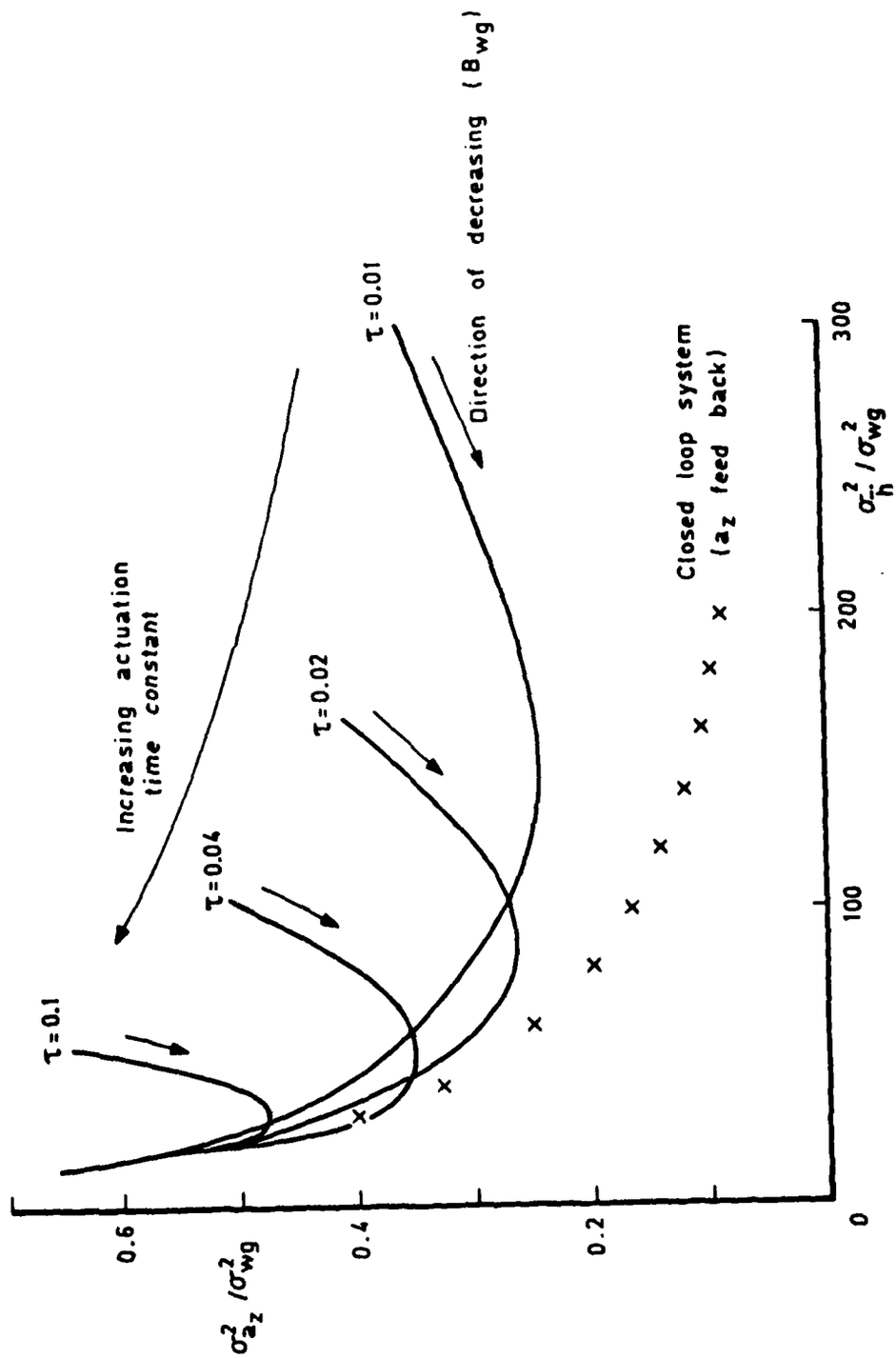

Fig 34 Conflict curves of $\sigma^2_{a_z}$ and variance of rate of change of normal acceleration (open-loop system)

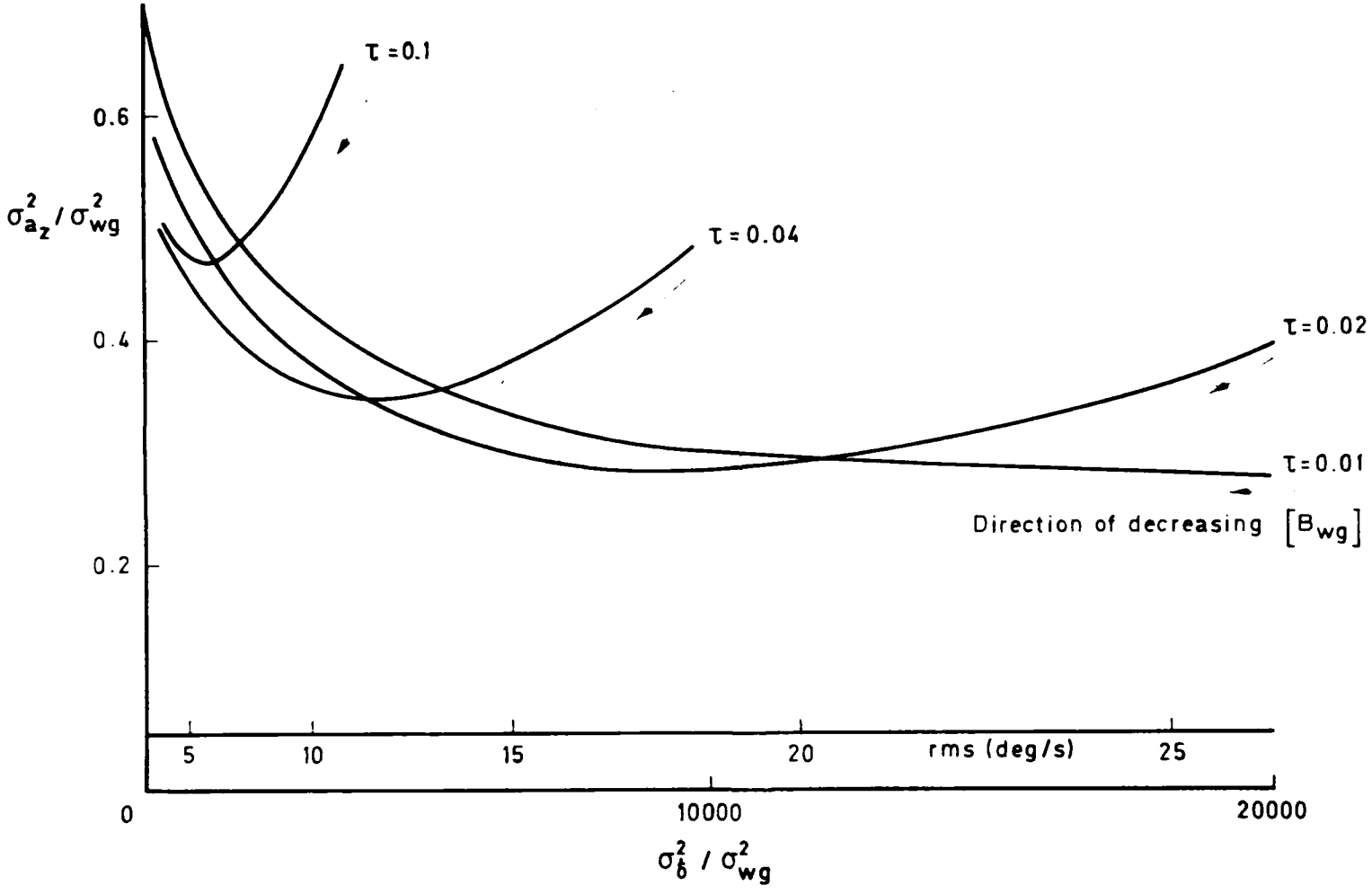

Fig 35 Conflict curves for $\sigma^2_{a_z}$ and $\sigma^2_{\dot{\delta}}$ (open-loop system)

Fig 35

Fig 36

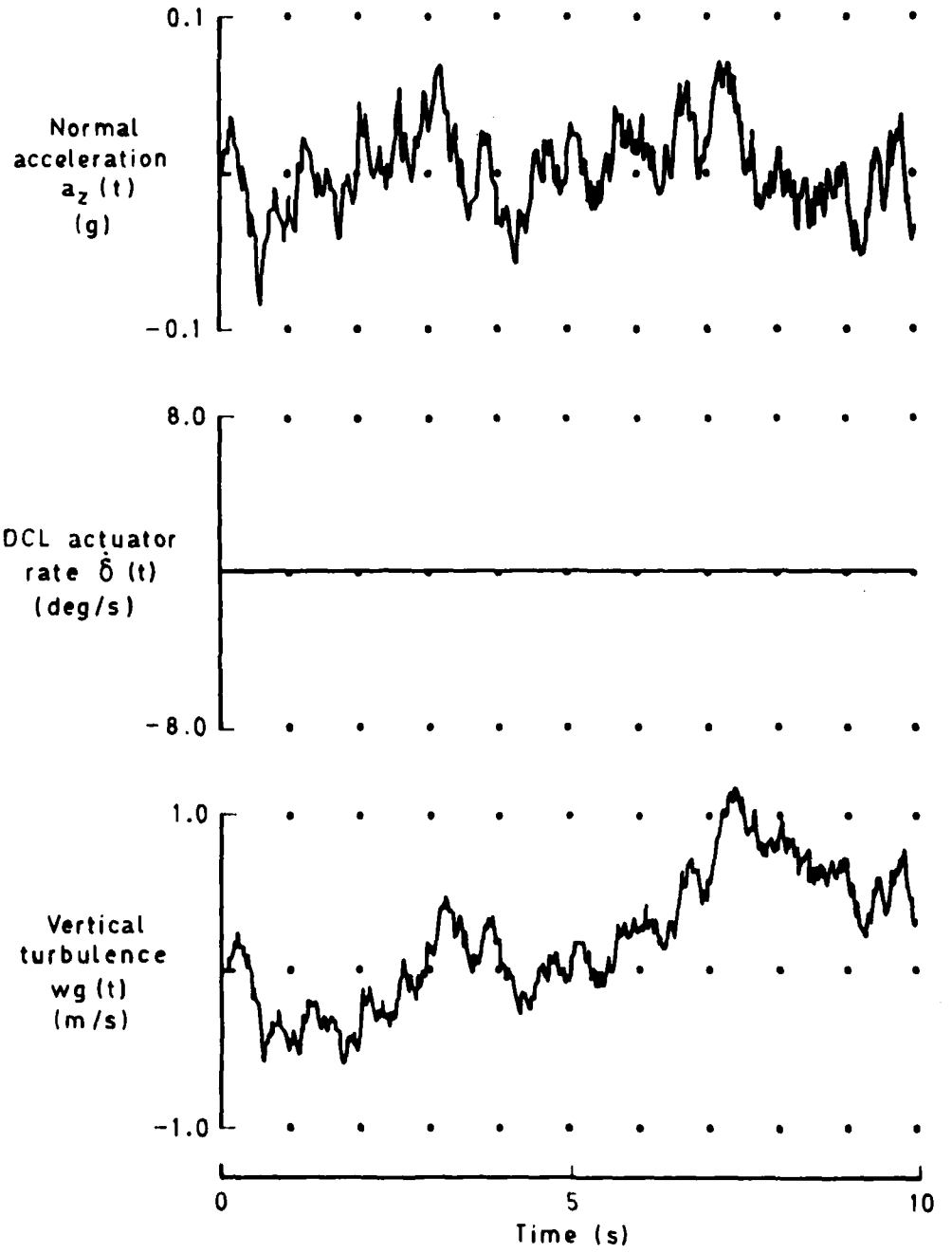

Fig 36 Response of elevator only system to band limited white noise (σ_{w_g} = 0.32 m/s)

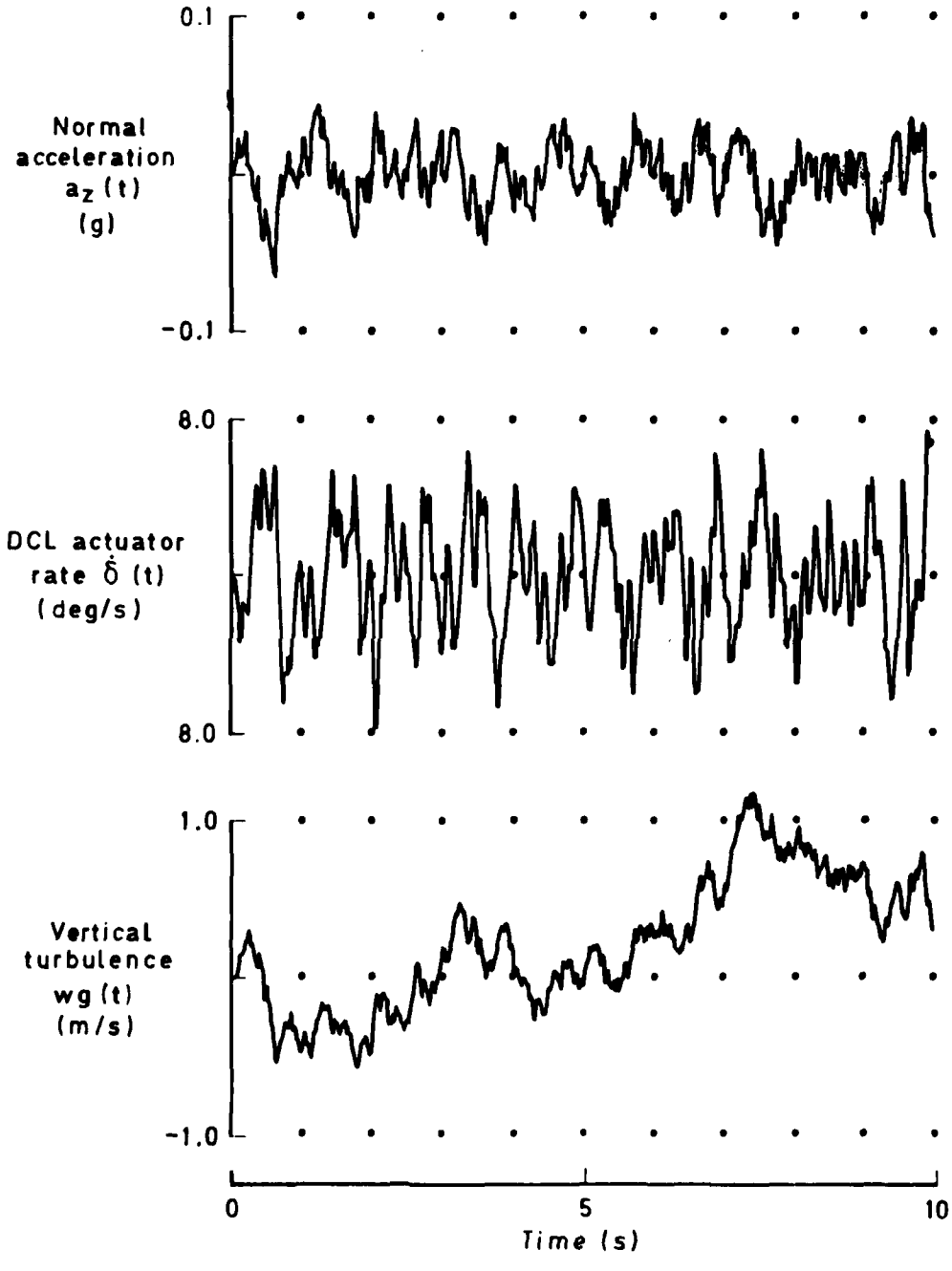

Fig 37 Response of linear RCS ($B_{a_z} = -12$, $\tau = 0.04$) to band limited white noise ($\sigma_{w_g} = 0.32$ m/s)

Fig 38

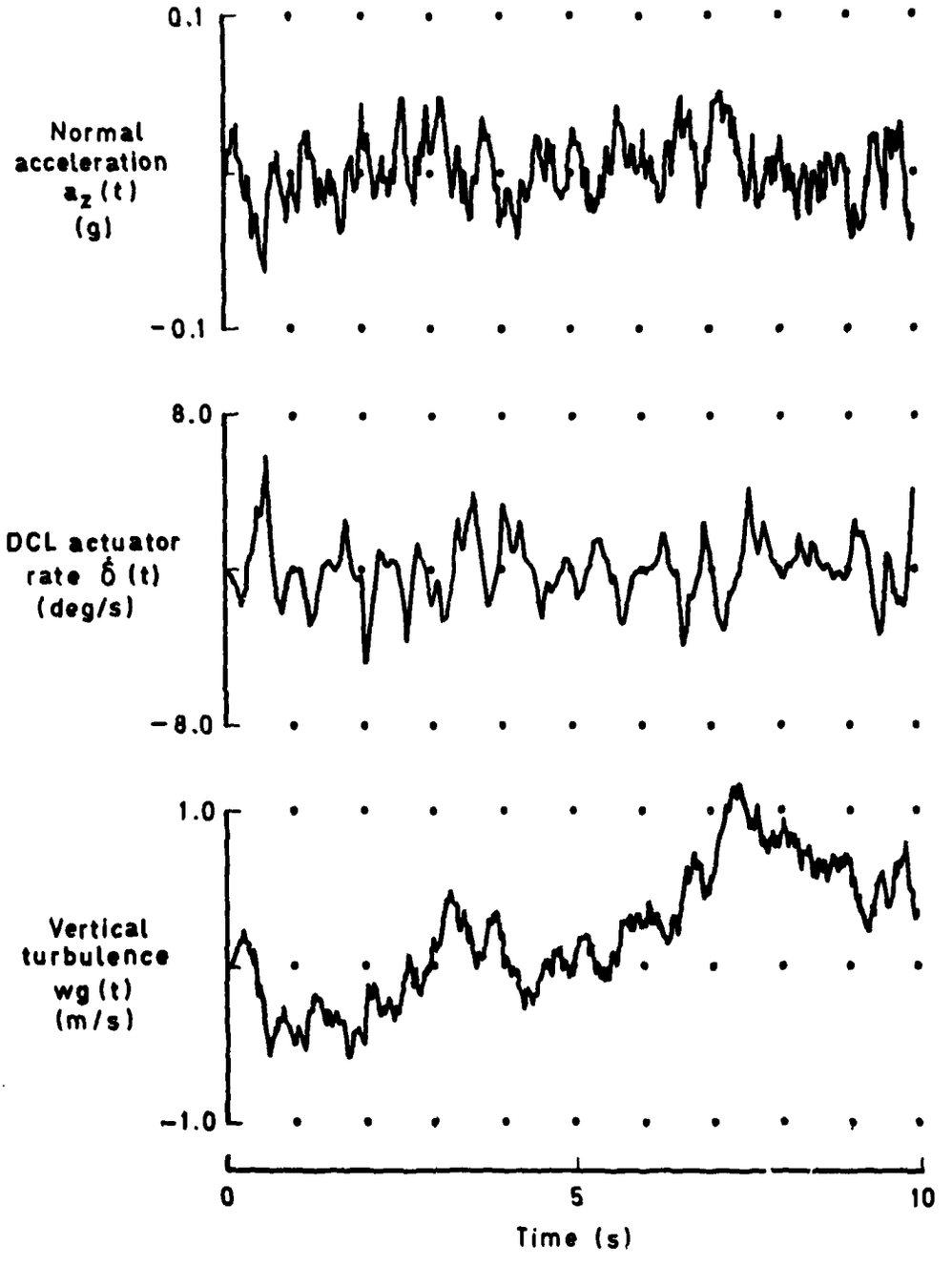

Fig 38 Response of nonlinear RCS ($B_{a_{z_1}} = 20$, $B_{a_{z_2}} = -1$, $\tau_f = 200$) to band limited white noise ($\sigma_{w_g} = 0.32$ m/s)

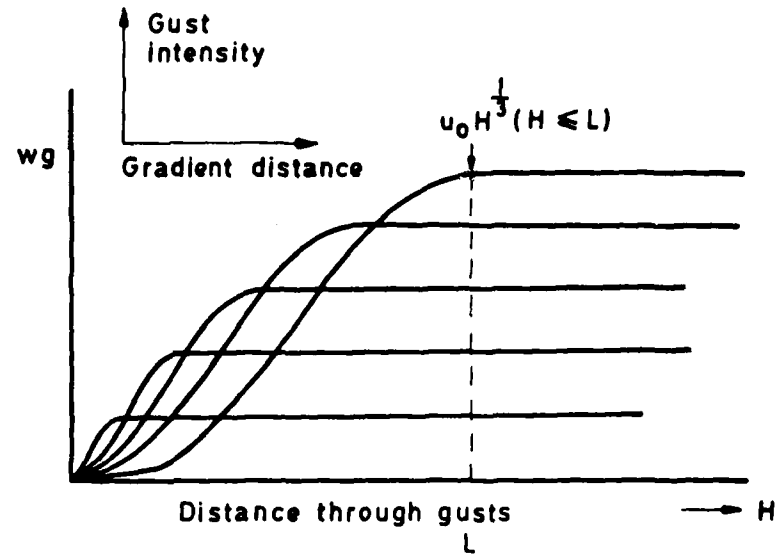

a Family of discrete gusts

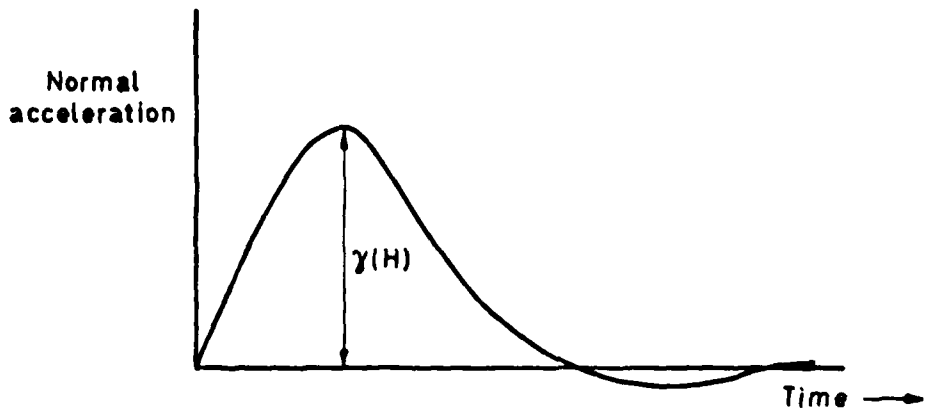

b Typical normal acceleration response to a discrete gust of gust length H

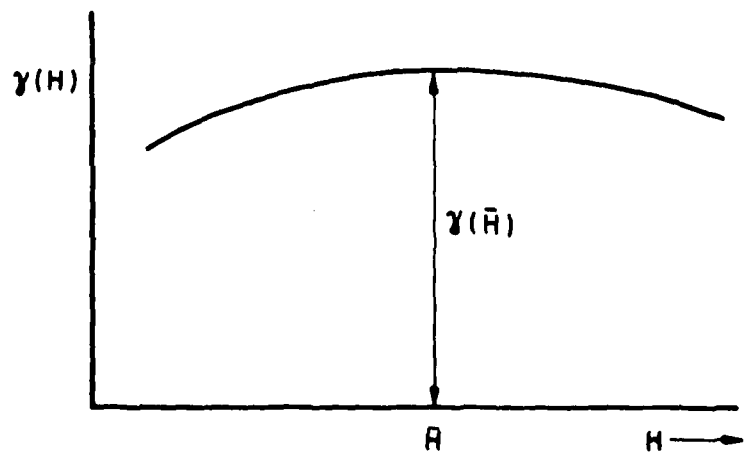

c Illustration of the tuned gust length H̄

Fig 39 Illustration of discrete gust terminology

REPORT DOCUMENTATION PAGE

Overall security classification of this page

UNCLASSIFIED

As far as possible this page should contain only unclassified information. If it is necessary to enter classified information, the box above must be marked to indicate the classification, e.g. Restricted, Confidential or Secret.

1. DRIC Reference (to be added by DRIC)	2. Originator's Reference	3. Agency Reference	4. Report Security Classification/Marking
	RAE TR 79045	N/A	UNCLASSIFIED UNLIMITED

5. DRIC Code for Originator	6. Originator (Corporate Author) Name and Location
7673000W	Royal Aircraft Establishment, Farnborough, Hants, UK
5a. Sponsoring Agency's Code	6a. Sponsoring Agency (Contract Authority) Name and Location
N/A	N/A

7. Title

The design of aircraft automatic ride-smoothing systems using direct-lift control

7a. (For Translations) Title in Foreign Language

7b. (For Conference Papers) Title, Place and Date of Conference

8. Author 1. Surname, Initials	9a. Author 2	9b. Authors 3, 4	10. Date	Pages	Refs.
Fry, D.E.	Winter, J.S.		May 1979	91	23

11. Contract Number	12. Period	13. Project	14. Other Reference Nos.
N/A	N/A		FS 98

15. Distribution statement

(a) Controlled by –

(b) Special limitations (if any) –

16. Descriptors (Keywords) (Descriptors marked * are selected from TEST)

Active control. Ride-smoothing. Gusts. Turbulence. Gust-alleviation.

17. Abstract

This Report shows how a direct-lift motivator can be used to alleviate the response to vertical turbulence of a rigid, combat-type aircraft. Optimal-control and parameter-optimisation techniques are used to design both 'open' and 'closed' loop control systems. Alternative criteria other than simply reducing the normal acceleration response are discussed. The effects of system nonlinearities such as position and rate limits are explored. Both discrete and continuous models of turbulence are used in the analysis. Some nonlinear control solutions are discussed.

F5910/1


ILMED
8